Natural Resources
Conservation and Research

Natural Resources Conservation and Research

Editor-in-Chief

Prof. Ali Mostafaeipour

Industrial Engineering Department,

Yazd University

Iran, Islamic Republic of

Dr. Richard Kwasi Bayitse
CSIR-Institute of Industrial Research
Ghana

Dr. Mehari Alebachew Tesfaye
Bern University of Applied Sciences
Ethiopia

Dr. Joanna Nowosad
Faculty of Environmental Sciences, University of Warmia and Mazury
Poland

Dr. Ekundayo Peter Mesagan
University of Lagos
Nigeria

Dr. Mohsen Abbasnia
Department of Meteorology, Istanbul Technical University
Turkey

Dr. Tri Dinh Bao Ong
Lincoln University
Viet Nam

Prof. Alaa M. Rashad
Housing & Building National Research Center (HBRC)
Egypt

Sherif Ali Younis
Egyptian Petroleum Research Institute
Egypt

Dr. Muhammed Cihat Tuna
Firat University
Turkey

Dr. Chandra Shekhar Kapoor
Department of Environment Science, Pacific Academy of Higher Education and Research University
India

Dr. Abderrahim Lakhouit
University of Tabuk
Canada

Prof. Hasan Yilmaz
Suleyman Demirel University
Turkey

Dr. Gioacchino Francesco Andriani
University of Bari ALDO MORO
Italy

Rashmi Yadav
ICAR- National Bureau of Plant Genetic Resources
India

Dr. Dmitry Mikhailovich Bezmaternykh
Institute for Water and Environmental Problems, Siberian Branch of Russian Academy of Sciences
Russian Federation

Dr. Shakti Suryavanshi
Sam Higginbottom University of Agriculture Technology and Sciences
India

Dr. Nazile Ural
Bilecik Şey Edebali University
Turkey

Dr. Sridhar Pilli
Mahindra École Centrale
India

Dr. Yaser Safari
Shahrood University of Technology
Iran, Islamic Republic of

Dr. Xu Gao
Wonkwang University
China

Dr. Somayeh Rahimi
University of Tehran
Iran, Islamic Republic of

Dr. Mamdouh El Haj Assad
University of Sharjah
United Arab Emirates

Dr. Emrah Yalcin
Ahi Evran University
Turkey

Prof. Chakravarthi Vishnubhotla
University of Hyderabad
India

Prof. Romesh Kumar Salgotra
SKUAST-Jammu
India

Prof. Eldar Magomedovich Eldarov
Dagestan State University
Russian Federation

Khurshid Ahmad Tsriq
Islamia College of Science and Commerce
(Autonomous)
India

Umaru Mohamed Gassama
College of Health and Environmental Science
Sierra Leone

Dr. Kai Ahrendt
Company for Environment and Coast
Germany

Dr. Mehdi Zarei
Shiraz University
Iran, Islamic Republic of

Dr. Roberto Rico-Martínez
Universidad Autonoma de Aguascalientes/
Centro de Ciencias Basicas-Departamento de
Quimica
Mexico

Dr. Paulo Jorge Silva Pereira
University of Minho Pole
Portugal

Dr. Abhay Kumar Pandey
Tocklai Tea Research Institute
India

Victor Cypren Nwaezeapu
Nnamdi Azikiwe University
Nigeria

Jairo José de Oliveira Andrade
Pontifical Catholic University of Rio Grande
do Sul
Brazil

Dr. Dinesh Singh
Division of Plant Pathology, ICAR- Indian
Agricultural Research Institute
India

Da Huo
Robert W. Baird. Stanford University
United States

Susan Horton Bragdon
Quaker United Nations Office Geneva
United States

Dr. Mohamed Galal Eltarabily
Civil Engineering Department, Port Said
University
Egypt

Dr. Ali Akbar Kakouei
University of Tehran
Iran, Islamic Republic of

Natural Resources Conservation and Research

Contents

ORIGINAL RESEARCH ARTICLE

Managerial approach for transplanted rare plants: A proposal

Akira Matsui

Keifuku Consultant Co., Ltd., 11-2-1 Tada, Obama, Fukui 917-0026, Japan. E-mail: matsuiakira1972@yahoo.co.jp

ABSTRACT

The species currently listed as rare plants are roughly divided into two types. The populations of one type of rare plants (including *Pellionia minima* Makino) have decreased due to habitat changes (e.g., from a wet environment to a dry environment) by human-driven development. The populations of the other type of rare plants (including disturbance-dependent species) have decreased because they are unmanaged. The former type of plants is stress tolerance-strategy or competition-strategy species, whereas the latter is only ruderal-strategy species. The stress tolerance-strategy or competition-strategy species do not need management after the protection period ends, but the ruderal-strategy species require adaptive management even after the protection period expires. The protection period of *P. minima* (a stress-tolerant competitor) is estimated to be approximately 1 year after transplant because *P. minima* have sufficient ecological adaptability and resilience, and growth in these plants is confirmed roughly 1 year after transplant.

Keywords: Growth Rate; *Pellionia Minima* Makino; Stress-tolerant Competitor; Survival Rate

ARTICLE INFO

COPYRIGHT

1. Introduction

In Japan, the Ministry of the Environment, local governments and nongovernmental organization (NGOs) together created Japan's Red List of Threatened Species. In Japan's Red List 2017 published by the Ministry of the Environment[1], the total number of threatened species (animals, fungi and plants) is 3,634 species. The National Biodiversity Strategy of Japan 2012–2020 defines four crises of biodiversity: (1) crises due to human activities such as development; (2) crises due to reduced intervention in nature; (3) crises due to alien species brought by humans and (4) crises due to changes of the global environment[2]. In the planned construction site of Kochigawa Dam (Wakasa Town, Fukui Prefecture, Japan), the presence of the rare plant *Pellionia minima* Makino was confirmed in July 2004. The *P. minima* was later transplanted from a flooded/submerged area at that site and their growth was monitored. The results of the transplantation and monitoring were presented in Matsui[3]. Herein I make a proposal concerning the managerial approach for transplanted rare plants based on the results of the *P. minima* transplantation.

Kochi River is located in Wakasa Town, Fukui Prefecture, on Japan's main island of Honshu. Its basin area is 16.3 km², and the length of the river channel is 6.4 km. The Kochi River has undergone from many floods and droughts, and Kochigawa Dam (**Figure 1**) is being constructed to address these problems. The Kochigawa Dam has a catchment area of 14.5 km², a submerged area of 0.37 km², a dam height of 77.5 m, a crest length of 202.3 m, a surcharge water-level

altitude of 197.7 m, a full water-level altitude of 190.5 m, a lowest low-water-level altitude of 162.7 m, and a reservoir capacity of 8 million m³. Construction started in 2012 and is scheduled to be completed in 2019. The construction objectives are flood control, normal functioning of the river water, agriculture water supply, city water supply and industrial water supply.

An evaluation of the animals and plants in the planned construction site of Kochigawa Dam confirmed the presence of *P. minima* in a flooded/submerged area of the planned construction site. This species is a rare perennial herb that grows in wet places in mountains. The stem crawls across the ground, is approximately 10 cm–30 cm long, and the leaf has obtusely saw teeth with dense short hair. The flower season is from April to June, and it is a dioecious plant. This species has shown a declining trend due to the deterioration of growing conditions by deforestation. According to the Fukui red data book, *P. minima* is now classified as near-threatened in Fukui Prefecture. This species is distributed from the west of the main island of Honshu to Okinawa, and only in the south area of Fukui Prefecture[4].
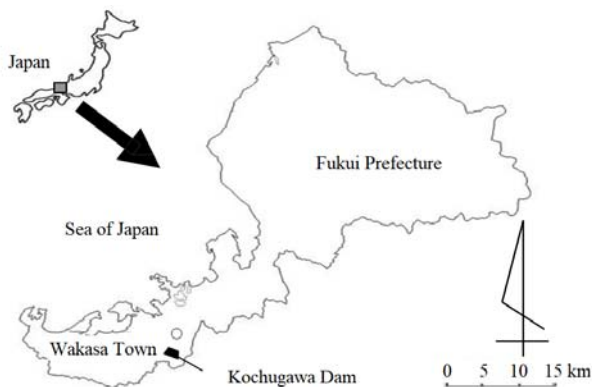
Figure 1. Location of survey area.

As a conservation measure of this species, the plants' transplantation to areas outside the submerged site and subsequent monitoring were selected. Other rare plants have been transplanted as part of road projects' conservation measures[5,6] and as a compensation method for the impact of dam projects[7]. However, there has been no case study of *P. minima* transplantation.

In the present study by Matsui[3], the transplanting of *P. minima* began in 2013 and ended in 2016. A total of 461 individual plants were transplanted: 56 in 2013, 100 in 2014, 205 in 2015, and 100 in 2016 (**Table 1**). The transplant destinations were three districts designated A, B and C outside the submerged area in the Kochigawa Dam's planned construction site. Ten separate transplantation sites (A-1, A-2, A-3, A-4, B-1, B-2, B-3, B-4, C-1 and C-2) were used. Sites B-2 and B-3 and Sites C-1 and C-2 were transplanted in the same year, but they were handled separately because these sites were distant from each other. The leaf size and vitality in each of the four seasons (spring, summer, autumn and winter) were then monitored. Here the results were reported and a proposal regarding the monitoring period for the transplantation of rare plants in future dam projects was made.

Table 1. Number of individuals of *Pellionia minima* bedded out in the transplant sites

Site	2013	2014	2015	2016	Total
A-1	56				186
A-2		50			
A-3			30		
A-4				50	
B-1		50			170
B-2			30		
B-3			40		
B-4				50	
C-1			60		105
C-2			45		
Total	56	100	205	100	461

This table is derived from Matsui[3].

Alteration of natural ecosystems is often necessary as human societies expand and develop. Mitigation measures such as avoidance, reduction and compensation must then be considered as environmental conservation measures. The transplanting of rare plants described herein corresponds to the compensation. Although wild animals and plants have varying degrees of ecosystem resilience, a protection period is necessary immediately after the transplantation of rare plants. The transplanted individuals can be expected to survive in the natural ecosystem after a protection period ends. If the protection period becomes too long, it will delay the plants' opportunity to return to a natural ecosystem. It is thus necessary to determine the optimal protection period of the transplanted individuals by monitoring their health and growth.

2. Methods

2.1 Survey of transplant candidate sites

As a survey of candidate transplantation sites toward the selection of sites that are similar to the environment of the autogenesis ground of *P. minima*, growth location and physical environment items at the transplant districts A, B and C were examined. The growth location items were vegetation and the presence/absence of damage by wild animals (mainly Sika deer [*Cervus nippon*]). The physical environment items were soil (as soil texture, humus, soil hardness, water wettability and pH), light (as relative light intensity) and terrain. The survey demonstrated that the soil texture of all three transplant districts is composed of clay loam soil, with abundant humus, soil hardness = soft, water wettability = moistened, pH = weakly acidic (4.2–4.8) and relative light intensity = 3%–10% (**Table 2**). These results confirmed that districts A, B and C provide almost the same environment as the autogenesis ground.

Table 2. Physical environment items in habitat of *Pellionia minima*

Soil texture	Clay loam soil
Humus	Abundant
Soil hardness	Soft
Water wettability	Moistened
pH	Weakly acidic (4.2–4.8)
Relative light intensity	3%–10%

2.2 Transplant period and method

In the typical transplant period of herbaceous plants, the blooming of spring species is from mid-February to early March, or from mid-September to early October; the blooming of summer-to-autumn species is from early March to mid-April[8]. Since *P. minima* is a species that blooms in spring and its autogenesis area have snow in winter, the optimal transplant period is judged to be from September to October. The activity of the plants is higher in September, and because transplantation result in damage to the roots, all of the transplantations of the individual *P. minima* were done during the month of October in 2013, 2015 and 2016; the exception was November in 2014.

The transplant method was carried out in the order of land-conditioning of the transplant dis-

tricts, digging and transporting at the autogenesis ground, and planting at the transplant sites. First, the removal of fallen leaves and branches, graveling and landscaping were carried out at the transplant sites. *P. minima* was hand-picked from the autogenesis ground one by one. Pot seedlings were placed in order to suppress drying, and transported to the transplant sites. The graft holes were excavated at 30 cm intervals, and a single pot seedling was planted in each graft hole. The irrigation was done by hand, and care was taken to ensure that the soil clogged well between the roots. After the transplanting, mulch with fallen leaves was added to prevent the soil/plant from drying. The transplanting was carried out step-by-step to the A, B and C districts in that order from 2013 to 2016 in order to reduce the risk of transplanting fails.

2.3 Monitoring method

To obtain the size of the leaves of the transplanted individuals, a fold scale was used to measure the length of the longitudinal side (X) and the length of the transverse side (Y), which is orthogonal to X. The vitality of the transplanted individuals was visually evaluated based on the leaf state, flowering, the presence/absence of insect damage. In the transplant year, monitoring was carried out immediately after the transplantation and at ≥1 week and at ≥1 month, post-transplantation and before snowfall. During the year after the transplantation, monitoring was done once in each of the four seasons (spring, summer, autumn and winter).

3. Results

3.1 Survival rate

The survival rate at each site was determined as followed: the number of individual plants surviving in the winter of 2016 was divided by that of transplanted plants. **Table 3** summarizes the sequential changes in the surviving number of *P. minima* bedded out in the transplant sites. The numbers are those of the survivors in the winter of each year. For each transplant year, the number is that of the live individuals before snowfall. In winter 2016, the survival of 452 individual plants

was confirmed (98% average survival rate).

Table 3. Sequential changes in the surviving number of *Pellionia minima* bedded out in the transplant sites

Site	Transplanted number	2013	2014	2015	2016	Survival rate
A-1	56	56	56	51	50	89％
A-2	50		50	50	50	100％
A-3	30			30	30	100％
A-4	50				50	100％
B-1	50		50	49	49	98％
B-2	30			30	30	100％
B-3	40			40	38	95％
B-4	50				50	100％
C-1	60			60	60	100％
C-2	45			45	45	100％
Total	461	56	156	355	452	98％

This table is obtained from Matsui[3].

3.2 Growth rate

The growth rate was determined as followed: the leaf size in the winter of 2016 was divided by that before the snowfall of the transplanting year, and the median value was omitted from the outlier values. **Table 4** shows the sequential changes in the increases and decreases of the average leaf size of *P. minima* bedded out in the transplant sites. The av-erage growth rate of the eight transplant sites was 2.1. Student's t-test was used to determine the sig-nificance of the changes in the average value of the leaf size of the previous year for each transplant site. Significant changes (i.e., with $p < 0.05$) are shown in **Table 4** as "↗", and non-significant changes are indicated by "-".

Table 4. Sequential changes in the increases and decreases of the average leaf size of *Pellionia minima* bedded out in the transplant sites

Site	2013	2014	2015	2016	Growth rate
A-1	Transplantation	-	↗	-	1.2
A-2		Transplantation	↗	↗	5.6
A-3			Transplantation	↗	2.5
B-1		Transplantation	↗	-	5.8
B-2			Transplantation	-	0.9
B-3			Transplantation	-	0.8
C-1			Transplantation	↗	2.1
C-2			Transplantation	↗	3.1
Total					2.1

Note: ↗ : $p < 0.05$; -: $p > 0.05$.
This table is collected from Matsui[3].

4. Discussion

4.1 Growth rate

The leaf size of many of the transplanted in-dividuals increased in the year following the trans-plantation, but there were some sites (A-1, B-2 and B-3) where no increase in leaf size was observed in the year after transplantation. The infiltration of *Cervus nippon* and sediments is suspected at these sites, and it is therefore speculated that the growth suppression at these three sites is due to the penetra-tion of *Cervus nippon* and the influx of gravel from the upper slope at the sites.

4.2 Determination of transplant success

The determination of transplant success was based on the survival rate, growth rate and vi-tality of the transplanted individuals. Overall, the transplanted individuals generally survived in dis-tricts A, B and C. The growth rate exceeded 1.0 except for Sites B-2 and B-3. Large growth abnor-malities, e.g., feeding damage and insect damage were not observed at any of transplant sites, and the transplanted individuals grew steadily and sat-isfactorily. From the above results, it is apparent that the transplanted individuals were well estab-lished as of this writing in 2017.

4.3 Monitoring period proposal

The optimal monitoring period for the trans-

4

plantation of *P. minima* originally expected to be 3 years (including two overwintering years) for the plants' complete survival over several dormancy periods after transplantation. However, since the increase in leaf size was confirmed and no major abnormalities were observed in the present monitoring and the plants grew steadily and well, it is apparent that it will be not necessary to monitor *P. minima* for 3 years after they are transplanted. Confirmation of the leaf-size increase can be used to classify the transplanted individuals as established. At the time point at which the transplantation is defined as successful, it could be said that the monitoring period can be discontinued. However, monitoring at dam construction sites is often subject to period restrictions, and it is thus important to judge the success of the transplant at the earliest stage.

On the other hand, the habitats change for animals and plants are expected to be stressful. When possible, it is desirable to take evasive measures so that transplantation is not necessary. Transplantation as simply an easy first option should be avoided. In addition, a protection period will be necessary following transplanting, and the length of the period should be optimal. *P. minima* has sufficient ecological adaptability and resilience, and its growth was confirmed herein at roughly 1 year after transplant. Ecosystem adaptability and resilience are truly remarkable.

4.4 Conservation measures other than stock transplant

In the cases of stock transplant as described in this research, most of the practical applications are done as plant environmental conservation measures, and the effect of the measures is easy to grasp. However, there is a risk that target individuals will not settle in at the transplant sites and disappear. It is thus desirable to use multiple methods[6]. *P. minima* does not accomplish a generation update by seed propagation; it is maintained and expanded by vegetative propagation with stolons. When a seed-propagating plant is being transplanted, it is also possible to collect seeds from the stock and to transplant the soil. Transplanting the soil is a method that can efficiently move many individuals. It has been shown to be effective in the restoration

of lakeshore vegetation using sediment seed banks[9].

4.5 Management after protection period

The present study's results demonstrated that transplanted *P. minima* will return to the natural ecosystem after a protection period. As this species grows in wet places in the mountains, it can be left to the progress of the undisturbed ecological transition. On the other hand, for species that grow in an environment where disturbances occur (such as wetlands and paddy fields), it is necessary to carry out management similar to conventional farming work such as the plowing of rice fields, the regulation of the water level and the maintenance of ditches and mowing[10]. In other words, the management after the protection period must differ according to the type of transplant.
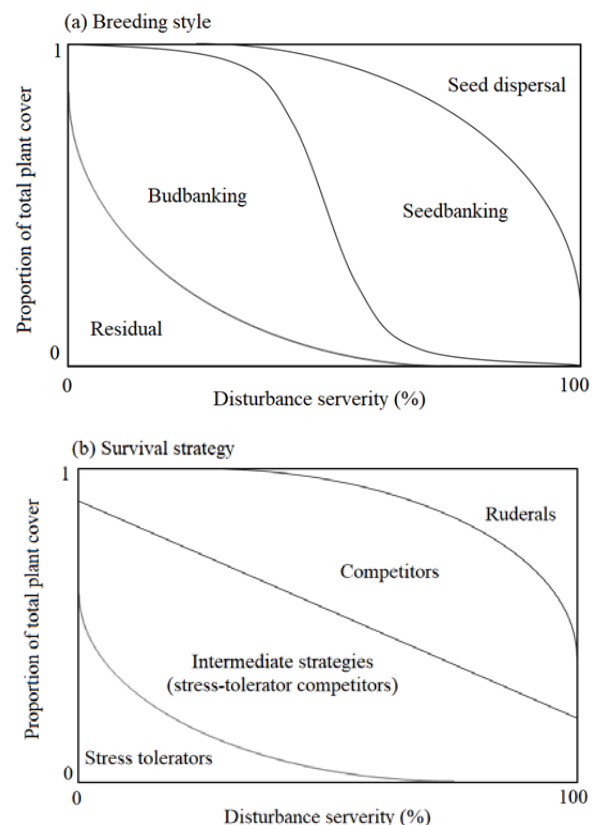
Figure 2. Changes in (a) the breeding style and (b) the survival strategy of plants with increasing disturbance severity. This figure is modified from Haeussler *et al.*[11]

According to Grime[11] and Haeussler *et al.*[12], the breeding style and the survival strategy of *P. minima* are budbanking and stress-tolerant competitor, respectively (**Figure 2**).

The species currently listed as rare plants are

roughly divided into two types. The populations of one type of rare plants (including *P. minima*) have decreased due to habitat changes (e.g., from a wet environment to a dry environment) by human-driven development. The populations of the other type of rare plants (including disturbance-dependent species) have decreased because they are unmanaged. The relationship between rare plant types and management methods is illustrated in **Table 5**. The former rare plant type is comprised of stress tolerance-strategy or competition-strategy species, whereas the latter rare plant type is comprised of only ruderal-strategy species. The stress tolerance-strategy or competition-strategy species do not need management after the protection period ends, but the ruderal-strategy species require adaptive management even after the protection period expires.

Table 5. Relationship between rare plant types and management methods

Type	Stress tolerance-strategy	Competition-strategy	Ruderal-strategy
Threat	Development	Development	Un management
Management	Unnecessity	Unnecessity	Adaptive management

Conflict of interest

The author declared no conflict of interest.

References

1. Ministry of the Environment Government of Japan. (2017) [Mammals] Ministry of the Environment Red List 2017. Tokyo: Ministry of the Environment. Available from: http://www.env.go.jp/press/files/jp/105449.pdf [Accessed 13 December 2017].

2. Ministry of the Environment Government of Japan. (2012). The National Biodiversity Strategy of Japan 2012–2020. Tokyo: Ministry of the Environment. Available from: http://www.env.go.jp/press/files/jp/20763.pdf [Accessed 13 December 2017].

3. Matsui A. Transplant and monitoring of Pellionia minima Makino live in planned construction site in Kochigawa Dam, Wakasa Town, Fukui Prefecture. Journal of the Japanese Society of Revegetation Technology 2017; 43: 339–342.

4. Fukui Prefecture. Revised version threatened wildlife of Fukui Prefecture. Fukui red data book. Fukui: Fukui Prefecture; 2016.

5. Hasegawa K, Ueno Y, Oshiro N, *et al*. Conservation measures for rare plants in road projects around the nation: Focus on difficult-to-transplant plants (epiphytic, mixotrophic, and mycoheterotrophic plants) (in Japanese with English Abstract). Ecology and Civil Engineering 2016; 19: 79–90.

6. Ueno Y, Kurihara M, Oshiro N, *et al*. The technical reference on environmental impact assessment technique for road project examples of environmental conservation measures on 13. Fauna, Flora, Ecosystem. Technical Note of National Institute for Land and Infrastructure Management 2016; 906.

7. Tajima A, Yagami T, Osugi T, *et al*. The current achievements and challenges of the transplant of plants as a compensation method for the impact of dam projects. Tokyo: Water Resources Environment Research Institute; 2013. p. 44–49.

8. Hisashi H. Deciding version how to enjoy wild grass. Tokyo: Kodansha, Ltd.; 2012.

9. Nishihiro J, Washitani I. Restoration of lakeshore vegetation using sediment seed banks; Studies and practices in Lake Kasumigaura, Japan. Global Environmental Research 2007; 11: 171–177.

10. Sekioka H, Shimoda M, Nakamoto M, *et al*. Vegetation management of abandoned rice fields for the conservation of water plants and wetland plants (in Japanese with English Abstract). Journal of the Japanese Institute of Landscape Architecture 2000; 63: 491–494.

11. Grime JP. Evidence for the existence of three primary strategies in plants and its relevance to ecological and evolutionary theory. The American Naturalist 1977; 111: 1169–1194.

12. Haeussler S, Bedford L, Leduc A, *et al*. Silvicultural disturbance severity and plant communities of the southern Canadian boreal forest. Silva Fennica 2002; 36: 307–327.

ORIGINAL RESEARCH ARTICLE

Prioritization for the conservation of Mexico's cloud forests

LM Ochoa-Ochoa[1*], NR Mejía-Domínguez[2], J Bezaury-Creel[3]

[1] *Departamento de Biología Evolutiva, Facultad de Ciencias, Universidad Nacional Autónoma de México, Ciudad de México 04510, México. E-mail: leticia.ochoa@ciencias.unam.mx*

[2] *Red de Apoyo a la Investigación, Coordinación de la Investigación Científica, Universidad Nacional Autónoma de México, Ciudad de México 04510, México.*

[3] *The Nature Conservancy, Programa México y Norte de Centroamérica, Ricardo Palmerin 110, Colonia Guadalupe Inn, Álvaro Obregón, Ciudad de México 01020, México.*

ABSTRACT

Cloud forests are ecosystems with a restricted distribution and high biodiversity, but they are highly threatened due to land use change. The objective of this study is to evaluate and prioritize existing cloud forest fragments to achieve their long-term conservation, combining threat levels and the potential response capacity of various conservation instruments in Mexico, through a triage tool. Threat levels were calculated based on human disturbance coverage, estimated specifically for Mexico. The response capacity was estimated using the presence of the different conservation instruments in each fragment. Once the triage level per fragment was obtained, these were analyzed by ecoregion. The results showed that the area of primary cloud forest has been reduced by 53–73%, and only 31.6% (including primary and secondary forest) is under some protection scheme. We identified a group of fragments on the Pacific slope that require special attention due to the small coverage and their high level of priority. The ecoregions: Sierra Madre del Sur of Guerrero and Oaxaca, Los Altos de Chiapas, Sierra Madre Oriental and Central Mexico corresponding to the largest concentration of cloud forest in the trans-Mexican volcanic belt, 70% of which are listed as a priority for emergency protection.

Keywords: Biodiversity; Government Protected Natural Areas; Social Instruments for the Conservation and Sustainable Use of Biodiversity; Montane Mesophyll Forest; Ecoregions

1. Introduction

One of the ecosystems that harbors the greatest biodiversity in Mexico is found in the montane forests of the intertropical zone in the form of discontinuous patches with limited extension[1-3]. This ecosystem is generally called "montane mesophyll forest" (MMF) in reference to the mesophilic characteristics of the leaves of the dominant tree species and the physiographic zone in which it is found[4,5]. Under this name we find a heterogeneous set of ecological communities, as they constitute a complex transition between lowland communities and those that develop at higher altitudes[6,7]. The heterogeneity of this set of communities is reflected in the variety of names by which they have been referred to in the literature, such as deciduous temperate forest[8], cloud forest[9], montane rain forest[10], fog forest[11], and montane mesophyll forest[4,12,13], to mention a few.

In spite of the wide variation in the names used to refer to these ecological communities, they are unified by the characteristics of the

climate where they develop, by the physiognomy and floristics of the vegetation[14]. This type of vegetation (**Figure 1**) develops in places where the mean annual temperature is between 12 and 23 °C, with a mean annual precipitation of not less than 1,000 mm, but reaching 3,000 mm and in some areas even more than 5,000 mm[15]. This indicates that it can be found in temperate or tropical climates with or without seasonality in precipitation[4]. Physiognomically, these forests are characterized by a great diversity of plants and a diversity of both vascular and non-vascular epiphytes[16,17]. In Mexico, in terms of floristic composition and number of species, there are important differences among authors. For example, González-Espinoza and collaborators[2,18] have described between 2,500–2,822 species, 650–815 genera and 144–176 families typical of this type of vegetation; highlighting the Lauraceae family and the Quercus genus as the best represented. On the other hand, Villasenor[7] mentions that in this type of forest there are at least 6,790 species belonging to 1,625 genera and 238 families of vascular plants. Of these, 2,361 species are endemic to Mexico. However, the main unifying characteristic is the constant or at least frequent presence of fog in the mountains where they develop[11]. In this context, without leaving aside the rest of their characteristics and complexity, it is more appropriate to call them cloud forests[1,2].

In the global context, cloud forests are rare. For example, it is estimated that they occupy about 0.26% of land area and 2.5% of the world's tropical forests[19]. In general, we can say that they are considered a priority worldwide both because of the small area they cover, as well as their distribution in relatively isolated fragments, but above all because of their unique particularity of capturing and filtering water through horizontal precipitation[20]. However, although in some places the cloud forest is maintained as such (Mexico is no exception), the surrounding matrix of tropical rainforests and temperate forests is not given the same priority. This could result in the elevation of the altitude at which clouds develop, causing the moisture of the forest floor to decrease with negative consequences for diversity (e.g. Anchukaitis and Evans[21]). Also, due to the close dependence on moisture in the form of both clouds and precipitation, these forests are particularly vulnerable to global climatic changes[22,23].

Figure 1. Examples of cloud forests of Teipan (upper left corner), Roayaga (lower left corner) and Sierra de Juárez (right); all from Oaxaca, Mexico. Photos: N. Mejía-Domínguez (Teipan) and L. Canseco-Márquez (Roayaga and Sierra de Juárez).

The combination of environmental factors that favor the development of a cloud forest can be found in all the montane regions of Mexico, depending on the altitude, between 600 and 3,200 m a.s.l.[5]. The distribution of cloud forests includes discontinuous regions of the montane zones of the Sierra Madre Oriental, Sierra Madre Occidental, Sierra Madre del Sur, Sierra Norte de Oaxaca, Faja Volcánica Transmexicana and Sierra Madre de Chiapas[24-26]. This distribution is the result of a complex biogeographic history and the environmental heterogeneity of the places where it is found[26,27]. These characteristics are considered to be the main causes of the great diversity of species and endemisms they harbor[3,28]. The high incidence of endemic species, as well as species of restricted distribution, attributes to highlight of cloud forests. A particularly interesting example is the tiny salamanders of the genus thorius. This genus is endemic to Mexico and has 23 restricted distribution species associated with the cloud forest. In addition, recent studies show that there is a distinct phylogenetic lineage of salamanders for virtually every cloud forest region[29]. In this context, the results of analyses to study the relationships of these areas indicate precisely that the evolutionary history of contemporary cloud forest lineages is complex. Although there are general patterns of vicariance, cloud forests have different biogeo-graphic-evolutionary histories, making each of their areas unique and of great importance for conservation[28-31].

Unfortunately, cloud forests are also characterized by a high loss of vegetation cover and a high incidence of other economic activities that modify their structure and species composition[32]. Globally, land use change is one of the greatest threats to biodiversity, and cloud forests are no exception. It should be noted that the loss of cloud forest area implies the loss of all ecosystem services, particularly hydrological services, provided. For the year 2007, it was reported that 71.5% of the primary cloud forest area remained of the 11,885 km^2 that existed in 1976. In addition, the area covered by secondary cloud forest increased by 52.7%[33]. Undoubtedly, estimating the area covered by this type of vegetation represents a

challenge. But assessing the degree of conservation of the remaining fragments is no less complicated[34,35]. In addition to these evaluations, conservation planning for cloud forests requires determining the degree of threat to them, and a good approximation is the level of human disturbance[25,36]. The only way to counteract these threats is conservation strategies. Bezaury-Creel and Gutiérrez-Carbonell in 2009[37] reported that of the more than 18,000 km^2 of cloud forest (primary and secondary) in Mexico, only 1,543 km^2 were under some conservation status. The case of cloud forests is not particularly encouraging and highlights the absence of conservation strategies, especially in the long term. In this context, our objective was to prioritize cloud forest fragments for long-term conservation, combining threat levels and the potential response capacity of conservation instruments located in each fragment. A triage tool was used for this purpose. This tool assigns each fragment a level that allows us to determine the most appropriate actions to follow in terms of conservation costs. Finally, considering the unique history of each of the cloud forest areas and the values obtained through the triage tool, the representation by ecoregions was evaluated to establish priority sites for conservation and propose strategies for their long-term protection.

2. Material and methods

2.1 Spatial data (vegetation coverages)

The vegetation layers generated by the National Institute of Geography and Statistics of Mexico (INEGI) were used. To date, INEGI has published 5 Series of vegetation types: I, II, III, IV and V in chronological order. The set of land use and vegetation layers Series I was published in 1993[38] contains information from 1968–1986. Series II[39] contains information from 1993–1996. Series III was published in 2005, Series IV in 2010[40] and Series V[41] contains information from 2011. For each layer, satellite images were used, mostly Landsat (which has changed in size and the latest resolution, the TM series, is 30 m), with field verification. The detailed process by which these spatial databases were generated can be consulted at

http://www.inegi.org.mx/.

Although more accurate vegetation coverages are now available, only general comparisons can be made between the estimated areas of cloud forest that originally existed in the country and what exists today. To make such a comparison, we used the layers of all Series I-V of land use and vegetation mapping, and the estimates of potential primary vegetation made by CONABIO, which are based on Rzedowski[42]. Area calculations were made in km^2 using Lambert's Conformal Conic plane projection, calculating the extent of cloud forest, both primary and secondary determined as arboreal, in order to obtain an estimate of cover loss and transformed area. The classifications of primary and secondary vegetation were taken directly from the metadata of the land use layers, as there may be controversy regarding their definition. Primary Vegetation: "natural condition, real or apparent (when there is no evidence of a different climax condition), and when disturbance factors have not yet affected the general structure and phlogistic composition of the community"[43]. Secondary Vegetation: "altered or modified state of the community in its floristic or structural composition, generally due to anthropogenic influence or natural catastrophes"[43].

To evaluate the proportion of cloud forests with conservation initiatives, we used the coverages of different types of conservation instruments and the latest land use coverage (Series V). These initiatives include government protected natural areas with three categories: Federal, State and Municipal; and in non-government protected areas or land conservation initiatives through social action that include: areas voluntarily set aside for conservation, payments for environmental services (updated to 2012), management units for wildlife conservation[44] and territorial community ordinances. The latter are not strictly conservation instruments, since their primary objective is to organize land use on ejido and communal lands[45], although they often present spaces for the conservation and sustainable use of ecosystems.

The layers of federal natural protected areas (NPA) that we used were modified from the coverages published by the National Commission of Natural Protected Areas[46], the rest was developed by Bezaury-Creel et al.[45]. Geographic overlaps between the coverages of the various instruments are common. In practice, there is no conflict since if there are resources from two different sources (e.g. federal and state), both are reversed. In addition, the hierarchy of laws on conservation instruments is very clear. However, when working only with coverages in the analysis, if these overlapping areas are not eliminated, overestimates can be generated and make it appear that a larger area is being protected than it should be. This is why we removed all duplicated areas, giving hierarchical priority; first, to federal natural protected area decrees over state natural protected areas, except in the case of natural resource protection areas where state decrees prevail by law; and second, state natural protected areas prevail over municipal natural protected areas in all cases. Finally, following the same logic, we only take into account land protection initiatives through social actions that are located outside of government natural protected areas. After extracting all overlapping areas, we determined the extent of cloud forests under some conservation instrument.

2.2 Risk classification

The Human Affectedness coverage over the Mexican land territory (Human Affectedness[47]) was used to determine the degree of threat. This layer has values of human affectation per pixel (–1 km^2), ranging from 1 to 15, from the lowest to the highest level of affectation. This layer combines different anthropogenic activities that can be a threat to biodiversity. For each fragment of cloud forest, the values of the corresponding pixels were extracted, as well as those within a buffer zone of 1, 5, 10 km and an average was calculated. Subsequently, 5 threat categories were assigned: Level I, when the area has an average value of 0.1 to 2.9 of human impact; Level II from 3 to 5.9; Level III from 6 to 8.9; Level IV from 9 to 12.9 and Level V from 13 to 15. An index was used to evaluate the potential response capacity to reduce the threat of conservation instruments, the classification and values were taken from Ochoa-Ochoa et al.[36]. The values used for the index were: federal natural protected areas = 5, state

and municipal = 4, areas voluntarily destined for conservation and private community protected areas = 3, community territorial ordinances (CTO) = 2, finally both payments for environmental services (PES) and wildlife conservation management units = 1. Although the theoretical maximum value of the response capacity index is 20, the probability of this happening is very low (not zero); therefore, the same ranges of values of the threats were chosen to determine the categories of the potential response index.
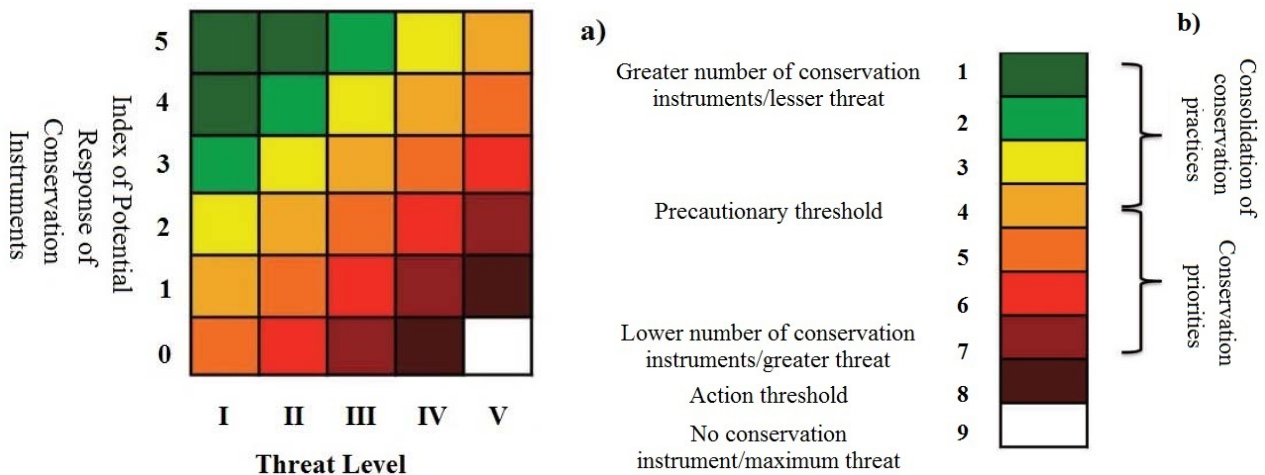
Figure 2. Triage tool to determine conservation priorities.

Subsequently, the cloud forest fragments were periodized by the triage tool proposed by Ochoa-Ochoa et al.[36]. The tool is based on the triage principle, commonly applied to accident victims, in which if a cloud forest fragment (in this case) has a too high level of threat and no conservation instrument (**Figure 2**) it is discarded because it is unlikely to be conserved in the long term, while forest fragments with medium levels of threat and with some conservation instrument are the priority ones to be addressed because the probability that they will be maintained in the long term is high. Finally, priority areas were established according to the percentage of cloud forest in the ecoregion and the percentage of forest at each triage level. Level III of the ecoregion layer proposed by INEGI et al.[48] was used.

This tool evaluates, on the one hand, the threats and determines the level/status of the forest fragment; on the other hand, it evaluates the potential response of the conservation instruments (NPA, CTO, UMA, private reserves, payment for environmental services, etc.) present in the fragment. Both aspects are integrated into the triage matrix (a), where the triage level is established for each forest fragment (b). Level 1 represents cloud forest fragments with a low level of threat with a high potential for response in terms of conservation instruments; levels 1 to 3 represent sites where, in order to preserve in the long term, it is only necessary to consolidate the conservation practices already existing in the area. Level 4 represents a precautionary threshold and it is from this value and up to level 7 where conservation priorities must be concentrated and adequate conservation strategies implemented. Level 7 represents cloud forest fragments with a high level of threat and a low conservation response potential; it is at this level where the threshold for action is established, i.e., it is necessary to evaluate whether it is worth investing, given the cost in terms of conservation, to establish conservation actions. Fragments located at level 9 represent sites with the highest level of threat and no conservation instrument, so it will be ineffective to invest in conservation actions.

3. Results

According to the analyzed coverages, between 26% (if secondary tree vegetation is taken into account) and 53% (if it is not considered) of the cloud forest in Mexico has been lost to date, according to the vegetation proposed by Rzedowski[42] (**Figure 3**). But it is more dramatic if we consider the primary vegetation chart as original

vegetation[49], where more than 57% has been lost if secondary vegetation is taken into account and more than 73%, if it is not considered (**Table 1**, **Figure 4**).

Approximately 31.56% of the cloud forest is within a conservation instrument (**Table 2**). Governmental instruments are the ones that protect the largest area of cloud forest. Of the government protected natural areas, it is not surprising that the Federal Protected Areas are the largest with more than 1,765 km^2, followed by the State ones with –536 km^2, and finally the municipal ones with 0.01 km^2. Among the social instruments for conservation, Community Land Use Plans are the main ones with –1,436 km^2, followed by management units for wildlife conservation (241.81 km^2), payments for environmental services (108.32 km^2), and of these, mainly hydrological ones with 104.41 km^2. Finally, there are areas voluntarily set aside for conservation together with private and community protected areas with almost 72 km^2.
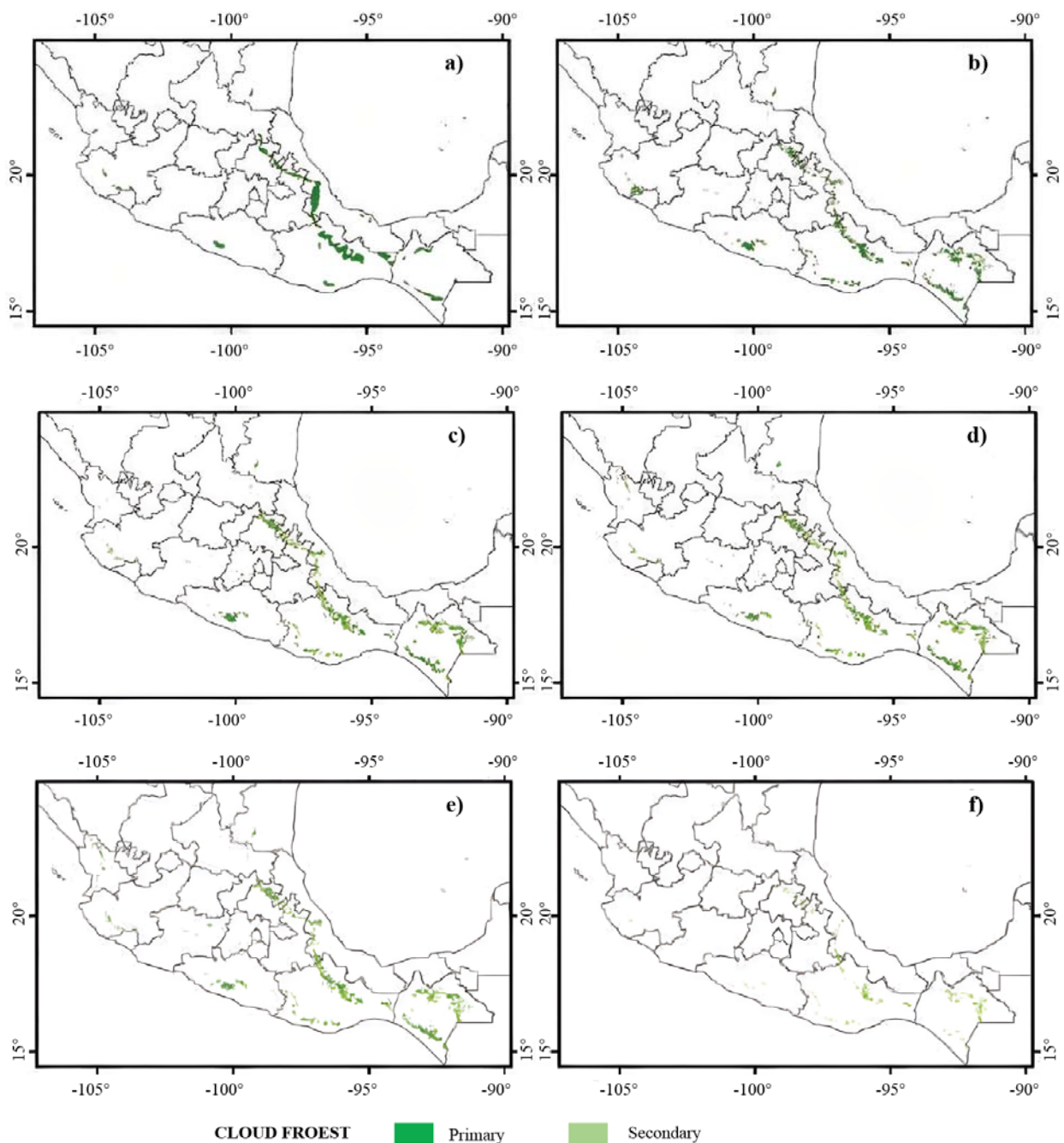
Figure 3. Distribution of montane mesophyll forest according to the different INEGI land use and vegetation coverages. Potential cloud forest according to CONABIO **(a)**, Series I **(b)**, Series II **(c)**, Series III **(d)**, Series IV **(e)** and Series V **(f)**.

Table 1. Area in square kilometers of cloud forest according to land use and vegetation coverage generated by INEGI in different years. *Sum of the area of primary and secondary tree vegetation.

Coverage	Primary vegetation	Secondary vegetation		Total
		Arborea	Shrub and herbaceous	
CONABIO potential	17.887			
INEGI potential	30.883			
Series I (1993)	18.113			
Series II (1999)	10.020	3.189	4.931	13.209
Series III (2005)	8.695	3.960	5.597	12.655
Series IV (2010)	8.475	4.528	5.415	13.003
V Series (2013)	8.472	4.708	5.348	13.180
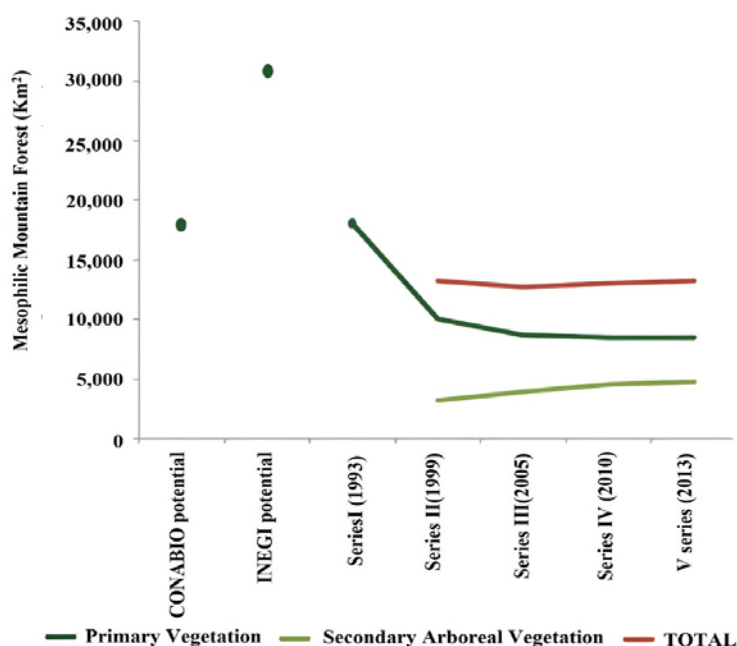
Figure 4. Area in square kilometers occupied by mesophyll mountain forest in Mexico according to different vegetation coverage and land use.

Table 2. Area of cloud forest under some type of protection in km^2

Type	Protected area of cloud forest (km^2)
Governmental	**2,301.59**
Federal natural protected areas	1,765.62
State natural protected areas	535.96
Municipal natural protected areas	0.01
Non-governmental	**1,857.49**
Areas voluntarily set aside for conservation and private and community protected areas	**71.80**
Community	69.43
Small property	2.36
Community land use planning	**1,435.56**
Community	689.25
Ejido	146.56
Others	599.75
Environmental services	**108.32**
Biodiversity conservation	3.90
Hydrological environmental services	104.41
Wildlife conservation management units	**241.82**
Total	4,159.08

In total, 747 fragments of cloud forest were detected, of which 291 are secondary forest and 456 primary forest. Threat levels, potential conservation response index and triage level are reported together (**Table 3**). The table shows the number of fragments that fall into each category of the tool (see **Figure 2**) depending on the buffer zone used. Of the total number of fragments, 85 have a value of zero, i.e., zero threat value and no conservation tools. These fragments were placed in a separate category because, although in these analyses they do not present any threat, they are still vulnerable to

13

Table 3. Evaluation of cloud forest fragments according to the triage tool based on threats and potential resilience of conservation instruments

		Triage	Mist forest Series V	Buffer 1 km	Buffer 5 km	Buffer 10 km
	Zero threat level/regardless of response rate	0	101			1
Consolidation of conservation practices	Greater number of conservation instruments/lesser threat	1				
		2				103
		3			82	
	Precautionary threshold	4				233
Conservation priorities		5	260	261		183
		6				
	Lower response rate/higher threat	7				0
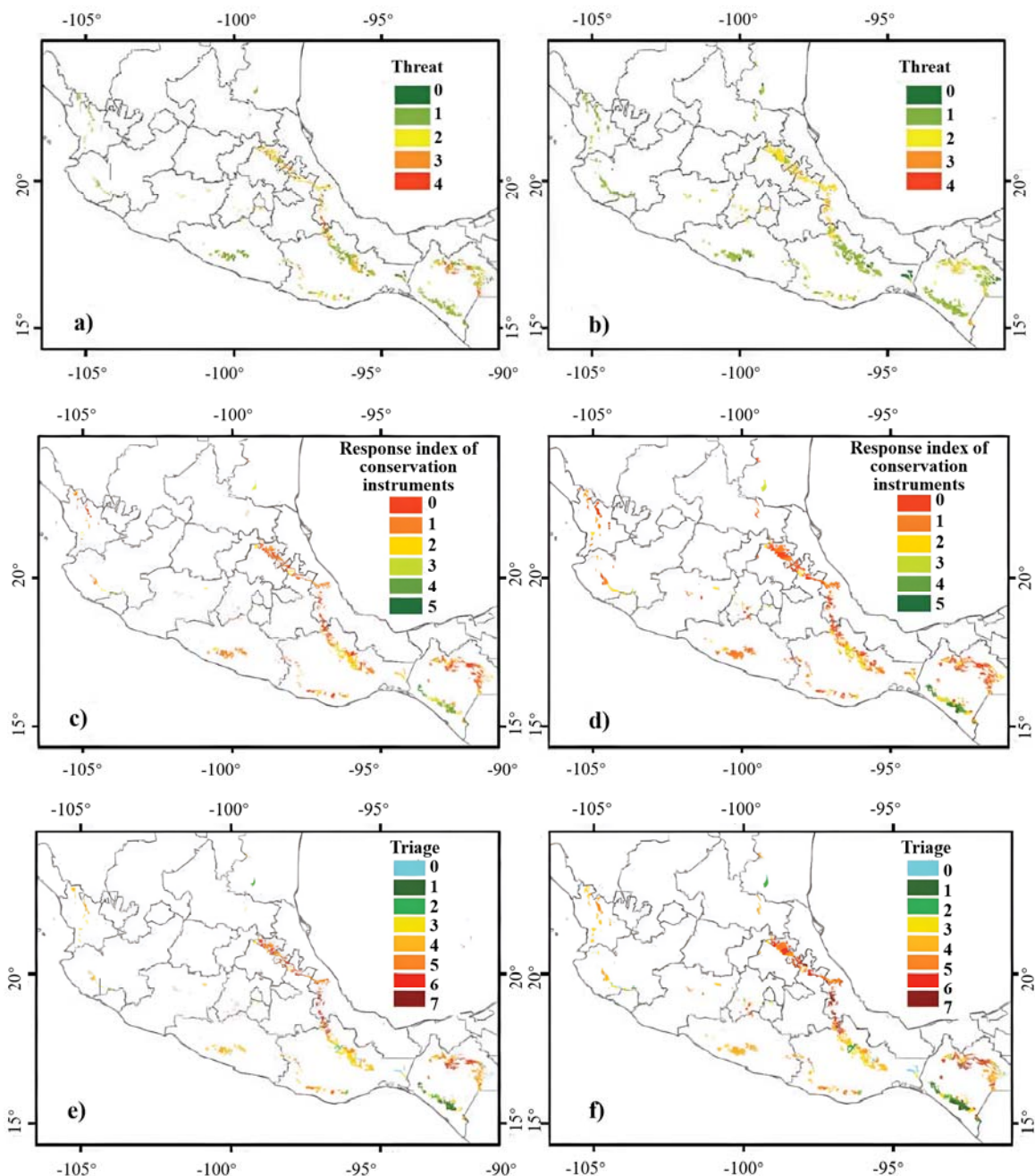
Figure 5. Evaluation of the fragments of montane mesophyll forest according to human disturbance; potential response index according to the presence of the different conservation instruments; and finally the evaluation of the triage tool. Fragments alone (**a**, **c**, **e** correspondingly) and fragments with a zone of influence of 1 km (**b**, **d**, **f**).

any that may arise. Of the remaining fragments, 89   should   have   their   conservation   strategies

consolidated and 531, 71%, are conservation priorities, i.e., strategies should be implemented for these sites. Finally, 42 fragments, equivalent to 5.6% of the total, need to be evaluated to verify whether it is worth investing in conservation strategies, to focus efforts on restoration or not to invest. Most of these fragments are located in the southern Sierra Madre Oriental, where the largest area is located between Coscomatepec and Huatusco, in Veracruz. Another group of sites in this category is located around Rayón and Simojovel, Chiapas (**Figure 5**).

The ecoregion with the largest area of cloud forest is the Sierra Madre del Sur of Guerrero and Oaxaca with more than 36%, of which almost 74% is classified as a priority to be conserved according to the triage results. This is followed by the Sierra Madre Centroamericana, an area more commonly known as Sierra Madre de Chiapas, with 16%, of which almost 83% only requires the consolidation of conservation instruments. This is followed by Los Altos de Chiapas with almost 15% of the country's cloud forest, of which more than 82% is classified as a priority. Then follows the cloud forests of the Sierra Madre Oriental with a little more than 11%, of which more than 85% is considered a priority. In fifth place is Central Mexico with more than 9%, of which almost 79% is considered a priority. These 5 ecoregions have almost 88% of the country's cloud forests. The next 5 ecoregions together have 11.35% (see **Table 4, Figure 5**), and the rest of the ecoregions together have less than 1% of the cloud forest. However, it is worth noting that in total 65.4% of cloud forests is a priority for conservation.

4. Discussion

Due to the nature of their distribution, restricted to islands and the large loss in the area they cover, cloud forests have always been considered a priority for conservation[1,2]. It has also been reported that there are overestimates in the calculation of cloud forest area in studies based on the quality of satellite images[50]. This means that it is possible that cloud forests are in a more precarious situation than currently believed[2]. Nevertheless, information and analytical tools based on remote sensing remain the most effective means for assessing the conservation status of vegetation in general[37], and is perhaps the only way to have an overall picture of the status of cloud forests, at least for the case of Mexico. The present study confirms the fact that the "primary" cloud forest has been dramatically affected, reducing its area by up to 73% (highest estimated value). Even the most encouraging figure (53% loss) almost doubles the loss value of 28.8% reported in 2007 for a 30-year period[33]. Although considering the secondary forest (only the tree component), the figure seems less discouraging, where only 31% of this area has some protection status.

Regardless of the conservation status, primary or secondary vegetation, due to the great wealth of natural resources, a high percentage of cloud forests have been settled by humans for a long time[51]. Studies on the diversity and structure of the vegetation have found evidence of their management; for example, it has been observed that forest harvesting has decreased species diversity, modified the spatial distribution of trees and changed the dimensional differentiation (diameter and height of trees). But the situation could be even worse, since in addition to land use change, there are other latent threats to cloud forests, such as climate change[32,51] and selective extraction of both orchid and tree litter[52]. These low-impact activities, apparently less serious, directly modify the composition of plant species and negatively affect the diversity and composition of animal species by modifying or losing microhabitats generated in the cloud forest[52,53]. However, it should be emphasized that almost no specific studies have been conducted in this regard for cloud forests in Mexico.

Due to the relative scarcity of cloud forests in Mexico and their biological importance[1,19], it is crucial to conserve 100% of their remaining cover and even consider the restoration of those portions of secondary forest with the potential to recover their structure and functions. However, achieving this figure is practically impossible, which is why the triage tool makes it possible to optimize the efforts and resources allocated to their conservation. Traditionally, natural protected areas have been seen as the ideal tool for conservation[54], but in

Table 4. Cloud forest, in percentage, according to the total area found in each ecoregion (INEGI *et al*.[48]) and the triage value obtained

Ecoregions	Triage value								
	0	1	2	3	4	5	6	7	Total
1. Coniferous, oak and mixed forests of the Sierra Madre del Sur of Guerrero and Oaxaca.	3.700		5.941	16.033	39.084	29.110	5.470	0.661	36.323
2. Coniferous, oak and mixed forests of the Central American Sierra Madre.	5.448	41.829	22.652	18.253	4.718	2.234	4.091	0.775	16.081
3. Coniferous, oak and mixed forests of the Chiapas highlands.	4.749		0.521	11.649	6.697	46.902	28.516	0.966	14.853
4. Coniferous, oak and mixed forests of the Sierra Madre Oriental.	1.091		10.845	1.167	10.210	33.614	41.571	1.502	11.294
5. Lomerios and Sierras with coniferous, oak and mixed forests of Central Mexico.	4.119	2.648	2.105	5.202	19.635	33.981	25.116	7.193	9.147
6. Lomerios with evergreen rainforest.	12.758		6.143	10.338	12.583	29.795	24.784	3.600	3.907
7. Coniferous, oak and mixed forests of the Sierra Madre Occidental.	11.876				30.580	57.006	0.538		2.439
8. Coniferous, oak and mixed forests of the Sierra Madre del Sur of Jalisco and Michoacan.	22.644		3.090	27.329	35.929	11.008			2.275
9. Soconusco Coastal Plains and Lomerios with evergreen rainforest.		57.561	14.165	24.545			1.079	0.027	1.499
10. Lomeríos and Coastal Plains of Nayarit and Jalisco with evergreen rainforest.	2.931				86.172	10.734	0.163		1.231
11. Lomerios and Piedemontes of the Mexican South Pacific with thorny forest.	0.656		0.525	6.966	75.279	16.574			0.505
12. Lomerios and Interior Plains with xerophytic scrub and lowland mesquite forest.						100.000			0.210
13. Sierra de los Tuxtlas with evergreen rainforest.				100.000					0.081
14. Central Depression of Chiapas with Caducifolia Forest.				0.404		33.300	66.296		0.072
15. Lomerios of Sonora and Sinaloa and Canons of the Sierra Madre Occidental with xerophytic scrub and deciduous forest.	2.530					97.470			0.063
16. Balsas depression with deciduous forest and xerophilous scrubland.					19.845	80.155			0.019
17. South Texas Plains/Inland Plains and Lomerias with xerophytic scrub and oak woodland.						100.0			0.001
18. Tehuantepec canyon and plain with deciduous forest and thorny forest.				1.00					0.0003
Total by triage value	4.770	7.832	7.821	12.608	22.398	28.137	14.920	1.516	

such a biologically diverse country (with high rates of species turnover; see Williams-Linera *et al*.[55]), not only biologically but also culturally (there is a great diversity of cultures with high turnover between regions), the use of a wide range of conservation instruments and/or strategies that adjust to the social requirements of each region is required for their use to be effective. Conservation instruments are not homogeneous and almost all of them contemplate a sustainable use of natural resources by human populations[37]. This means that in a certain way, cloud forests that are currently covered under some conservation instrument will continue to maintain some level of "threat". In this sense, the triage method is the most appropriate for prioritizing and making decisions about which fragments should be addressed first, in a long-term conservation context[36]. In a high percentage (>71%) of cloud forest fragments, it is necessary to implement conservation instruments immediately, either because of their high level of threat or because they are not yet covered by any instrument, i.e. they are a priority. The lesser ones are at a more affordable level for conservation, i.e., it is enough to consolidate the instruments currently in place. It is worth noting that the geographic location of the fragments is not only important in terms of their evolutionary history but also in terms of their social context, and is therefore a determining factor for the possible tools to be implemented to be truly effective. An interesting example is Oaxaca, where social/cultural issues have complicated the establishment of governmental natural areas, but social conservation initiatives have proven to be truly effective[56].

For a long time, there was discussion as to which were the best conservation strategies: top-down or bottom-up. There now seems to be a

consensus on the importance of using both strategies. However, it is worth emphasizing that in practice, conservation is carried out by people (governed by laws and/or resources). In this sense, it is people who perceive and are affected by changes in the ecosystem around them. Moreover, in general, top-down strategies depend on the resources allocated, which vary temporally and spatially; social conservation strategies do not. Therefore, at least in Mexico, social conservation strategies have been particularly successful[37,57]. These rural communities are immediately dependent on the conservation status of their natural resources.

Weighing by ecoregions, it is interesting that in the regions where cloud forest is concentrated, in most cases more than 70% of the fragments are a priority.

Undoubtedly, these fragments are the priority for long-term conservation. They are located in the ecoregions: Sierra Madre del Sur of Guerrero and Oaxaca, Los Altos de Chiapas, Sierra Madre Oriental and Central Mexico corresponding to the Trans-Mexican Volcanic Belt. By covering a larger area, these ecoregions guarantee' long-term success. However, it is very likely that ecoregions containing smaller areas of cloud forest are at a higher level of priority due to the small area of fragments they contain. The cloud forest fragments with the smallest area are mostly located on the Pacific slope and in areas where atmospheric humidity is lower on average than in the rest of the country's cloud forests[6]. This climatic variant represents another distinct set of cloud forest type that should be prioritized for conservation, as it surely represents rare and unique communities in terms of the composition and structure of the species that comprise them. The opposite case is the Sierra Madre de Chiapas, where only the federal protected natural areas of El Triunfo, the municipalities of La Concordia, Ángel Albino Corzo, Villa Flores and Jiquipilas (La Frailescana), La Sepultura and Volcán Tacaná, as well as the state protected natural area Cordón Pico El Oro Paxtal, need to be consolidated. Of course, this scenario is based on the assumption that the instruments will work ideally or adequately. Therefore, it is imperative to incorporate some measures related to socioeconomic variables as possible indicators of the success of the implementation and continuity of each of the conservation instruments as well as the surrounding area. In this sense, it would be important to evaluate the effectiveness of community land-use planning, since they cover a significant percentage of cloud forest fragments, mainly in areas where there are very few governmental reserves, such as Guerrero and Oaxaca. A relevant aspect of this type of conservation instrument is that it is the communities or ejidos that decide to manage, therefore they represent a "bottom-up" strategy where the landowners are the ones who are convinced that this measure is required[57]. And it is precisely the fact that they are convinced that favors or increases their success.

5. Final considerations

The overall conservation prioritization strategy for Mexico's cloud forests is a comprehensive and complex process. The assessment presented here is only a simplified guide to initiate a more comprehensive conservation planning process. This process should consider the effectiveness of the instruments and their viability in each proposed area. Likewise, socially owned lands (ejidos, agrarian communities, etc.) deserve special attention as they are home to a large area of cloud forest, so it is advisable to encourage long-term social conservation and/or reinforce it with other socially appropriate instruments. In this sense, the Payment for Environmental Services Component operated by the National Forestry Commission (CONAFOR), whose rules of operation favor the conservation of these cloud forests by granting them the highest payment per hectare, is of great importance. It is relevant that the first site supported by CONAFOR's Biodiversity Endowment Fund, through which the Commission makes payments for long-term environmental services, is the Sierra de Cacoma in Jalisco, which was selected precisely because of the presence of cloud forests.

Finally, the environmental services provided by cloud forests are broad and include the

seven aspects identified as environmental services (water capture and filtration, mitigation of climate change effects due to their strategic position in altitudinal gradients, oxygen generation, biodiversity protection, soil retention, wildlife refuge and, of course, scenic beauty). However, particularly these forests have an additional unique value in the capture of water by the condensation of clouds and fog, so they are recognized and even sought for payment for environmental services for the large amount of water they capture and filter[19]. Given the above, the conservation of these forests is of vital importance.

Although the primary focus of this assessment is on cloud forest fragments, it is highly relevant to integrate information on the matrix of other ecosystems in which these fragments are immersed. Therefore, the results obtained from fragments that include a buffer zone are particularly important. Because it is inevitable that the changes that occur within the in-mediated area surrounding the fragment, whatever they may be, will have an impact on it.

Acknowledgement

Conflict of interest

The authors declared no conflict of interest.

References

1. CONABIO. El Bosque Mesófilo de Montana en México: Amenazas y oportunidades para su conservación y manejo sostenible (Spanish) [The Montana Mesophilic Forest in Mexico: Threats and opportunities for its conservation and sustainable management]. Mexico: Comisión Nacional para el Conocimiento y Uso de la Biodiversidad; 2010.
2. González-Espinosa M, Meave JA, Ramírez-Marcial N, *et al*. Los bosques de niebla de México: conservación y restauración de su componente arbóreo (Spanish) [The cloud forests of Mexico: Conservation and restoration of its arboreal component]. Ecosistemas 2012; 21(1–2): 36–52.
3. Ochoa-Ochoa LM, Mejia-Dominguez NR. Fauna de los Bosques Mesófilos de Montaña (Spanish) [Fauna of the mesophilic forests of Montana]. In: Gual-Diaz M, and Rendón-Correa A (editors.). Bosques Mesófilos de Montana de México: Diversidad, Ecología y Manejo. Mexico: Comisión Nacional para el Conocimiento y Uso de la Biodiversidad; 2014. p. 237–247.
4. Rzedowski J. Vegetación de México (Spanish) [Vegetation of Mexico]. Mexico: Limusa; 1978.
5. Luna-Vega I, Velázquez A, Velázquez E. 2001b. Mexico. In: Kappelle M, Brown AD (editors). Bosques nublados del Neotrópico (Spanish) [Neotropical cloud forests]. San José, Costa Rica: Instituto Nacional de Biodiversidad; 2001. p. 183–229.
6. Mejía-Domínguez NR, Meave JA, Ruiz-Jiménez CA. Análisis estructural de un bosque mesófilo de montaña en el extremo oriental de la Sierra Madre del Sur (Oaxaca), México (Spanish) [Structural analysis of a montane cloud forest in the eastern end of the Sierra Madre del Sur (Oaxaca), Mexico]. Botanical Sciences 2004; (74): 13–29.
7. Villaseñor JL. El bosque húmedo de montaña en México y sus plantas vasculares: Catálogo florístico-taxonómico (Spanish) [The humid mountain forest in Mexico and its vascular plants: Floristic-taxonomic catalog]. DF, México: Comisión Nacional para el Conocimiento y Uso de la Biodiversidad-Universidad Nacional Autónoma de México; 2010.
8. Rzedowski J. El extremo boreal del bosque tropical siempre verde en Norteamérica continental (Spanish) [The boreal edge of tropical evergreen forest in continental North America]. Vegetatio 1963; 11(4): 173–198.
9. Gómez-Pompa A. Ecología de la Vegetación de Veracruz (Spanish) [Vegetation ecology of Veracruz]. A.C., Xalapa: Instituto de Investigaciones sobre Recursos Bióticos; 1982.
10. Beard JS. The classification of tropical American vegetation-types. Ecology 1955; 36(1): 89–100.
11. Hamilton LS, Juvik JO, Scatena FN. The Puerto Rico tropical cloud forest symposium: Introduction and workshop synthesis. Tropical montane cloud forests. New York: Springer; 1995. p. 1–18.
12. Miranda F. Estudios sobre la vegetación de México. V. Rasgos de la vegetación de la Cuenca del Río Balsas (Spanish) [Studies on the vegetation of Mexico. V. Characteristics of the vegetation of the Balsas River Basin]. Revista de la Sociedad Mexicana de Historia Natural 1947; 8: 95–114.
13. Rzedowski J, McVaugh R. La vegetación de la Nueva Galicia (Spanish) [The vegetation of Nueva Galicia]. Contributions of the University of Chicago Herbarium 1966; 9: 1–123.
14. Ortega Escalona F, Castillo Campos G. El bosque mesófilo de montaña y su importancia forestall (Spanish) [The mountain mesophyll forest and its forest importance]. Ciencias 1996; (43): 32–39.
15. Rzedowski J, Palacios-Chávez R. El bosque de Engelhardtia (Oreomunnea) mexicana en la región de la Chinantla (Oaxaca, México): Una reliquia del Cenozoico (Spanish) [The Mexican Engelhardtia (Oreomunnea) forest in the Chinantla region (Oaxaca, Mexico): A relic of the Cenozoic].

Botanical Sciences 1977; (36): 93–127.

16. Mayorga-Saucedo R, Luna-Vega I, Alcántara-Ayala O. Floristic of the cloud Forest of Molocotlan, Molango-Xochucoatlan, Hidalgo, Mexico. Botanical Sciences 1998; (63): 101–119.

17. Barthlott W, Schmit-Neuerburg V, Nieder J, *et al*. Diversity and abundance of vascular epiphytes: A comparison of secondary vegetation and primary montane rain forest in the Venezuelan Andes. Plant ecology 2001; 152(2): 145–156.

18. Gonzáalez-Espinosa M, Meave JA, Lorea-Hernáandez FG, *et al*. The red list of Mexican cloud forest trees [Master's thesis]. Cambridge, UK: Fauna & Flora International; 2011.

19. Sánchez-ramo SG, Dirzo R, Gual-Díaz M, *et al*. El bosque mesófilo de montaña: Un ecosistema prioritario amenazado (Spanish) [The montane cloud forest: A threatened priority ecosystem]. In: Gual-Díaz M, and Rendón-Correa A (editors). Bosques Mesófilos de Montaña de México: Diversidad, Ecología y Manejo (Spanish) [Mesophilic mountain forests of Mexico: Diversity, ecology and management]. México: Comisión Nacional para el Conocimiento y Uso de la Biodiversidad; 2014. p. 109–139.

20. Bruijnzeel LA, Proctor J. Hydrology and biogeochemistry of tropical montane cloud forests: What do we really know? Tropical montane cloud forests. , New York: Springer; 1995. p. 38–78.

21. Anchukaitis KJ, Evans MN. Tropical cloud forest climate variability and the demise of the Monteverde golden toad. Proceedings of the National Academy of Sciences 2010; 107(11): 5036–5040.

22. Mulligan M. Modeling the tropics-wide extent and distribution of cloud forest and cloud forest loss, with implications for conservation priority. Tropical montane cloud forests: Science for conservation and management 2010; 740: 16–38.

23. Rojas-Soto OR, Sosa V, Ornelas JF. Forecasting cloud forest in eastern and southern Mexico: conservation insights under future climate change scenarios. Biodiversity and Conservation 2012; 21(10): 2671–2690.

24. Rzedowski J. Análisis preliminar de la flora vascular de los bosques mesófilos de montaña de México (Spanish) [Preliminary analysis of the vascular flora of the montane cloud forests of Mexico]. Acta Botánica Mexicana 1996; (35): 25–44.

25. Challenger A. Utilización y conservación de los ecosistemas terrestres de México: Pasado, presente y future (Spanish) [Use and conservation of terrestrial ecosystems in Mexico: Past, present and future]. Mexico: Comisión Nacional para el Concimiento y Uso de la Biodiversidad; 1998.

26. Luna-Vega I, Morrone JJ, Ayala OA, *et al*. Biogeographical affinities among Neotropical cloud forests. Plant Systematics and Evolution 2001; 228(3): 229–239.

27. Halffter G, Llorente-Bousquets J, Morrone JJ. La perspectiva biogeográfica histórica, en Capital Natural de México, vol. I: Conocimiento actual de la biodiversidad (Spanish) [The historical biogeographical perspective, in Natural Capital of Mexico. vol. I: Current knowledge of biodiversity]. Mexico: CONABIO; 2008.

28. Ornelas JF, Sosa V, Soltis DE, *et al*. Comparative phylogeographic analyses illustrate the complex evolutionary history of threatened cloud forests of northern Mesoamerica. PloS One 2013; 8(2): e56283. doi: https://doi.org/10.1371/journal.pone.0056283.

29. Rovito SM, Vásquez-Almazán CR, Papenfuss TJ, *et al*. Biogeography and evolution of Central American cloud forest salamanders (Caudata: Plethodontidae: Cryptotriton), with the description of a new species. Zoological Journal of the Linnean Society 2015; 175(1): 150–166.

30. Watson DM, Peterson AT. Determinants of diversity in a naturally fragmented landscape: humid montane forest avifaunas of Mesoamerica. Ecography 1999; 22(5): 582–589.

31. Marshall CJ, Liebherr JK. Cladistic biogeography of the Mexican transition zone. Journal of Biogeography 2000; 27(1): 203–216.

32. Toledo-Aceves T, Meave JA, González-Espinosa M, *et al*. Tropical montane cloud forests: Current threats and opportunities for their conservation and sustainable management in Mexico. Journal of Environmental Management 2011; 92(3): 974–981.

33. Rosete-Vergés FA, Pérez-Damián JL, Villalobos-Delgado M, *et al*. El avance de la deforestación en México 1976–2007 (Spanish) [The advance of deforestation in Mexico]. Madera y Bosques 2014; 20(1): 21–35.

34. Mas JF, Velázquez A, Couturier S. La evaluación de los cambios de cobertura/uso del suelo en la República Mexicana (Spanish) [The evaluation of land cover/use changes in the Mexican Republic]. Investigación Ambiental 2009; 1(1): 23–39.

35. CONABIO-SEMARNAT. Cuarto Informe Nacional de México al Convenio sobre Diversidad Biológica (CDB) (Spanish) [Fourth National Report of Mexico to the Convention on Biological Diversity (CBD)]. México: Comisión Nacional para el Conocimiento y Uso de la Biodiversidad y Secretaría de Medio Ambiente y Recursos Naturales; 2009.

36. Ochoa-Ochoa LM, Bezaury-Creel JE, Vázquez LB, *et al*. Choosing the survivors? A GIS-based triage support tool for micro-endemics: Application to data for Mexican amphibians. Biological Conservation 2011; 144(11): 2710–2718.

37. Bezaury-Creel J, Gutiérrez-Carbonell D. Áreas naturales protegidas y desarrollo social en México (Spanish) [Protected natural areas and social development in Mexico]. México: CONABIO; 2009. p. 385–431.

38. INEGI. Conjunto Nacional de Uso de Suelo y Vegetación (1968, 1971–1986) (Spanish) [National set of land use and vegetation (1968, 1971–1986)]. Scale 1:250 000, Series I. Mexico: DGG-INEGI; 1993.

39. INEGI. Conjunto Nacional de Uso de Suelo y

Vegetación (1993–1999) (Spanish) [National set of land use and vegetation (1993–1999)]. Scale 1:250 000, Series II. Mexico: DGG-INEGI; 1999.

40. INEGI. Conjunto Nacional de Uso de Suelo y Vegetación (2007–2008) (Spanish) [National set of land use and vegetation (2007–2008)]. Scale 1:250 000, Series IV. Mexico: DGG-INEGI; 2010.

41. INEGI. Conjunto Nacional de Uso de Suelo y Vegetación (2012–2013) (Spanish) [National set of land use and vegetation (2012–2013)]. Scale 1:250 000, Series V. Mexico: DGG-INEGI; 2013.

42. Rzedowski J. Vegetación Potencial (Spanish) [Potential vegetation]. IV.8.2. Atlas Nacional de México. Vol II. Escala 1:4 000 000. México: Instituto de Geografía, UNAM; 1990.

43. INEGI. Conjunto Nacional de Uso de Suelo y Vegetación (2002–2005) (Spanish) [National set of land use and vegetation (2002–2005)]. Scale 1:250 000, Series III. Mexico: DGG-INEGI; 2005.

44. SEMARNAT. Unidades de Manejo para el Aprovechamiento Sustentable de la Vida Silvestre 2016 (Spanish) [Management units for the sustainable use of wildlife 2016]. Scale: 1:0. Edition: 2a. México: Secretaría de Medio Ambiente y Recursos Naturales; 2016.

45. Bezauri-Creel JE, Torres-Origel JF, Ochoa-Ochoa LM, *et al*. Áreas naturales protegidas y otros espacios dedicados a la conservación, restauración y uso sustentable de la biodiversidad en México (Spanish) [Protected natural areas and other spaces dedicated to the conservation, restoration and sustainable use of biodiversity in Mexico]. Capas ArcGis [CD-ROM]. México: The Nature Conservacy; 2012.

46. Bezauri-Creel JE, Torres-Origel JF, Ochoa-Ochoa LM. Base de datos geográfica de áreas naturales protegidas federales y áreas bajo manejo de conservación federal en México (Spanish) [Geographic database of federal natural protected areas and areas under federal conservation management in Mexico]. Modified and adapted from CONANP 2016–Version 3.0. Updated 30/12/2016. 8 ArcGIS 9.2 layers + 3 Goggle Earth KMZ layers + 1. Word metadata file.

47. Bezauri-Creel JE, Ochoa-Ochoa LM. Base de Datos Geográfica de la Afectación Humana sobre el Territorio Mexicano (Spanish) [Geographic database of human impact on the Mexican territory]. Version 1.0, 07/2009. 2 raster format layers + 1 Goggle Earth KMZ layer + 1 Word Metadata File.

48. INEGI, CONABIO, INE. Ecorregiones terrestres de México (Spanish) [Terrestrial ecoregions of Mexico]. Scale: 1:1000 000. México: Instituto Nacional de Estadística, Geografía e Informática, Comisión Nacional para el Conocimiento y Uso de la Biodiversidad, Instituto Nacional de Ecología; 2008.

49. INEGI. Carta de Vegetación Primaria (Tipos de Vegetación) (Spanish) [Primary vegetation chart (types of vegetation)]. Aguascalientes, México: INEGI; 2000.

50. Cayuela L, Golicher JD, Rey JS, *et al*. Classification of a complex landscape using Dempster–Shafer theory of evidence. International Journal of Remote Sensing 2006; 27(10): 1951–1971.

51. Williams-Linera G. El bosque de niebla del centro de Veracruz: ecología, historia y destino en tiempos de fragmentación y cambio climático (Spanish) [The cloud forest of central Veracruz: Ecology, history and destiny in times of fragmentation and climate change]. AC, CONABIO, Xalapa: Instituto de Ecología; 2007.

52. Ruiz-Jiménez CA, Téllez-Valdés O, Luna-Vega I. Classification of the Mexican cloud forests: Floristic affinities. Revista Mexicana de Biodiversidad 2012; 83(4): 1110–1144.

53. Toledo-Aceves T, García-Franco JG, Williams-Linera G, *et al*. Significance of remnant cloud forest fragments as reservoirs of tree and epiphytic bromeliad diversity. Tropical Conservation Science 2014; 7(2): 230–243.

54. Bezaury-Creel JE. El valor de los bienes y servicios que las áreas naturales protegidas proveen a los mexicanos (Spanish) [The value of goods and services that protected natural areas provide to Mexicans]. México: The Nature Conservancy; 2009.

55. Williams-Linera G, Toledo-Garibaldi M, Hernández CG. How heterogeneous are the cloud forest communities in the mountains of central Veracruz, Mexico? Plant Ecology 2013; 214(5): 685–701.

56. Bray DB, Merino-Pérez L. La experiencia de las comunidades forestales en México: veinticinco años de silvicultura y constucción de empresas forestales comunitarias (Spanish) [The experience of forest communities in Mexico: Twenty-five years of forestry and the construction of community forestry companies]. México: Instituto Nacional de Ecologíap; 2004.

57. Martin GJ, Camacho-Benavides C, del Campo-Garcia C, *et al*. Indigenous and community conserved areas in Oaxaca, Mexico. Management of Environmental Quality: An International Journal 2011; 22(2): 250–266.

Original Research Article

Future forecast of global land wind and light resources in the context of climate change

Feimin Zhang[1], Chenghai Wang[1*], Guohui Xie[2], Weizheng Kong[2]

[1*] *College of Atmospheric Sciences, Lanzhou University, Key Laboratory for Arid Climatic Change and Disaster Reduction of Gansu Province, Lanzhou 730000, Gansu province, China. E-mail: wch@lzu.edu.cn*

[2] *State Grid Energy Research Institute, Co., Ltd., Beijing 102209, China.*

ABSTRACT

Based on the multi-model ensemble average results of the CMIP5 program, we predict the changes of global terrestrial wind and solar energy resources from 2020 to 2030 under different future climate change scenarios. The results show that the multi-mode ensemble average results have high confidence in the simulation of global wind and solar energy resources. Under different climate scenarios (RCPs), the changes in global terrestrial wind and solar energy resources in the next 2020–2030 (relative to 1986–2005) will have significant regional differences. Among them, wind resources in the Americas, Africa and Australia increased, while European wind-rich areas decreased; those in Asia (e.g., Northwest China and Central Asia) increased in RCP2.6, but decreased in RCP4.5 and RCP8.5. Global terrestrial solar energy resources are increasing in different RCPs scenarios in the future, especially in European solar energy-rich areas. Wind energy and solar energy resources on the global land have obvious seasonal variation characteristics, and the seasonal variation rate varies greatly in different regions. The change trend and change range of wind energy and solar energy resources in different rich areas are different. There are some differences in the RCPs scenario. It shows the complexity of future changes in wind and solar energy resources in response to global climate change.

Keywords: Wind and Solar Energy; Future Projection; Climate Change Scenario; CMIP Project

COPYRIGHT

1. Introduction

In recent years, as an important part of clean energy, the utilization of wind and solar energy has developed rapidly around the world. The Global Wind Energy Commission (GWEC) forecast for the future global wind market suggesting that the global demand for renewable energy will gradually increase in the future and the wind market will grow steadily, especially in Asia, Europe and North America.

As the basic elements of renewable energy, near-stratigraphic wind speed and surface solar radiation have significant inter-chronological changes and regional differences. In recent years, the evaluation and estimation of renewable resources have become one of the hotspots of global attention[1-10]. Studies show that near-stratigraphic wind speeds decrease in most of the tropical and middle latitudes, while increasing in high latitudes[11,12]. In China, the daily average wind speed is greater than 3 m·s⁻¹ decreases, and the overall wind speed shows a decreasing trend[13]. The change of wind energy is closely related to the east Asian monsoon circulation and under cushion surface[14]. The inter-decadal variation of surface solar radiation in China is characterized by an "ascending-descending" variation, and the overall trend is also decreas-

ing[15], which is mainly related to low cloud changes and human activities[16], while the solar radiation reaching the surface in Europe is on the increase, with an increase of about 5%[17].

With global climate change, the reserves and distribution of wind and solar energy resources will change accordingly in the future. The study concluded that, due to global warming, the average wind energy in the northern hemisphere mid-latitudes will decrease in the future, while the average wind energy in the tropics and southern hemisphere will increase[18]. In the 21st century, the annual mean wind speed at 10 m height in China tends to decrease in the high emission (A2), medium emission (A1B) and low emission (B1) scenarios, and the decreasing trend becomes more significant as the emission scenario increases[19]. Under the A2 emission scenario, the spatial distribution of wind energy resources in the 21st century is essentially the same as in the last 40 years of the 20th century, and the annual mean wind speed has a weakening trend in the first half of the 21st century, while an increasing trend dominates in the second half[20]. In the medium emission (A1B) scenario, the annual mean wind speed tends to increase over most of the United States, with a maximum increment of about 0.4 m·s^{-1}[21]. Under the RCP4.5 and RCP8.5 emission scenarios, the wind speed increment in the South African region does not exceed 6%[22]. Under climate change scenarios, wind energy resources will increase in the future in north-central Europe (e.g., in and around the Baltic Sea), while they will decrease along the Mediterranean coast and in most of France, with insignificant interannual variability[23,24]. In the context of global warming, estimates of future solar energy resources indicate a 0% to 20% decrease in solar radiation on a seasonal scale in the continental United States[25]. In Japan, solar radiation will increase in the warm season and decrease in the cool season[26]. The overall solar radiation in central and southern Europe will increase by 5% to 10%, while the winter solar radiation in northern and eastern Europe will decrease by 5% to 15%[27]. Solar radiation in Nigeria will be reduced, especially in the southern part[28].

In summary, it can be seen that the near-surface wind speed and surface solar radiation as wind and light resources respond significantly to future climate change, but there are large uncertainties. The future changes of wind and light resources involve the development and utilization of global renewable resources, enterprise development, and resource construction layout. It is of great practical and scientific significance for national economic development to predict in advance the possible changes of future wind and solar resources in the context of climate change.

This paper attempts to use the simulation results of the international Coupled Mode Inter-comparison Project Phase 5 (CMIP5) to estimate the possible changes of global land wind and light elements from 2020 to 2030, and give the spatial and temporal change characteristics of wind and light resources, so as to provide scientific reference for the medium and long-term planning of the development and utilization of wind and light resources.

2. Materials and methods

Despite the large uncertainties in climate models, they are still the most reliable and indispensable tool to estimate the future climate change. The monthly data of air temperature, wind velocity and downward short-wave radiation in CMIP5 are used to study the future changes of global land wind velocity and solar radiation. In order to ensure model uniformity, 16 climate models including the above variables were selected from the historical test (RCP2.6, RCP4.5, RCP8.5) and the future tests with different typical emission concentration scenarios. Considering that the resolution of different climate models will have differences on the simulation results under the same emission scenario, a bilinear interpolation method is used to uniformly interpolate the results of all models to the bilinear interpolation method was used to uniformly interpolate all model results to a 2.5° × 2.5° grid point. For comparison, the period 1986–2005 is used as the current climate reference period, using the definition of the IPCC (Intergovernmental Panel on Climate Change) Working Group I Fifth Assessment Report (AR5, fifth assessment report).

There are few tests and assessment analyses on

the ability of GCMs to simulate near-surface wind speed and surface solar radiation, which are mainly limited by the large uncertainties in the model simulations of the two elements. Loew *et al*.[29] showed that the assessment results of CMIP models on a global scale rely heavily on the reanalysis of model information, and the simulation of interdecadal variability of solar radiation is subject to large errors and uncertainties. In this paper, eight models (**Table 1**) were selected for equal-weighted ensemble averaging to estimate the changes of global terrestrial wind and solar resources in 2020–2030 under different future climate scenarios (RPCs) based on the

comparative analysis of the simulation capability of temperature and precipitation in the CRU (climate research units, version 4.01) reanalysis data for the same period. The global terrestrial wind and solar resources in 2020–2030 under different future climate scenarios (RPCs) are estimated relative to the historical reference period. It should be noted that the soundness of the above methods has been widely recognized in the field of climate change prediction, and the simulation capability of multi-model ensemble averaging is more reliable than that of a single model.

Table 1. Basic information of CMIP5 model for wind and light resource estimation

Model name	Country	Resolution	Points period	
			Historical experiments	Future prognostic tests
CanESM2	Canada	2.8° × 2.8°	1850–2005	2006–2100
MIROC5	Japan	2.8° × 2.8°	1850–2012	2006–2100
NorESM1-M	Norway	2.5° × 1.875°	1850–2005	2006–2100
IPSL-CM5A-LR	France	3.75° × 1.875°	1850–2005	2006–2300
IPSL-CM5A-MR	France	2.5° × 1.25°	1850–2005	2006–2100
HadGEM2-ES	United Kingdom	1.875° × 1.25°	1859–2005	2006–2299
HadGEM2-AO	Korea	1.875° × 1.25°	1859–2005	2006–2299
MRI-CGCM3	Japan	1.125° × 1.125°	1850–2005	2006–2100

Wind energy is the kinetic energy of air movement, which is the product of the wind turbine blade area, 3 times of wind speed and the air density. Wind energy per unit area of the wind turbine blade is defined as:

$$W = \frac{1}{2}\rho v^3$$

(1)

Where: W is the wind energy per unit area of the wind turbine blade (W·m^{-2}); ρ is the air density (g·m^{-3}); v is the wind speed at the height of the wind turbine hub (m·s^{-1}).

The above equation shows that wind energy is proportional to air density and wind speed, i.e., the greater the air density and wind speed, the greater the wind energy. However, air density has spatial variability. In order to eliminate the deviation of wind energy caused by spatial differences in density, a relationship between air density and altitude is established to make corrections based on the gas equation of state[30].

$$\rho_H = \rho_0 \left(1 - a\frac{H}{T_0}\right)^{4.26}$$

(2)

Where: ρ_H is the density of air at altitude H, ρ_0

is the density of air at room temperature and standard atmospheric pressure, taking the value of 1225 g·m^{-3} (the density of air at 15 °C at sea level); H is the altitude (m); T_0 is the absolute temperature (K), taking the value of 273 K; a is the decreasing rate of atmospheric vertical temperature, taking the value of 0.0065 °C·m^{-1}.

The magnitude of solar energy depends mainly on the density of solar shortwave radiation flux (also known as irradiance, W·m^{-2}) that reaches the ground. In general, the stronger the solar irradiance reaching the ground, the more abundant the solar energy.

The rate of change of global land-averaged wind and solar energy (R_{RCPs}) for 2020–2030 under different climate scenarios (RPCs) relative to the historical reference period (1986–2005) is calculated as follows:

$$R_{RCPs} = \frac{M_{RCPs} - M_{his}}{M_{his}}$$

(3)

Where: M_{RCPs} are the global terrestrial annual (seasonal) average wind and solar energy for different future climate scenarios; M_{his} is the global terrestrial annual (seasonal) average wind and solar

23

energy for the historical reference period.

2. Simulation capability of multi-model ensemble for global near-surface wind speed and solar irradiance

Figure 1 shows the global near-surface wind speed and solar irradiance distributions based on multi-model ensemble averaging. As seen in **Figure 1(a)**, there are significant regional differences in the global distribution of near-surface wind energy resources. The overall wind energy resources on the ocean are higher than on land, and the wind energy-rich areas on the ocean are mainly concentrated in the vast areas south of the equator near the poles, especially in the eastern hemisphere region, where the wind speed is above 7 m·s^{-1} in most of the sea. Onshore wind energy-rich areas are concentrated in North Africa, central North America, northwestern China, Central Asia and Australia, with relatively few wind energy resources at low latitudes near the equator. Compared with the global near-surface wind speed based on ground station observations released by NASA[31], the multi-model ensemble averaging results better reflect the approximate distribution of the actual global near-surface wind speed, but the simulated values are small, which may be related to the inconsistency between the simulated and observed altitudes of the near-surface wind speed.

From **Figure 1(b)**, it can be seen that global solar energy resources are mainly concentrated between the Tropic of Cancer near the equator, with solar irradiance usually above 200 W·m^{-2}, and are most abundant in the Sahara region of northern Africa, while the eastern and southern parts of the African continent, Australia and northwestern China are also solar resource-rich areas. Compared with the solar irradiance observed by global ground-based weather stations published by NASA[31], the multi-model ensemble averaging results not only effectively reflect the approximate distribution of the actual global solar radiation, but also have a better reproducibility of the solar radiation magnitude values in different regions.

Comparing the multi-model ensemble averaging results with the observed spatial distribution of global near-surface wind speed and solar irradiance, the multi-model ensemble averaging results can reproduce the distribution and magnitude of global wind and solar energy resources better, which has high reliability. Therefore, this paper estimates the possible trend and distribution of wind and solar energy resources from 2020 to 2030 by using multi-model ensemble averaging results.
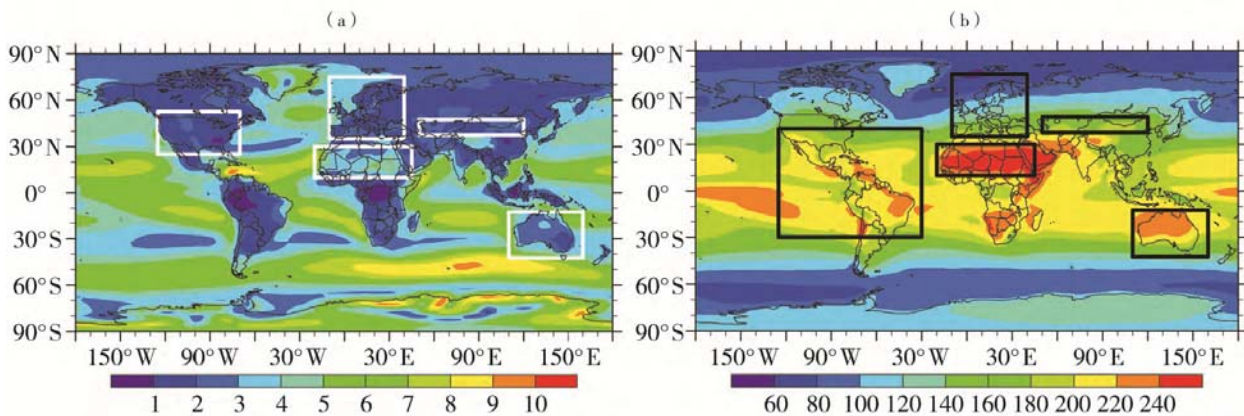
Figure 1. Multi-model ensemble-averaged global near-surface wind speed (**a**, unit: m·s^{-1}) and surface solar irradiance (**b**, unit: W·m^{-2}) distributions (high value areas are in the box).

3. Possible future changes in global terrestrial near-surface wind power density and solar irradiance

Figure 2 shows the annual rate of change distribution of global terrestrial near-surface wind and solar resources for the period 2020–2030 for different climate scenarios relative to the reference period (1986–2005). It can be seen that under different climate scenarios

24

(RCPs), the changes of global terrestrial wind energy resources from 2020 to 2030 are obviously spatial different. Under the RCP2.6 and RCP8.5 climate scenarios, compared with the period 1986–2005, most of the terrestrial wind energy resources show an increasing trend in 2020-2030, and some regions such as conti-nental Antarctica, Greenland, western Canada, and Russia show a decreasing trend, and the wind-rich areas are mainly distributed in East Asia, Southeast Asia, northern and eastern China, Mongolia, Central Asia, 30°S–30°N region of America, northeastern Australia, and sub-Saharan Africa.
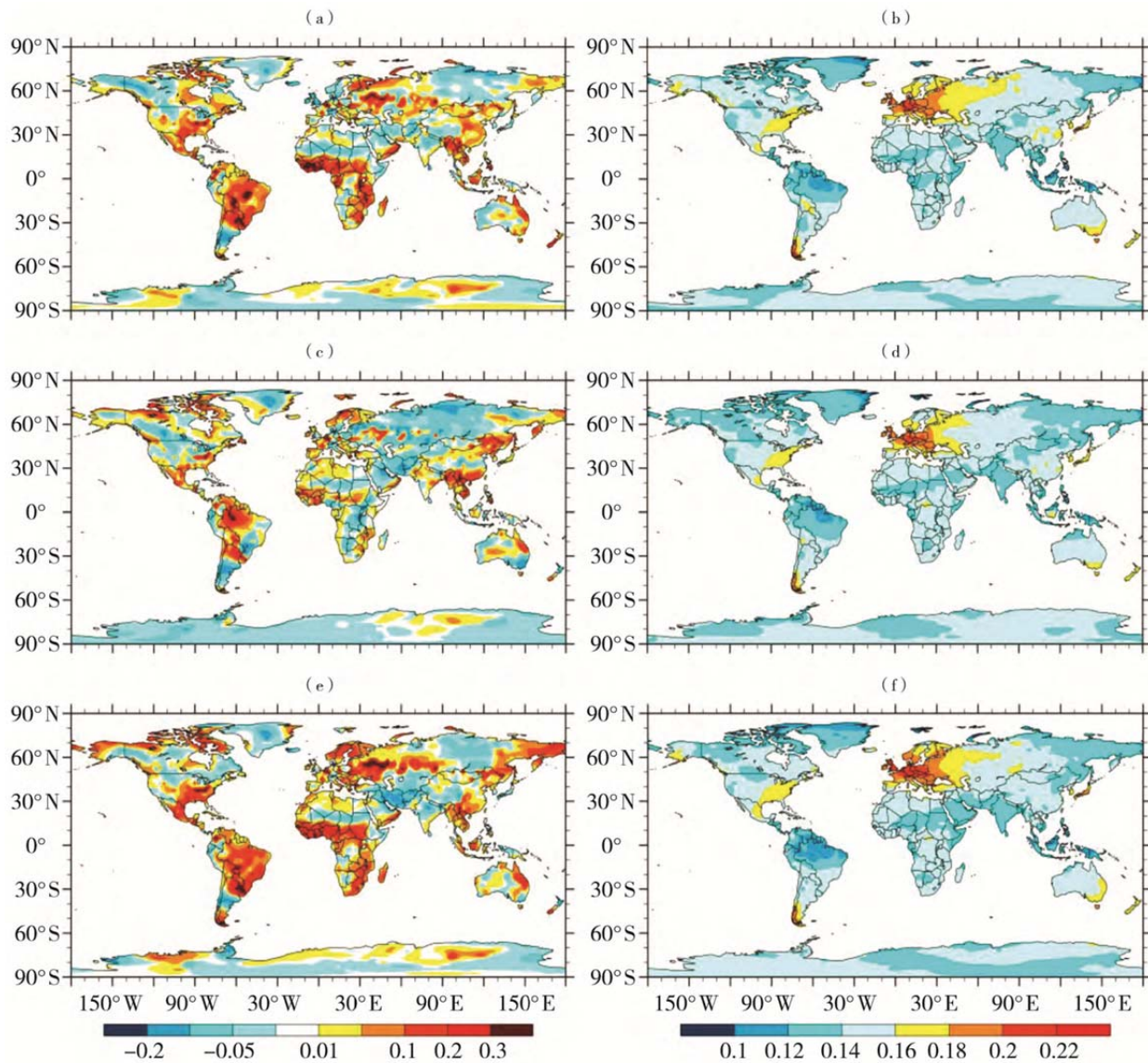
Figure 2. Rates of change in global land-averaged wind (**a**, **c**, **e**) and solar energy (**b**, **d**, **f**) for 2020–2030 under different climate scenarios (compared with the period from 1986 to 2005, the same as below). (**a**, **b**) RCP2.6, (**c**, **d**) RCP4.5, (**e**, **f**) RCP8.5.

At present, eastern China, Inner Mongolia, Hexi Corridor, Xinjiang and other regions are the places with the most abundant wind energy resources in China, in the past 10 a, the above areas have established large-scale wind power bases; under the RCP2.6 and RCP8.5 climate scenarios, these regions of China are still rich in future wind energy resources. Under the RCP4.5 scenario, the change distribution characteristics of wind energy resources from 2020 to 2030 are similar to that of RCP2.6 and RCP8.5 climate scenarios, but the increase range of wind energy resources is significantly reduced, and the increase range is relatively weak, among them, the European continent, Antarctica continent and most regions of Central Asia showed a decreasing trend. The spatial differences in the change of ter-restrial wind energy resources from 2020 to 2030 under different RCPs scenarios may be related to

25

the change of polar climate and global sea and land thermal gradient in the context of global warming. The reasons still need to be further analyzed. Compared with the reference period, under different RCPs scenarios, the global solar energy resources increased between 2020 and 2030, and the most significant increase was in Europe, southeastern United States, southwest South America, and Southeast Australia, the increase in solar resources in these regions was most pronounced under the RCP8.5 climate scenario, indicating a significant increase trend in solar resources between 2020 and 2030 under the high emission scenario. This may be related to the future reduction in cloud volume for reasons that need further investigation.

According to the NASA global near-surface wind speed and solar radiation observation material[31] and multi-mode ensemble averaging results (**Figure 1**), the onshore wind and solar-rich areas are mainly concentrated in the Americas, the Sahara region in Africa, Australia, Europe, Northwest China and Central Asia. Therefore, for the above five regions, this paper further discusses the characteristics of wind energy, solar energy resources annually and seasonal changes under different climate scenarios. January, April, July and October were selected to represent winter, spring, summer and autumn, respectively.

Figure 3 shows the annual and seasonal average percent change in global terrestrial wind and solar resources for 2020–2030 under different RCPs climate scenarios relative to the reference period. It can be seen that there are significant seasonal differences in global terrestrial wind and solar energy resources under different future climate scenarios, and the response to different RCPs varies greatly.

Figure 3. Annual and seasonal average rates of change in global land-based wind (**a**) and solar (**b**) resources for 2020–2030 under different climate scenarios.

From **Figure 3(a)**, it can be seen that relative to the reference period (1986–2005), the global land-based annual average wind resource increases during the period 2020–2030 under the RCP2.6 and RCP8.5 climate scenarios, and increases more significantly under the RCP8.5 scenario than the RCP2.6 scenario, while decreases under the RCP4.5 scenario, but the trend varies from season to season. Among them, the land average wind energy resources in winter, summer and autumn all decreased under different RCPs (except for the winter RCP2.6 scenario), wind energy resources in winter and summer are most significantly in the RCP8.5 scenario, in autumn, the wind energy resources decreased most significantly in the RCP2.6 scenario; the change trend of wind energy resources in spring

is consistent with the whole year, in a slight reduction in the RCP4.5 climate scenario, while the increase is significant in the RCP2.6 and RCP8.5 scenarios, and the rate of increase is higher than the annual average. It can be seen that under the future high and low emission scenarios, the onshore wind energy resources show a general decreasing trend during the period 2020–2030, except for a significant increase in spring.

As seen in **Figure 3(b)**, the global terrestrial annual and seasonal average solar resources increase from 2020 to 2030 relative to the reference period, and the increase is most pronounced in the RCP2.6 and RCP8.5 scenarios, with the largest increase in summer.

To sum up, compared with the reference period,

26

the changes in the global terrestrial average wind and solar resources between 2020 and 2030 did not increase or decrease with the increasing RCP emission concentration, indicating that future changes in wind and solar resources are nonlinear in response to climate change.

Table 2 statistics the annual and seasonal average change rates of wind and solar energy resources over the reference period from 2020 to 2030 for different RCPs. It can be seen that the annual average wind energy resources in the rich regions of America, Africa and Australia show an increasing trend under different climate scenarios, and the increasing trend is most pronounced in the rich regions of Africa. The annual mean wind resource variability in the Asian rich region (Northwest China and Central Asia, hereafter) is relatively complex, with an increasing trend under the RCP2.6 scenario and decreasing trends under the RCP4.5 and RCP8.5 scenarios. In different seasons, wind energy resources in the rich regions of the Americas and Africa in winter show consistent decreasing and increasing trends under different climate change scenarios; The wind resource in the Asian rich region tends to increase under the RCP2.6 scenario and decrease under the RCP4.5 and RCP8.5 scenarios, with the most significant decrease in the RCP4.5 scenario. Wind resources in Australia and the European rich zone decrease under the RCP4.5 scenario and increase under the RCP2.6 and RCP8.5 scenarios. In spring, the wind energy resources showed a consistent increasing trend across climate change scenarios, except in the African rich zone, where the trend varied across climate change scenarios. In particular, wind energy resources in the Asian rich region show a decreasing trend under the RCP2.6 scenario and an increasing trend under the RCP4.5 and RCP8.5 scenarios, which is the opposite of the winter season. In summer, wind energy resources in the Americas, Africa and Europe increase under different climate change scenarios, wind energy resources in Asian rich region are decreasing under different climate change scenarios, and the reduction is the most obvious in the RCP4.5 scenario, but the changing trends of Australia's rich regions are different. In autumn, wind energy resources in rich areas of the Americas and Australia increase under different climate change scenarios; Wind energy resources in the rich regions of Asia increased in the RCP2.6 and RCP8.5 scenarios, but decreased in the RCP4.5 scenario.

According to the above analysis, the wind energy resources in the five major rich regions of the world, except for Europe and Asia, will generally show an increasing trend from 2020 to 2030 under different climate scenarios in the future. In addition, global terrestrial wind energy resources are significantly seasonal and regional under different climate change scenarios, indicating that wind energy resources in different seasons and regions have different responses to different climate change scenarios.

Table 2. Annual and seasonal average rates of change of wind and solar energy resources in different parts of the global land under different climate scenarios, relative to the reference period 2020–2030

Enrichment area	Future climate scenarios	Wind energy					Solar energy				
		Winter	Spring	Summer	Autumn	All year	Winter	Spring	Summer	Autumn	All year
Americas	RCP2.6	-10.8	0.99	17.79	3.02	3.02	15.97	16.28	15.62	16.40	16.08
	RCP4.5	-0.63	-10.68	14.52	11.35	0.25	15.94	15.82	16.08	16.11	16.20
	RCP8.5	-5.93	-2.94	20.45	6.18	3.16	15.62	15.87	15.91	16.17	16.10
Africa	RCP2.6	0.87	5.43	3.17	1.2	3.33	16.68	16.61	16.92	15.84	16.85
	RCP4.5	0.58	8.01	3.21	-1.96	3.22	16.75	17.01	16.60	16.61	17.05
	RCP8.5	3.51	7.89	1.95	-1.89	3.32	16.71	16.68	16.53	15.56	16.67
Asia	RCP2.6	0.43	-1.09	-1.11	3.52	0.63	16.10	17.00	18.34	17.17	17.54
	RCP4.5	-1.82	1.59	-5.00	-5.34	-0.98	15.20	16.39	18.08	16.35	17.20
	RCP8.5	-0.17	1.84	-0.28	4.36	-0.48	16.32	16.70	18.74	17.08	17.58
Australia	RCP2.6	3.10	2.38	3.00	12.10	3.11	17.98	17.33	18.41	17.64	17.66
	RCP4.5	-6.96	1.12	-1.02	10.00	1.24	17.11	17.23	18.00	16.85	17.06
	RCP8.5	4.36	-9.14	5.80	6.98	2.08	17.10	18.04	18.19	17.54	17.22
Europe	RCP2.6	4.33	-1.14	2.43	0.51	-0.29	15.88	17.74	18.23	17.04	18.00
	RCP4.5	-0.95	-1.22	2.39	-2.72	-1.86	15.47	17.24	17.83	16.15	17.46
	RCP8.5	0.55	1.89	3.22	-0.13	-0.03	15.97	17.35	17.95	16.68	17.82

According to the annual and seasonal average rate of change of solar energy resources from the five major global land rich regions in the 2020–2030 which relative to the reference period (**Table 2**), solar energy resources in different regions show an increasing trend in different climate change scenarios and different seasons, that is, solar energy resources in the rich areas of the global land always show an increasing trend in the future climate change scenarios.

In terms of annual averages, solar resources in the global continent-rich regions increase most significantly in Europe under different climate change scenarios in 2020–2030, followed by Asia and Australia, with relatively small increases in solar resources in the Americas and Africa.

Under different climate change scenarios, the increase in solar energy resources is most pronounced in winter in the Australian-rich region and least in the European-rich region. In spring, the most significant increases in solar resources were seen in Australia and Europe, with relatively small increases in other regions; in summer and fall, the most significant increases were seen in Asia, Australia and Europe, with relatively small increases in the Americas and Africa. Among them, the solar energy resources in the Asian-rich regions increased the most significantly under the RCP8.5 scenario. It can be seen that there are also significant regional and seasonal differences in the increase of global terrestrial solar resources in 2020–2030 under different climate change scenarios. It should be noted that under future climate change scenarios, wind energy resources vary significantly more than solar energy resources across seasons, which is related to the strong transient and volatile nature of wind speed itself (small spatial and temporal scales)[2].

4. Conclusion and discussion

(1) The multi-model ensemble averaging results based on the CMIP5 program can better reproduce the global near-surface wind speed and the distribution of surface solar short-wave radiation, and the simulation performance for solar radiation is better. It shows that the multi-model ensemble averaging results have high confidence in the simulation of wind and solar resources on a global scale.

(2) Compared with the reference period, the changes of global terrestrial wind and solar energy resources between 2020 and 2030 under different RCPs scenarios have obvious regional differences. The regional difference of solar energy resources was small. Each rich area showed an increasing trend under different RCPs, and showed the most obvious increasing trend under the high emission (RCP8.5) scenario. The regional variation of wind energy resources is great, and the change trend of different rich areas under different RCPs is also quite different.

(3) Compared with the reference period, there are still obvious seasonal differences in wind and solar energy resources in different regions of the world between 2020 and 2030 under different climate scenarios, and the seasonal differences of wind energy resources are stronger than those of solar energy resources. The changes in wind and solar energy resources from 2020 to 2030 did not increase or decrease with the increasing emission concentration, indicating the complexity and non-linearity of future wind and solar energy resource responses to global climate change.

It should be noted that although the climate system model has been continuously improved in the past decade and the simulation capacity has gradually improved, the model still has great uncertainty, also reflected in the simulation of near-surface wind speed and surface solar radiation[32]. Moreover, the climate model has a "climate drift" phenomenon in the long integration process, which manifests itself as spurious changes independent of internal variability or external forcing[33,34]. It has been shown that the near-surface wind speeds from GCM results and reanalysis data differ significantly at high altitudes, especially north of 30°N, where the correlation coefficients between the two are low[35]. Among them, the GCM simulation of near-surface wind speed in China is small[36].

The mechanisms of wind and solar resource changes in the context of climate change are more complex, and atmospheric circulation, ENSO (El Niño-Southern Oscillation), topographic thermo-dynamic effects, subsurface changes, and anthropogenic effects all have an impact on the changes of wind speed in the global terrestrial near-surface

layer, but the corresponding explanations of the mechanisms still differ greatly[37-40]. Therefore, with the continuous improvement and development of the model, the predicted results of wind and solar resources will be more credible in the future.

Conflict of interest

The authors declared that they have no conflict of interest.

Reference

1. Wang C, Liu C. Woguo fengdian jianshe zhong fengziyuan pinggu cunzai de wenti he yingduicuoshi (Chinese) [Problems and countermeasures existing in the stroke resource evaluation of wind power construction in China]. Proceedings of the CSEE 2011; 31(Suppl.): 242–245.

2. Zhang F, Wang C. The application of observation data assimilating in wind power prediction. 2nd International Conference on Applied Robotics for the Power Industry (CARPI); 2012 Sep 11–13; Zurich, Switzerland. New York: IEEE; 2012. p. 137–139.

3. Zhang F, Yang Y, Wang C. The effects of assimilating conventional and ATOVS data on forecasted near-surface wind with WRF-3DVAR. Monthly Weather Review 2015; 143(1): 153–164.

4. Wang C, Jin S. Error features and their possible causes in simulated low-level winds by WRF at a wind farm. Wind Energy 2014; 17(9): 1315–1325.

5. Wang C, Jin S, Hu J, et al. Comparing different boundary layer schemes of WRF by simulation the low-level wind over complex terrain. 2011 2nd International Conference on Artificial Intelligence, Management Science and Electronic Commerce (AIMSEC); 2011 Aug 8–10; Zhengzhou, China. New York: IEEE; 2011. p. 6183–6188.

6. Zhang F, Wang C. Experiment of surface-layer wind forecast improvement by assimilating conventional data with WRF-3DVAR. Plateau Meteorology 2014; 33(3): 675–685.

7. Xing T, Zheng Y, Zhu Y. Research on the development and exploitation of wind energy resources in Yunnan Province. Meteorological and Environmental Sciences 2013; 36(4): 55–61.

8. Fei Y, Xia X. Decadal variations of aerosol-cloud-radiation in Eastern China and their relationships during 1980–2009. Meteorological and Environmental Sciences 2016; 39(2): 1–9.

9. Zhu X, Li H. Analysis and evaluation of solar energy resources in Luoyang area. Meteorological and Environmental Sciences 2015; 38(1): 67–72.

10. Si F. Assessment analysis of solar radiation resources in Jiaozuo. Meteorological and Environmental Sciences 2013; 36(2): 87–91.

11. Vautard R, Cattiaux J, Yiou P, et al. Northern hemisphere atmospheric stilling partly attributed to an increase in surface roughness. Nature Geoscience 2010; 3(11): 756–761.

12. Mcvicar TR, Roderick ML, Donohue RJ, et al. Global review and synthesis of trends in observed terrestrial near-surface wind speeds: Implications for evaporation. Journal of Hydrology 2012; 416: 182–205.

13. Jiang Y, Luo Y, Zhao Z. Jin wushi nian zhongguo fengsu bianhua ji yuanyin fenxi (Chinese) [Analysis of wind speed changes and causes in China in the last 50 years]. Proceedings of the 24th Annual Meeting of the Chinese Meteorological Society; 2007 Oct 13–16; Qingdao. Beijing: Chinese Meteorological Society; 2007.

14. Zhang T, Yan J, Li S, et al. Influence of climate change on wind energy resources in agriculture and stock-raising interlaced region of Northern China. Journal of Arid Meteorology 2012; 30(2): 202–206.

15. Wang C, Zhang Z, Tian W. Factors affecting the sur-face radiation trends over China between 1960 and 2000. Atmospheric Environment 2011; 45: 2379–2385.

16. Ma J, Luo Y, Shen Y, et al. Regional long-term trend of ground solar radiation in China over the past 50 years. Science China: Earth Sciences 2012; 42(10): 1597–1608.

17. Turnock ST, Spracklen DV, Carslaw KS, et al. Modelled and observed changes in aerosols and surface solar radiation over Europe between 1960 and 2009. Atmospheric Chemistry and Physics 2015; 15(9): 13457–13513.

18. Karnauskas KB, Lundquist JK, Zhang L. Southward shift of the global wind energy resource under high carbon dioxide emissions. Nature Geoscience 2018; 11(1): 38–43.

19. Jiang Y, Luo Y, Zhao Z. Projection of wind speed changes in China in the 21st century by climate models. Chinese Journal of Atmospheric Sciences 2010; 34(2): 323–336.

20. Li Y, Tang J, Wang Y, et al. Prediction of climate change of the near-surface wind energy potential over China. Acta Energiae Solaris Sinica 2011; 32(3): 338–345.

21. Liu B, Costak B, Xie L, et al. Dynamical downscaling of climate change impacts on wind energy resources in the contiguous United States by using a limited-area model with scale-selective data assimilation. Advances in Meteorology 2014; 2014: 1–11.

22. Herbst L, Rautenback H. Climate change impacts on South African wind energy resources. Africa Insight 2016; 45: 1–31.

23. Carvalho D, Rocha A, Gomez-Gesteira M, et al. Potential impacts of climate change on European wind energy resource under the CMIP5 future climate projections. Renewable Energy 2017; 101: 29–40.

24. Najac J, Lac C, Terray L. Impact of climate change on surface winds in France using a statistical-dynamical downscaling method with mesoscale modelling. International Journal of Climatology 2011; 31: 415–430.

25. Pan Z, Christensen JH, Arritt RW, *et al*. Evaluation of uncertainties in regional climate change simulations. Journal of Geophysical Research: Atmospheres 2001; 106: 17735–17751.

26. Iizumi T, Nishimori M, Yokozawa M. Combined equations for estimating global solar radiation: Projection of radiation field over Japan under global warming conditions by statistical downscaling. Journal of Agricultural Meteorology 2008; 64: 9–23.

27. Ruostenja K, Raisanen P. Seasonal changes in solar radiation and relative humidity in Europe in response to global warming. Journal of Climate 2013; 26: 2467–2481.

28. Ohunakin OS, Adaramola MS, Oyewola OM, *et al*. The effect of climate change on solar radiation in Nigeria. Solar Energy 2015; 116: 272–286.

29. Loew A, Anderson A, Trentmann J, *et al*. Assessing surface solar radiation fluxes in the CMIP ensembles. Journal of Climate 2016; 29(20): 7231–7246.

30. Bai S, Lu J. Analysis on influence of Tibet High Plateau climate on wind power generation. Electric Power Construction 2006, 27(11): 37–40.

31. Nema P, Nema RK, Rangnekar S. A current and future state of art development of hybrid energy system using wind and PV-solar: A review. Renewable and Sustainable Energy Reviews 2009; 13(8): 2096–2103.

32. Knutti R, Sedláček J. Robustness and uncertainties in the new CMIP5 climate model projections. Nature Climate Change 2013; 3(4): 369–373.

33. Dirmeyer PA. Climate drift in a coupled land atmosphere model. Journal of Hydrometeorology 2009; 2(1): 89–102.

34. Gupta AS, Muir LC, Brown JN, *et al*. Climate drift in the CMIP3 models. Journal of Climate 2012; 25(13): 4621–4640.

35. Mcinnes KL, Erwin TA, Bathols JM. Global climate model projected changes in 10 m wind speed and direction due to anthropogenic climate change. Atmospheric Science Letters 2011; 12(4): 325–333.

36. Jiang Y. Zhongguo feng he fengneng bianhua yanjiu (Chinese) [Study on wind and wind energy change in China] [PhD thesis]. Nanjing: Nanjing University of Information Science and Technology; 2009. p. 1–192.

37. Li Y, Wang Y, Chu H, *et al*. Zhongguo luyu jindiceng fengneng ziyuan de qihou bianyi he xiadianmian ren wei gaibian de yingxiang (Chinese) [Effects of climate variability and anthropogenic modification of subsurface on near-surface wind energy resources in China's land area]. Chinese Science Bulletin 2008, 53(21): 2646–2653.

38. Zhao Z, Luo Y, Jiang Y. Is global strong wind decling? Advances in Climate Change Research 2011; 7(2): 149–151.

39. Li X, Zhong S, Bian X, *et al*. Climate and climate variability of the wind power resources in the Great Lakes region of the United States. Journal of Geophysical Research: Atmospheres 2010; 115(D18).

40. Berg N, Hall A, Capps SB, *et al*. El Niño-Southern oscillation impacts on winter winds over Southern California. Climate Dynamics 2013; 40(1): 109–121.

Rᴇᴠɪᴇᴡ Aʀᴛɪᴄʟᴇ

Thinking about the development of solar energy resources in Wulian County, Shandong Province

Zhichao Chen

Wulian Meteorological Bureau, Rizhao 262300, Shandong province, China. E-mail: czc0102@126.com.

ABSTRACT

In order to cope with the shortage of conventional energy and curb the sustainable development of global warming, it expounds on the natural conditions and national policies for the development of solar energy in Wulian County, and points out that the development and utilization of solar energy resources is an inevitable trend to cope with climate change, introduces the current situation of solar energy utilization in Wulian County, as well as the lack of specific policies and perfect economic subsidy measures, insufficient understanding of the strategic significance of solar energy resources, the fact that resource advantages have not been converted into economic advantages, and the prospects for solar energy utilization, such as solar water heaters. Solar ovens, solar cells, and solar power generation were analyzed, and the development and utilization of solar energy resources were promoted by formulating mandatory policies for the development and utilization of new energy, government incentive subsidies, and formulating development plans.

Keywords: Solar Energy; Current Situation; Prospects; Countermeasure Suggestions

1. Introduction

As global temperatures continue to rise, weather conditions continue to deteriorate, and experts have predicted that "extreme weather may become the norm in the future". Compared to the past 500,000 years, the concentration of CO_2 in the atmosphere has exceeded the safe limit, and after the industrial age, its proportion has increased by 30%, mainly due to the combustion of fossil fuels. The average annual temperature of Wulian County from 2011 to 2015 has increased steadily, and there is a trend of increasing year by year compared with the average of the calendar year, of which the average temperature in 2014 is 14.2 °C, which is as high as 1.0 °C compared with the average of 13.2 °C in the calendar year, and the precipitation is unbalanced, the drought and flood are uneven, and the spring drought and autumn drought are serious. In 2016, the World Meteorological Organization proposed the theme of Meteorological Day, "Facing a Hotter, Drier, and More Waterlogged Future", and a slight increase in global average temperature may bring frequent climate disasters—excessive rainfall, widespread drought, and persistent high temperatures, resulting in large-scale disaster losses. Therefore, countermeasures should be taken to reduce greenhouse gas emissions and fully develop pollution-free energy[1]. The world is very rich in clean energy, as long as 0.5‰ can meet the needs of human beings. Solar energy is the largest, followed by wind and electricity, and there is also hydropower. The world develops new energy at an average annual growth rate of 12.4% every

year, and by 2050, the global new energy can reach more than 80% of the total energy, achieving a sustainable and clean energy supply and completely getting rid of the fossil energy dilemma. By then, global annual carbon emissions will return to 10.5 billion T, which is the level of the early 1990s, so the problem of controlling temperature rises at 2 °C or 1.5 °C can be solved, and China's smog problem can also be alleviated. Solar energy resources are abundant, can be used free of charge, without transportation, and have no pollution to the environment. The development and utilization of solar energy resources can not only solve the energy crisis, but also be a guarantee for coping with climate change, and the full use of solar energy will create a new model of life for mankind so that society and mankind can enter an era of energy conservation and emission reduction.

Since the 1970s, solar technology has advanced by leaps and bounds, and the use of solar energy has continued to evolve. In 2000, 70,000 households in Japan had installed solar power generation equipment, and in 2011, Texas, the United States, invented a new solar cell, which is only 2 US dollars per watt of power generation equipment. Domestic research on solar energy has also made great progress, Huang[2] pointed out that Shandong Province is relatively rich in solar energy resources, and solar water heater production in scale and competitiveness are at the forefront of the country's provinces and cities, but the photovoltaic industry is still in its infancy while analyzing the main problems in the development and utilization of solar energy in Shandong Province. Shen *et al.*[3-7] estimated the reserves of Solar Energy Resources in China, pointing out that China's solar energy resources have great potential, providing a way for various regions to develop and utilize solar energy. The author analyzes the development conditions, utilization status, and former[8-15] solar energy resources in Wulian County, Shandong Province, and puts forward countermeasures and suggestions for the development and utilization of solar energy in Wulian County, with a view to providing clean and safe modern new energy sources for residents' lives to cope with the climate crisis and alleviate the shortage of traditional energy.

2. Conditions for the development of solar energy resources in Wulian County

2.1 Natural conditions for the development of solar energy resources

Wulian County is located at 119.2 °E, 35.74 °N, located in the south of Shandong Peninsula, the northeast end of Rizhao City, east of Qingdao West Coast New Area, south of Rizhao City Donggang District, west of Ju County, north of Zhucheng, with a total area of 1,500 km², belonging to the warm temperate continental monsoon climate.

2.1.1 Characteristics of sunshine hours

The average annual sunshine hours in Wulian County are 2,393.5 h, and the number of sunshine hours in each month is the most in May and the least in December, and among the four seasons of the year, the spring season has the most sunshine hours, followed by summer, and the winter is the least. The annual percentage of sunshine is 54%, and the percentage of sunshine in each month is the largest in October, the lowest in July, and the average annual number of days with ≥ of 60% sunshine is 207.3 days.

2.1.2 Sunny days and cloud cover characteristics

The number of days on rainy days is low, with an average annual sunny day The number of days (average total cloud cover per day ≤20%) is 86.8 days, with the highest average number of sunny days in December at 12.8 days and the lowest number of sunny days in July. Wulian average annual total cloud cover is 55%, with the monthly average total cloud cover peaking in July and the least in December.

2.1.3 Characteristics of precipitation

In the same season as rain and heat, Wulian precipitation shows obvious seasonality, the degree of seasonal change is obvious, the average precipitation in summer is 489.7 mm, accounting for 62% of the whole year, and the average precipitation in winter is 36.8 mm, accounting for 5% of the whole year, and the rainfall is mostly concentrated in hot

season from June to August, and the precipitation in spring, autumn and winter is small, which is prone to drought.

2.1.4 Characteristics of foggy days

Since Wulian County is located in a hilly and mountainous area, the wind speed is large, the average number of fog days per year is 13.9 days, the maximum number of fog days in the year is 25 days, and the minimum number of fog days in the year is 4 days.

2.2 National and local policies for the development of solar energy resources

2.2.1 The State Council formulates new energy development prospects

In May 2015, the State Council issued the "Made in China 2025", which is the first ten-year action plan for China's implementation of the manufacturing power strategy, focusing on the development of a new generation of information technology, high-end CNC machine tools, and robots, aerospace equipment, energy-saving, and new energy vehicles, electric equipment, new materials, and other ten major areas.

2.2.2 National leaders point out the way to address climate change

On September 26, 2015, President Xi Jinping announced to the world at the United Nations Development Summit that "China's initiative to explore the construction of a global energy Internet and promote the clean and green way to meet global electricity demand" is a wise decision that depicts the prospects for the development of green and low-carbon energy for the world, points out a new way to deal with climate change, and demonstrates China's strength and Chinese style to the world.

2.2.3 The Energy Administration issued new energy guidance

On February 29, 2016, the National Energy Administration issued the Guiding Opinions of the National Energy Administration on Establishing a Guiding System for Renewable Energy Development and Utilization Targets. According to the current mining intensity, the world's coal can be mined for 110 years, natural gas can be extracted for 54

years, oil can be exploited for 53 years, facing the problem of depletion, solar energy resources are very important for promoting world peace and harmony and eliminating poverty. With the continuous innovation of making full use of solar energy technology, its economy will become more and more prominent, and its competitiveness will become stronger and stronger.

2.2.4 The national "13th Five-Year Plan" program actively supports solar power generation

In March 2016, China's "13th Five-Year Plan" was officially promulgated, and Chapter 30 of the Outline—Building a Modern Energy System", proposes to continue to promote the development of photovoltaic power generation, actively support solar thermal power generation, and put solar energy utilization in a very important position.

2.2.5 Wulian County government continues to promote photovoltaic power generation projects

In March 2016, Wulian County issued its 13th Five-Year Plan, which mentioned the implementation of six major environmental protection and energy-saving projects, of which the circular economy development project includes the exploration and development of photovoltaic power generation projects for large-scale factories in agriculture and enterprises in townships and towns of Zhongzhi, Wanghu, Street and Xumeng.

3. Overview of solar energy utilization in Wulian County

3.1 Solar energy to internal energy

3.1.1 Solar water heaters achieve large-scale popularization of Wulian from the 20th century

In the early 1990s, solar water heaters were vigorously promoted, from smoldering, collector pipe to vacuum tubes, and with the continuous development of new rural construction projects such as water supply villages and villages, the popularity of rural solar water heaters is also increasing year by year. Up to now, the urban solar water heater in Wulian County has been basically covered,

and the utilization rate of rural solar water heaters has reached more than 10%.

3.1.2 Passive solar greenhouses have been effectively promoted and applied

In the construction of the Central Primary School of Gongguan Town, Dujiagou Primary School, Wangjiazhuangzi Village Committee Office, etc. Solar greenhouses 2,880 m^2, the main structure is a vertical heat collection wall, heat collection wall. These include transparent materials, endothermic coatings, collector panels and insulation materials, roof ceiling panels with perlite and straw, and cinder on the ground.

3.1.3 Sun stove was further developed and utilized

Since 2002, Wulian County has taken the implementation of the project as an opportunity to introduce, develop and promote more than 4,000 solar stoves in street towns, which have been promoted to more than 6,000 households, and that has achieved great social benefits. At present, the solar cooker independently developed and developed by Wulian County has been exported to Qinghai, Tibet and other plateau areas.

3.1.4 The benefits of solar energy companies are prominent

The Wulian County produces solar water heater enterprises mainly have 2 homes, namely Rizhao Zhongke Meiyang Solar Manufacturing Co., Ltd. and Rizhao Leyu Solar Energy CO., Ltd. The annual output of the two companies reaches nearly 200,000 units, and the collector area exceeds 600,000 m^2.

3.2 Solar to electrical energy

Wulian Medium to Photovoltaic Power Generation Project is located in Wulian County, Rizhao City, Shandong Province, near Yaoyuzi and Shanghejiagou Village, covering an area of about 40 hm^2. Invested by Wulian Jingke Photovoltaic Power Generation Co., Ltd., the planned capacity is 20 MWp, which started in April 2016, went into production at the end of June 2016. A total of 1,331 solar street lights were installed on Fuqiang Road, Yantai Road, Changqing Road and other sections of Wulian County.

4. Problems in the development and utilization of solar energy resources

4.1 There are shortcomings in policy guarantees

Although a unified goal and program of struggle have been formulated and the Corresponding Wulian "13th Five-Year Plan" Circular Economy Development Project has been promulgated, specific support policies on how to achieve the ultimate goal have not yet been introduced, and the mandatory policies and regulations applicable to the region need to be refined as soon as possible.

4.2 Lack of understanding of the strategic significance of solar energy resources

The consumption of fossil energy in Wulian County is bound to cause energy and environmental pressure and increase greenhouse gas emissions. The development and utilization of solar energy are of epoch-making significance for rationally controlling the total amount of energy consumption, harnessing the ecological environment, and promoting sustainable economic and social development; large-scale solar power generation can adjust the power supply structure of Wulian County, which is mainly coal power generation, not to produce any degree of pollution, and to give people a hometown with blue skies and white clouds, green waters, and green mountains.

4.3 Lack of well-systematic economic subsidy measures

According to the actual situation of the development of the solar energy industry in Wulian County, there has been no relevant policy on whether to subsidize enterprises, purchasers, and solar products. Japan is already planning to introduce a series of preferential measures, and in 2016, the price of solar power generation systems will be reduced to 60,000 to 70,000 yuan. Foreign countries use economic leverage to promote the popularization of home solar systems. In Japan, households with solar power systems install two meters, one to record household consumption of the state grid' electricity, which is consumed by the household; the other calculates the amount of electricity transmit-

ted by the household power generation system to the national grid, which the government forces the grid to acquire. In Germany, the benign stimulus of the price difference is used to incentivize residents to use solar power generation systems, and the German electricity price alone is 0.1 EUR/kWh, while the price of the State Grid to acquire solar power generation is as high as 0.5 EUR/kWh.

4.4 Resource advantages are not translated into economic advantages

The transformation of solar energy resources into economic benefits is reflected by driving the development of industries related to the manufacture and processing of solar power generation products, and the second is the conversion of solar energy resources into electric energy, and the direct economic benefits are obtained through the sale of electric energy. Therefore, the transformation of solar energy resources into significant economic benefits requires the large-scale installation of solar power generation systems everywhere. Although Wulian County is rich in solar energy resources and has unique superiority, there is still a clear gap between the scientific research and utilization of solar energy resources and other areas with the same light energy conditions, and there is still a long way to fully transform the advantages of solar energy resources into economic advantages.

5. Prospects of solar energy utilization in Wulian County

5.1 Solar water heater

One of the most competitive ways of using energy economically and conventionally is that solar energy heats water from low to high temperatures to meet people's use of hot water in life and production. Solar water heater structure is simple, and low price, but also because domestic hot water is a perennial need, so solar water heaters can play a role throughout the year, there is a high utilization rate[16-18], and the current need to start to develop Wulian rural solar water heater applications. Liu *et al*.[19] conducted a study on the application status and prediction of solar water heaters in rural areas, and proposed that the premise of improving the uti-

lization rate of solar water heaters in rural areas is to start from the regional economy, make farmers affluent as a whole, and add policies to benefit the people to promote the promotion of rural solar water heaters.

5.2 Construction of solar houses

The one-time investment in solar greenhouses is large, about 20% higher than that of ordinary houses, but the heating effect is quite impressive, which can bear 50% of the auxiliary heat source throughout the year, and generally recover the investment in the utilization of solar energy resources in 5 to 8 years. According to the test, when the outdoor is -1 °C, the indoors is maintained at about 15 °C; when the outdoors is above 30 °C in summer, the indoors can be maintained at about 18 °C. Compared with ordinary houses, solar greenhouses can save 22.60 kg/m^2 of coal for heating, and the energy-saving benefits are very significant. Liang *et al*.[20] have done research on the design and experiment of active solar houses, through the rational use of solar energy and surface water, it can effectively change the micro-environment in the room, save conventional energy, reduce environmental pollution, and achieve warm winter and cool summer.

5.3 Promote solar stoves

The solar stove is easy to operate, easy to use, clean and hygienic, and pollution-free, the service life is generally up to 15 years, longer than the service life of the liquefied gas stove. The use of solar-powered stoves not only improves the defects of cutting wood in rural areas and destroying the ecological environment, but also does not produce pollution, promotes environmental protection work, saves energy, and can return the cost within two years. Solar stoves that can be used for cooking throughout the day, in sunny weather, can ensure three meals a day, the temperature can reach 250 °C, can be used normally within 36 hours, can be steamed, boiled, fried, stewed, fried and other ways to cook. The scope of use of solar stoves is wide, as long as there is a sun, they can also be used in winter, and can be used for daily life, picnics, disaster prevention, and emergency occasions.

5.4 Solar greenhouses

The photovoltaic vegetable greenhouse is to install solar energy thin film panels on top of ordinary vegetable greenhouses, absorb solar energy, and divide solar radiation into light energy needed by plants and solar power generation, which not only ensures plant growth but also realizes photoelectric conversion. Photovoltaic vegetable greenhouses can not only generate electricity but also grow vegetables, one shed for dual use, increasing renewable energy, making agriculture move towards low-carbon, efficient, green, and circular agriculture. Shouguang City, Shandong Province, invested in solar photovoltaic vegetable greenhouses in 2014 and has been running well since the grid was connected, achieving gratifying economic and ecological benefits. The solar photovoltaic vegetable greenhouse is the product of the combination of solar photovoltaic energy technology and winter warm vegetable greenhouse, which can effectively use the existing vegetable greenhouse without occupying new land resources. Solar cell modules have a very high transmittance, greenhouse solar panels can be designed according to different areas of vegetable planting 97% or 75%, and other styles of light transmittance, in the power generation at the same time, can also meet the needs of plant photosynthesis on sunlight. Not only that, but solar cell components can also block some of the damage of ultraviolet rays to plants, which can effectively reduce vegetable diseases and insect pests and improve vegetable quality. In addition, the greenhouse photovoltaic system can also be matched with the LED system, and the night LED system can use the electricity generated during the day to provide lighting for plants, extend the irradiation time of vegetables, shorten the production cycle, and ensure the stable production of vegetables. At present, there are 53,000 hm^2 of vegetable greenhouses in Shouguang City, and if all solar photovoltaic vegetable greenhouses are built, they can generate 42.4 billion kW·h of electricity a year to meet the city's industrial and agricultural production and residents' daily electricity.

5.5 Launch of the sun roof program

After the installation of the household solar power generation system, on the one hand, the household electricity consumption system can be solved, on the one hand, the inexhaustible electricity can be sold to the state power grid, so as to activate the people's roof power generation and guide the generation of "zero energy construction" and "production capacity building" in Wulian. The Zhejiang government strongly supports the photovoltaic industry and plans to achieve 1 million rooftop power generation projects by 2020. In the first quarter of 2016, Jiaxing Xiuzhou Photovoltaic Town invested 562 million yuan in fixed assets ranked fifth in the second batch of 42 provincial-level characteristic towns. For one of the 10 provincial-level demonstration towns in Zhejiang, the "Jiaxing model" has been emulated by the whole country, and the essence of the "Jiaxing model" is to unify the roof development by playing the role of the government, and after power generation, in addition to the proceeds sold to the power grid, the state will receive an additional subsidy of 0.4 yuan/kW·h, Zhejiang subsidy 0.1 yuan/kW·h, basically, one year can recover the purchase cost of solar equipment.

5.6 Solar baking room

Tobacco production mode is changing from traditional labor-intensive to modern tobacco agriculture, especially tobacco roasting is transforming into a labor-saving, time-saving, and money-saving system. Because of the tax credit, the cost of building a solar oven in the United States is lower than that of a standard grill. In the bright and clean solar roasting room, the use of clean solar energy to replace coal-roasted tobacco leaves shortens the tobacco roasting time, the roasting efficiency can be increased by 29%, and zero emissions of tobacco roasting gas are realized. Wang et al.[21] conducted a study on the baking effect of the solar grilled tobacco in Guizhou, and the appearance quality and chemical composition of the flue-cured tobacco leaves were similar to those of the ordinary densely packed baking room, and the dry tobacco baking cost was 13% lower than that of the ordinary dense baking room. Solar roasting rooms can not only dry tobacco leaves but also other agricultural and sideline products and medicinal materials. Sav-

ing time and money with solar grilling houses, in winter, the electricity generated by the solar grilled roof power generation system is recycled by the National Grid.

5.7 Solar power generation

In recent years, the cost of thermal power has been rising day by day, and the development of the solar energy industry is just in time, and the rising "solar economy" will surely become the mainstream of global energy. For the development of the photovoltaic industry at this stage, Liang Zhipeng, deputy director of the New Energy Department of the National Energy Administration, said that if the photovoltaic industry wants to develop, it must be driven by innovation and upgraded. At the same time, reduce costs and reduce prices, so that large-scale applications can be realized. In order to promote technological progress and reduce prices, the State Energy Administration should expand the scale of the photovoltaic front-runner base and introduce a more perfect competition mechanism. Wulian's photovoltaic power generation industry started late, there are many difficulties and bottlenecks, the current solar photovoltaic utilization technology is still in its infancy, and subject to cost constraints, the effect is not ideal. However, with the advancement of scientific research projects and the research and development of new materials, the optoelectronic industry will gradually reach a mature stage of development[22-28].

5.8 Solar cells

China has successfully developed solar cells for rainy days, and on March 21, 2016, the research team of ocean university of China and Yunnan Normal University published a research report in the German journal "Applied Chemistry International Edition" to elaborate on this achievement, and the future development trend of solar cells may be all-weather. Solar cells can be used in illuminated lamps, electric vehicles, etc.[29]. The first choice is lighting, solar lamps have economic and environmental protection, energy saving, safety, long life, no need for wiring when installing, low operating costs, simple installation, and other characteristics, the more scale of the installation, com-

pared to ordinary lamps and lanterns, the more saving investment. At present, electric vehicles are mainly based on the development of old scooters, and with the aging of the Population of Wulian, electric vehicles have great business opportunities.

6. Suggestions for the utilization of solar energy resources in Wulian County

6.1 Promulgate mandatory policies for the development and utilization of new energy sources

In hotels, hospitals, shopping malls, and other public places, it is mandatory to install solar energy power generation equipment[30] and make full use of solar power generation, so that it will have a certain peak regulation effect on the state grid; green quotas[31] are adopted, stipulating that power enterprises must produce a certain proportion of solar power, and the State Grid will buy back and implement more rewards and fewer penalties. Special funds for the development of solar energy resources must be put in place and law enforcement inspections must be carried out in depth.

6.2 Implement policies related to the promotion of solar energy development and utilization

Correctly interpret the special fund policy for energy conservation and actively implement it, and cooperate with the departments of the Development and Reform Commission to increase economic support for the promotion and application of the solar energy industry. Implement the state's tax reduction and reduction policy on new energy, and set up supporting encouragement awards.

6.3 Develop development plans

The competent department of solar energy will convene well-known domestic experts and local high-end skill-based professionals to draw a grand plan for the development of solar energy in Wulian County, plan a new pattern of solar energy development and utilization in Wulian County, and clearly put forward the strategic layout of solar energy development and utilization and short-, medium-term and long-term development plans.

6.4 Implement solar energy demonstration projects

Advocate the construction of a demonstration project for the integration of solar energy and buildings[32-35], actively guide and encourage solar water heater enterprises to participate in the construction of demonstration projects, and support the construction of integrated solar energy collectors systems for public buildings. Solar energy enterprise products in the street lamps, signal lights, and urban landscape lighting to expand the demonstration application.

6.5 Establish R&D institutions

The county government should attach great importance to technological development, introduce high-level technical personnel, improve the level of new energy research, encourage enterprises to participate in scientific research projects, and use scientific and technological innovation to promote industrial development and reduce costs. The solar energy industry is an emerging industry[36-38], with technological development by leaps and bounds, it is necessary to strengthen exchanges and cooperation with photovoltaic power generation research institutions and universities, follow up the latest trend of photovoltaic industry technology, combined with reality, according to the needs of industrial development to do a good job in the introduction of technology absorption, innovation. The government has given a certain degree of support in terms of funds and economic policies to promote the comprehensive strength of the development and utilization of Wulian Solar Energy.

6.6 Strengthen publicity and education

Give full play to the role of various news media platforms, publicize the great significance of solar energy development and utilization, promote and popularize the application of solar energy products in various fields, improve social recognition, and form a public opinion atmosphere conducive to the development of the solar energy industry[39-42]. To strengthen publicity and education aimed at government leaders at all levels and responsible persons of relevant departments, we should have a forward-looking awareness and establish a correct outlook on political achievements. The development of solar energy is in the contemporary era, the benefits are in the future, and the "sunshine economy" will be an inevitable choice for achieving economic development and protecting resources and the environment win-win situations and an inevitable trend of economic sustainable development.

Conflict of interest

The author declares no conflict of interest.

Reference

1. Gao G. Jianhuan quanqiu qihou bianhua de benzhi he zhongguo yingdui celve (Chinese) [The nature of global climate change mitigation and China's response strategy]. Energy of China 2002; (7): 4–8, 12.
2. Huang T. The strategies research on promoting the development and utilization of solar energy in Shandong Province [Master's thesis]. Qingdao: Qingdao University; 2009.
3. Shen Y. The spatial distribution of solar energy and the comprehensive potential evaluation of regional exploitation and utilization in China [Master's thesis]. Lanzhou: Lanzhou University; 2014.
4. Gao F, Sun C, Liu Q. Woguo taiyangneng kaifaliyong de xianzhuang ji ruogan sikao. (Chinese) [The current situation and some thoughts on solar energy development and utilization in China]. Energy Engineering 2000; (5): 8–11.
5. Yang Q. Current status and development of solar thermal conversion in China. Energy Technology 2001; (4): 162–164.
6. Zhuang Y, Jia Z. The status quo and suggestion for solar energy development and utilization in China. Science Technology and Industry 2008; (9): 5–6.
7. Li K, He F. Analysis on mainland China's solar energy distribution and potential to utilize solar energy as an alternative energy source. Progress in Geography 2010; (9): 1049–1054.
8. Miao R, Li S. Actuality and prospect of solar energy's application. Applied Energy Technology 2007; (5): 28–33.
9. Zhao Y. Development status and prospect of solar energy application technology. Electric Power 2003; (9): 63–64.
10. Gao F, Sun C, Liu Q. The status and trends of solar energy utilization. World SCI-TECH R & D 2001; (4): 35–39.
11. Lu W. The development trend of solar utilization technology. World SCI-TECH R & D 2007; (2): 95–99.
12. Zhao L, Hu M, Yang Z. Taiyangneng liyongjishu yu fazhan (Chinese) [Solar energy utilization technology and development]. Energy and Environment 2007; (4): 55–57.

13. Zhang S, Guan X, Wang D, *et al*. Research development of solar thermal utilization and photovoltaic power generation. Chemical Industry and Engineering Progress 2012; (S1): 323–327.

14. Yao W. Taiyangneng liyong yu kechixu fazhan (Chinese) [Solar energy utilization and sustainable development]. Energy of China 2007; (4): 46–47.

15. Yu H. Taiyangneng liyong zongshu ji tigao qi liyonglv de tujing (Chinese) [Review of solar energy utilization and ways to improve its utilization rate]. New Energy Research & Utilization 2004; (3): 34–37.

16. Wei X, Gao L, Gao Y, *et al*. Chongqing nongcun diqu taiyangneng guangre liyong pingjia (Chinese) [Evaluation of solar photothermal utilization in rural areas of Chongqing]. South China Agriculture 2008; 2(7): 14–16.

17. Liu W. Woguo taiyangneng reshuiqi chanye fazhan xianzhuang ji zhanwang (Chinese) [Development status and prospect of solar water heater industry in China]. Renewable Energy 2002; (4): 4–6.

18. Hu R, Li J. Quanqiu taiyangneng reshuiqi chanye yu jishu fazhan xianzhuang ji qishi (Chinese) [Global solar water heater industry and technology development status and enlightenment]. Solar Energy 2007; (2): 8–11.

19. Liu J, Sun Q. Woguo nongcun diqu taiyangneng reshuiqi yingyong xianzhuang diaocha ji yuce (Chinese) [Investigation and prediction of solar water heater application in rural China]. Keji Zhifu Xiangdao 2013; (24): 244–248.

20. Liang P, Liu S, Sun B, *et al*. Zhudongshi taiyangnengfang de sheji yu shiyan de yanjiu (Chinese) [Design and experiment research of active solar energy house]. Journal of Henan Agricultural University 2011; (2): 201–203.

21. Wang G, He B, Gu R, *et al*. Guizhou kaoyan taiyangneng rebeng mijixing kaofang hongkao xiaoguo yanjiu. (Chinese) [Study on the baking effect of flue-cured tobacco solar heat pump intensive baking room in Guizhou province]. Gengzuo yu Zaipei 2010; (1): 10–11.

22. Wang W, Wang K. Taiyangneng fadian jishu jianjie (Chinese) [A Brief Introduction to Solar Power Generation Technology]. Beijing: Machinery Industry Press; 1998. p. 115–137.

23. Zhang B, Yang Y. Status and trend of wind/photovoltaic power development. Electric Power 2006; 39(6): 65–69.

24. Yang J Chen Z. Prospect of photovoltaic in 21st Century. Journal of Shanghai University of Electric Power 2001; 17(4): 23–28.

25. Lin Y. Taiyangneng bingwang fadian jishu gaishu (Chinese) [Overview of solar grid-connected power generation technology]. China Electrical Equipment Industry 2009; (12): 42–45.

26. Li B, Li A. Taiyangneng fadian jishu (Chinese) [Solar energy and thermal power generation technology]. Shanghai: Higher Education Press; 2004:

80–92.

27. Ji X. Taiyangneng refadian jishu (Chinese) [Solar thermal power generation technology]. Yangguang nengyuan; 2005; (4): 2–3.

28. Wu F, Wang X. Characteristics and development of photovoltaic power generation technology. Power & Energy 2011; (1): 74–79.

29. Zhang Z. Youji taiyang dianchi yu suliao taiyang dianchi (Chinese) [Organic solar cells and plastic solar cells]. Beijing: Chemical Industry Press; 2004: 25–28.

30. Yang J. Zang Y. Legislation status and prospect on utilization of solar energy resource in China. Nanjing Journal of Social Sciences 2011; (10): 97–103.

31. Zhang X. Discussions on the urgent need of supportive policy for PV industry. Energy Technology and Economics 2011; 23(12): 14–17.

32. Xiao X, Li D. The application situation and the development trend to BITV. Energy Conservation 2010; 29(2): 12–18.

33. Gao H, He Q. Integrated design of solar energy utility and building. Huazhong Architecture 2007; (1): 70–72.

34. Li T, Zhu T. Taiyangneng liyong yu zhuzhai jianzhu yitihua yanjiu (Chinese) [Research on solar energy utilization and residential building integration research]. Engineering and Construction 2010; (2): 236–238.

35. Li S, He S, Cai Y, *et al*. The practice of integration application for photovoltaic and architecture. Chinese & Overseas Architecture 2010; (1): 135–137.

36. Guo T, Liu J. Taiyangneng de liyong (Chinese) [The utilization of solar energy]. Beijing: Science and Technology Literature Press; 1987.

37. Wang J. Taiyangneng liyong jishu (Chinese) [Solar energy technology]. Beijing: Jindun Publishing House; 2008.

38. Luo Y, He Z, Wang C. Taiyangneng liyong jishu (Chinese) [Solar energy utilization technology]. Beijing: Chemical Industry Press; 2005.

39. Ai X. Lun woguo fengneng he taiyangneng fadian jishu de fazhan xianzhuang ji weilai fazhan qushi (Chinese) [On the development status and future development trend of wind energy and solar power generation technology in China]. Dianyuan Jishu Yingyong 2012; (10): 134–134.

40. Kong H, Xiong S. Quanqiu guangfu chanye fazhan xianzhuang ji fazhan qushi fenxi (Chinese) [Analysis of the development status and development trend of global photovoltaic Industry]. Solar Energy 2009; (6): 10–12.

41. Duan X. Taiyangneng fazhan qianjing ji yingyong yanjiu (Chinese) [Solar energy development prospect and application research]. Modern Business Trade Industry 2010; 22(20): 283–284.

42. Zheng L. Fengneng, taiyangneng fazhan zhengfengshi (Chinese) [Wind and solar energy develop]. Chuangxin Shidai 2011; (4): 32–33.

ORIGINAL RESEARCH ARTICLE

Spatio-temporal coupling suitability of solar energy resources and distributed photovoltaic power generation projects in Beijing

Zhenyu Zhao[*], **Yujia Yang**

Beijing Key Laboratory of New Energy and Low Carbon Development, School of Economics and Management, North China Electric Power University, Beijing 102206, China. E-mail: zhaozhenyuxm@263.net

ABSTRACT

Distributed photovoltaic power generation projects contribute to the coordinated and sustainable development of "energy—economy—environment". The spatio-temporal coupling relationship between regional solar resources and distributed photovoltaic power generation projects is studied. Taking Beijing area as the research object, a variety of spatial analysis methods are proposed to explore the relationship between solar resources and distributed photovoltaic power generation projects from a new perspective of spatial geography. The spatio-temporal coupling suitability of regional solar energy resources and distributed photovoltaic power generation project development area was scientifically evaluated. The research results can provide suggestions and decision support for optimizing the timing of regional development of photovoltaic power generation, and also provide reference for planning and layout optimization of photovoltaic power generation projects in the Beijing-Tianjin-Hebei region and other regions.

Keywords: Solar Energy; Distributed Photovoltaic Power Generation Project; Spatio-Temporal Coupling; Suitability; Beijing

1. Introduction

Currently, distributed photovoltaic power generation projects based on the utilization of solar energy occupy a leading position in the field of distributed energy construction in China[1]. Beijing is a Class II solar resource region with good resource endowment, coupled with the high demand for low-carbon and safe energy in Beijing, it is therefore important to study the correlation between solar resources and distributed photovoltaic power generation projects in Beijing, to fully explore the potential of solar resource development and utilization in Beijing, and to develop and utilize clean energy resources in Beijing according to local conditions.

The current research on the resource–project–demand chain of distributed energy can be divided into three parts. (1) From the perspective of resources, Zhao and Fan[2] evaluates the abundance of energy resources in Beijing on the basis of solar energy, wind energy and biomass energy; Qi *et al.*[3] established an evaluation model for the development level of provincial renewable energy projects from the perspective of resource development and consumption. (2) From the project side, scholars at home and abroad have conducted comprehensive studies on the operation mode, risk assessment and economic benefits of distributed photovoltaic power generation projects. For example, Li *et al.*[4] discussed the operation mode and adaptability

of distributed photovoltaic power generation system in remote areas through feasibility analysis. Lu *et al.*[5] quantified the benefits of participants of distributed photovoltaic power generation projects adopting contract energy management mode from three perspectives: economy, environment and society. (3) From the perspective of demand side, researches mainly focus on demand response[6], virtual power plant[7], energy storage and integrated energy system[8]. Dynamic balance of energy supply chain can be maintained by adjusting flexible resources on the demand side, so as to optimize system resources and comprehensive benefits.

To sum up, this paper will focus on the "resource—project" association, and use a variety of spatial statistical methods to explore the suitability of solar resources and distributed photovoltaic power generation projects in Beijing from the perspective of the spatio-temporal coupling of resource endowment, in order to provide reference for distributed photovoltaic power generation projects in Beijing.

2. Research methods

Spatial statistical method is a method to study the geospatial relationship among various attribute factors, which is suitable for statistical analysis of data with spatial distribution characteristics[9]. This paper introduces kernel density estimation method, standard deviation ellipse method and bivariate spatial autocorrelation model to conduct an in-depth exploration of the static geospatial distribution law and dynamic spatio-temporal coupling relationship between solar resources and distributed photovoltaic power generation projects in Beijing.

2.1 Kernel density estimation method

Kernel density estimation is a spatial statistical method to simulate and explore the density and distribution characteristics around spatial points by fitting the observed data points with smooth peak kernel function.

Suppose the sample point is n, then the probability density function $f(x)$ can be expressed as:

$$f(x) = \frac{1}{n} \sum_{i=1}^{n} K_\mu(x - x_i)$$
$$= \frac{1}{n\mu} \sum_{i=1}^{n} K \frac{(x - x_i)}{\mu}$$

(1)

Where, x is the project point for which the estimated probability is to be obtained; μ is a smoothing parameter, that is, bandwidth, $\mu > 0$; x_i are other project points around the desired project point which are limited to μ, $i \in n \in$; K is the kernel density function, and the integral of $\int K(t)\,dt = 1$, where $t \geq 0$, when $0 \leq t \leq 1$, $K(t) = 1/2$; K_μ is the kernel density function of the μ bandwidth.

2.2 Standard deviation ellipse method

Standard deviation ellipse method adopts the deviation angle (long half-axis) to reflect the dominant direction of the pattern, which can be expressed as:

$$\begin{cases} SDE_X = \sqrt{\dfrac{\sum_{i=1}^{n}(X_i - \bar{X})^2}{n}} \\ \\ SDE_Y = \sqrt{\dfrac{\sum_{i=1}^{n}(Y_i - \bar{Y})^2}{n}} \end{cases}$$

(2)

$$\tan\theta = \frac{\left(\sum_{i=1}^{n}\tilde{X}_i^2 - \sum_{i=1}^{n}\tilde{Y}_i^2\right) + \sqrt{\left(\sum_{i=1}^{n}\tilde{X}_i^2 - \sum_{i=1}^{n}\tilde{Y}_i^2\right)^2 + 4\left(\sum_{i=1}^{n}\tilde{X}_i\tilde{Y}_i\right)^2}}{2\sum_{i=1}^{n}\tilde{X}_i\tilde{Y}_i}$$

(3)

In the formula, SDE_X and SDE_Y are the lengths of the short axis x and long axis x of the standard deviation ellipse, respectively, representing the major and minor development directions of the spatial distribution of project sites. θ is rotation Angle, $tan\theta$ is used to explain the development trend of the project site; X_i and Y_i are the coordinate points of the ith project site; $\bar{X}$ and $\bar{Y}$ are the center of gravity of all project points in the map; $\tilde{X}$ and $\tilde{Y}$ are the deviation between the coordinates and the center of gravity of the ith project points.

2.3 Bivariate spatial autocorrelation model

Bivariate spatial autocorrelation model is used to describe the coupling between multiple variables in space, which can be expressed as:

$$\begin{cases} I = \dfrac{m\sum\limits_{v=1}^{m}\sum\limits_{r=1}^{m}w_{vr}(c_v-\bar{c})(c_r-\bar{c})}{\left(\sum\limits_{v=1}^{m}\sum\limits_{r=1}^{m}w_{vr}\right)\sum\limits_{v=1}^{m}(c_v-\bar{c})^2} \\ z = \dfrac{1-E(I)}{\sqrt{\text{var}(I)}} \end{cases}$$

(4)

Where, m is the number of object grids; w_{vr} is spatial weight matrix; c_v and c_r are grid specific values of elements v and r respectively, $v \in m$, $r \in m$; $\bar{c}$ is the mean value of all grid specific values; z is the test value; I is the correlation value; var (I) is the variance of I; E(I) is the expected value of I.

v and r grids are selected here to describe the spatial autocorrelation model of bivariate, namely:

$$\begin{cases} I_v = \dfrac{c_v-\bar{c}}{S^2}\sum\limits_{v}^{m}w_{vr}(c_v-\bar{c}) \\ E(I_v) = -\dfrac{1}{m-1}\sum\limits_{r}^{m}w_{vr} \\ z(I_v) = \dfrac{I_v-E(I_v)}{S(I_v)} \end{cases}$$

(5)

$$\begin{cases} z_1^v = \dfrac{\beta_1^v-\overline{\beta}_1}{\sigma_1} \\ z_G^r = \dfrac{\beta_G^r-\overline{\beta}_G}{\sigma_G} \\ I_{1G}^v = z_1^v\sum\limits_{r=1}^{m}w_{vr}z_G^r \end{cases}$$

(6)

Where, β_I^v is the attribute I value of v grid; $\overline{\beta}_I$ and $\overline{\beta}_G$ are the mean values of attribute I and attribute G, respectively. σ_I and σ_G are the variances of I and G, respectively. S is the discrete standard deviation of c_v; I_v is the correlation value of v; z_I^v is the test value of attribute I value of v grid. z_g^r is the test value of attribute G value of r grid. I_{1G}^v is the correlation value of I and G under v grid; β_I^v is attribute G value of r grid; when $|z| < 1.96$ and $v < 0.05$, it is spatially aggregated; otherwise, it is randomly distributed and has no spatial coupling relationship.

3. Distribution of distributed photovoltaic power generation projects in Beijing

Beijing is a typical temperate monsoon climate area. According to the classification of solar energy resources distribution in China, Beijing belongs to class II solar energy resource area, with rich resources. The annual total solar radiation is 1,393.9 ~ 1,463.3 kWh/m². In terms of spatial distribution of Beijing, the annual total solar radiation of Yanshan Mountains, Western Hills and the areas with relatively high altitude in the northwest direction is larger, which can reach more than 1,450 kWh/m². The average annual total solar radiation in the central and southeastern plains is less than 1,400 kWh/m².

In recent years, Beijing has developed a series of distributed photovoltaic power generation projects in batches. The distributed photovoltaic power generation projects published in *The Beijing Distributed photovoltaic Power Generation Project Award List* (hereinafter referred to as the Award List) from March 2016 to March 2020 are selected as the research objects. The Award List is divided into two parts: "legal entity" and "natural person", containing two batches each year. A total of 9 batches were selected for this study. The new annual grid-connected installed capacity and the number of new projects of distributed photovoltaic power generation in the Award List are shown in **Figure 1**.

As can be seen from **Figure 1**, from March 2016 to March 2020, the newly installed grid-connected capacity of distributed photovoltaic power generation projects in Beijing showed a trend of continuous growth. The number of new projects in that year showed a trend of rising first and then falling, among which, the number of new projects in 2018 was the largest, 6,423.
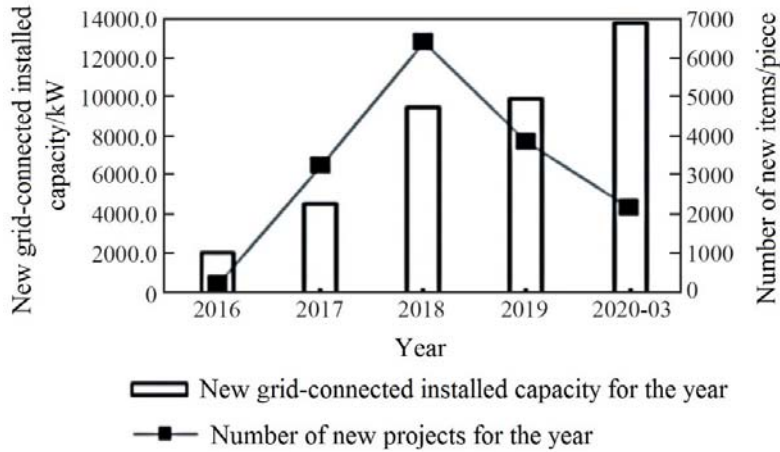
Figure 1. Change of annual newly grid-connected installed capacity and new projects number in *Award List.*

Among the above-mentioned 9 batches of projects, the area of newly added distributed photovoltaic power generation projects in Beijing has grown from 5 districts (Shunyi District, Haidian District, Changping District, Pinggu District, Tongzhou District) in March 2016 to 16 districts. The regional distribution has expanded, showing a trend from centralized development in some regions to decentralized development in multiple regions. At present, Beijing's distributed photovoltaic power generation projects are mostly distributed in Shunyi District, Tongzhou District and other areas around Beijing. According to different development speed, these areas can be divided into three categories: (1) decelerating development areas: Fangshan District, Daxing District, Changping District and Yanqing District, where the proportion of new projects is decreasing year by year. (2) Emerging development areas: including Shunyi District, Tongzhou District and Yizhuang Economic Development Zone, where the proportion of new projects is increasing year by year. (3) Traditional development areas: including Miyun District, Pinggu District and Huairou District, where the growth rate of new projects basically maintains a balanced state.

4. Spatio-temporal coupling relationship between solar energy resources and distributed photovoltaic power generation projects in Beijing

This study explores the multi-spatio-temporal coupling heterogeneity between solar energy resources and distributed photovoltaic power generation projects in Beijing from three aspects of the characteristics of circle, cluster and development. Considering the scale of distributed photovoltaic power generation project in Beijing and the availability and completeness of the relevant data, select 541 projects with legal entities as the main body from the *Award List*, whose total grid-connected installed capacity accounts for 65% of the nine batches of the *Reward List*, and therefore is representative.

The project data sources will query relevant enterprise information in the national Enterprise Credit Information Disclosure System (http://bj.gsxt.gov.cn/) through the enterprise information list of legal entities recorded in the *Award List*, delete the legal entities that have been revoked, expired or non-compliant as of 2020, and verify and supplement the legal entities whose information registration is unknown; then extract the spatial coordinates of the company name and address through the API development platform of Baidu Maps, and combined with AutoNavi map to supplement the spatial coordinate data.

4.1 Characteristics of the circle layer

Kriging interpolation is an optimal, linear and unbiased spatial interpolation method, which is widely used in geospatial isoline drawing[9]. In this study, total solar radiation (GHI) was used to measure solar resource margin, which was collected from Global GIS, and information of 10 points evenly distributed in 16 regions of Beijing was

43

collected, namely 160 GHI data. The kriging interpolation method was used to assign weights based on the spatial relationship of GHI, and the weighted average interpolation results were used to divide Beijing into 9 layers with a resolution of about 2 km. Then the results were verified, 15% GHI samples were randomly selected and compared with the original results after fitting. Kriging interpolation rendering results and standardized error verification figure are shown in **Figure 2**.
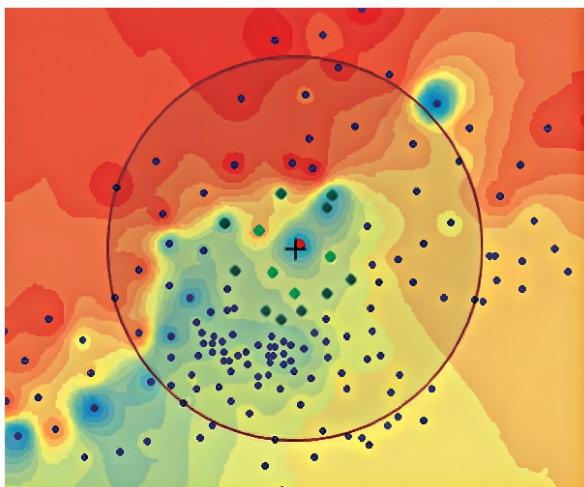
a. Kriging interpolation rendering results
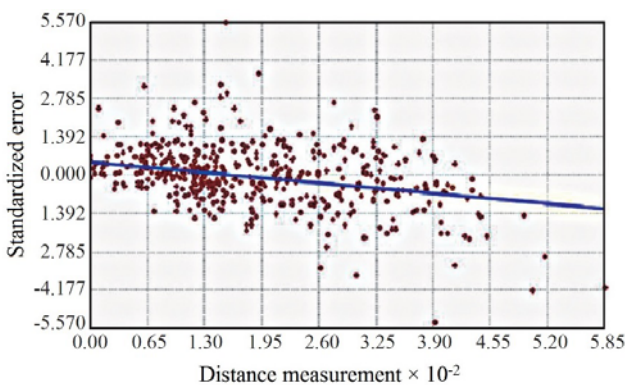
b. Verification of standardization error of Kriging interpolation method

Figure 2. Kriging interpolation method rendering results and standardized error verification chart.

It can be seen from **Figure 2** that the standardized error fitting curve is basically close to the horizontal, and the standardized error value fluctuates near the zero value, which indicates that the kriging interpolation method adopted is relatively ideal. The obvious circles and differences in the figure indicate that the spatial distribution of solar energy resources and distributed photovoltaic power generation projects in Beijing has significant circle differentiation and heterogeneity.

The kriging interpolation diagram is coupled with distributed photovoltaic power generation project sites in Beijing to obtain the circle layer distribution of distributed photovoltaic power generation projects in Beijing, as shown in **Figure 3**.

As can be seen from **Figure 3**, from the perspective of development sequence, distributed photovoltaic power generation projects in Beijing show a trend of developing from the middle resource valley area to the surrounding resource peak area, and their integration with the development of solar energy resources in Beijing gradually increases.

Considering the geographical location of Beijing, the first batch of distributed photovoltaic power generation projects are mainly distributed in the central region of Beijing. The second group is spread out across the city's central district; the third to fifth batch of projects were concentrated around the cluster area of the first and second batch of projects, showing a tendency of clustering in the middle. The sixth batch of projects keeps the development trend of centralization and gradually begins to expand outward. The seventh batch of projects shows obvious characteristics of development towards the southeast of the city; the number of projects in the eighth and ninth batches increased significantly and began to move toward the peak solar resource area around the city. According to the results of **Figure 3**, at present, distributed photovoltaic power generation projects in Beijing are still mostly concentrated in areas with relatively poor solar energy resources, and the spatial distribution of distributed photovoltaic power generation projects and solar energy resources is not balanced.

The solar energy resources in Beijing show a basin distribution. According to GHI value, the solar energy resources in Beijing can be divided into three grades: (1) the general resource area where the GHI value is 1,384.10 ~ 1,402.90 kWh/m^2; (2) the area with medium resource where the GHI value is 1,402.90 ~ 1,411.18 kWh/m^2; (3) the resource-rich region where the GHI value is 1,411.18 ~ 1,508.00 kWh/m^2. As can be seen from

Figure 3, 36.87% of the 9 batches of distributed photovoltaic power generation projects in Beijing are distributed in areas with general resources, namely Haidian District and Fengtai District in central Beijing. 38.48% of the projects are located in medium resource areas. 24.65% of the projects are located in resource-rich areas, namely Huairou District, Yanqing District and other surrounding areas of Beijing.

GHI/kWh•m^{-2}

1384.10 ~ 1395.60	• The first batch of projects
1395.60 ~ 1400.66	• The second batch of projects
1400.66 ~ 1402.90	• The third batch of projects
1402.90 ~ 1403.88	• The fourth batch of projects
1403.88 ~ 1406.11	• The fifth batch of projects
1406.11 ~ 1411.18	• The sixth batch of projects
1411.18 ~ 1422.68	• The seventh batch of projects
1422.68 ~ 1448.78	• The eighth batch of projects
1448.78 ~ 1508.00	• The ninth batch of projects

Figure 3. Circle distribution map of distributed PV power generation projects in Beijing.

To sum up, the spatial matching degree between solar resources and distributed photovoltaic power generation projects in Beijing is low at present, but the projects gradually begin to radiate to resource-rich areas with a positive development trend, and the spatial matching degree between energy utilization and project construction is gradually enhanced.

4.2 Agglomeration characteristics

A bivariate spatial autocorrelation model was established to analyze the spatial coupling between solar energy resources and distributed photovoltaic power generation projects in Beijing. There were two variables in the model: variable 1 was the geographical location of different projects, and variable 2 was GH value. In view of the total area and layer characteristics of Beijing, the grid function of ArcGIS software is used to divide Beijing into 6,043 grids of 1.5 km × 1.5 km. After linking and importing into GeoDa software, and several tests, the default distance threshold of 1.5 km was selected as the weight matrix of the bivariate spatial autocorrelation model.

After simulation, the value of Moran's I, which measures the spatial correlation index, is -0.30, indicating that there is a negative correlation between solar energy resources and distributed photovoltaic power generation projects in Beijing, which conforms to the distribution law of circle layer. According to the significant difference of spatial coupling relationship, the spatial coupling relationship between solar resources and distributed photovoltaic power generation projects in Beijing can be divided into four types: Low radiation–weak construction (L-L), low radiation–strong construction (L-H), high radiation–weak construction (H-L), and high

45

radiation–strong construction (H-H), the specific distribution is shown in **Figure 4**.

(1) Type 1: Low radiation–weak construction (L-L). This type refers to the regions with low GHI value and weak development of distributed photovoltaic power generation projects, which are distributed at both ends of the central belt region of Beijing and have 677 grids, accounting for 11.20% of the total grids, mainly including Mentougou District, Haidian District and the southern part of Pinggu District. The spatial distribution of solar resources and distributed photovoltaic power generation projects in this type of region does not show the characteristics of agglomeration, and the GHI value shows large horizontal change, and the utilization degree of solar resources of projects is not high. Affected by the level of economic development, user demand, geographical location and energy span, the development of photovoltaic power generation industry in this type of region is relatively weak.
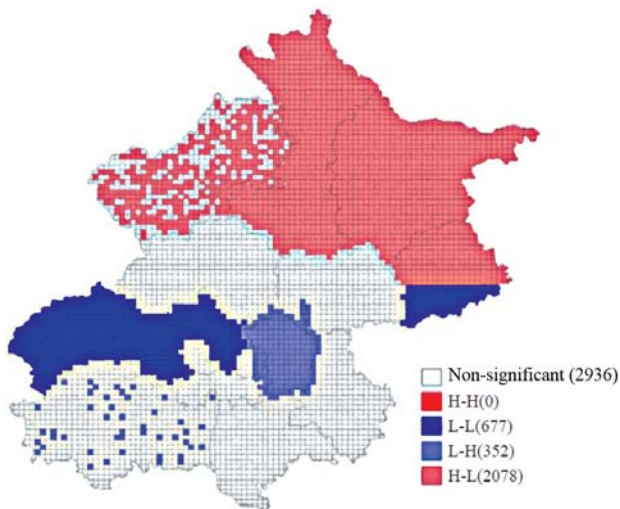
Figure 4. Spatial autocorrelation distribution of solar energy resources and distributed PV power generation projects in Beijing.

(2) Type 2: Low radiation–strong construction (L-H). This type refers to the region with low GHI value and agglomeration of distributed photovoltaic power generation projects, mainly distributed in Chaoyang District in central Beijing, with obvious agglomeration of projects and 352 grids, accounting for 5.82% of the total number of grids. The development of solar resources and distributed photovoltaic power generation projects in this type

of region presents obvious heterogeneity characteristics, with less resource endowment but higher project development degree. Resource capacity lags behind project construction, that is, the adaptability of resource and project spatial distribution is poor. Due to the high level of economic development, the shortage of land resources and the large demand for energy on the user side in this type of region, the projects in this type of region are mostly rooftop distributed photovoltaic power generation projects, mainly utilizing roof resources, which is an application form of photoelectric architecture.

(3) Type 3: High radiation–weak construction (H-L). This type refers to the regions with high GHI value but weak development of distributed photovoltaic power generation projects, mainly distributed in the northern part of Beijing, with the Miyun area in the northeast having the most obvious agglomeration. The number of projects in this category is the largest, with 2,078 grids, accounting for 34.39% of the total grids. This type of region has a good resource endowment, but the agglomeration of projects is not obvious

On the one hand, the surrounding areas of the northern region of the city are mostly rural areas, and the distributed photovoltaic power generation projects are mostly dominated by natural people, while the projects dominated by legal entities are relatively few. On the other hand, the economic development of the surrounding rural areas in the northern region is relatively backward compared with that of the central region, with small energy demand from users and loose land resources use. As a result, a number of large-scale photovoltaic power generation projects are built, leading to weak clustering of distributed photovoltaic power generation projects. Therefore, there is significant spatial heterogeneity between the development and utilization of solar energy resources and distributed photovoltaic power generation projects in this type of region.

(4) Type 4: High radiation–strong construction (H-H). This type refers to the region with high GHI value and the agglomeration of distributed photovoltaic power generation projects. According to data analysis, there is no such area in Beijing.

To sum up, the spatial coupling relationship between solar resources and distributed photovoltaic power generation projects in Beijing mainly includes L-L, L-H and H-L, as well as areas with no significant autocorrelation of spatial distribution, and there are spatial differences between solar resources and distributed photovoltaic power generation projects, which is mainly reflected in the weak matching development between the north and the central region, and the development trend of the project shows a pattern of weak in the north and strong in the south.

4.3 Development characteristics

In order to explore the temporal and spatial development trend and evolution law of solar resources and distributed photovoltaic power generation projects, and to optimize the layout of future development and site selection of distributed photovoltaic power generation projects, this study uses standard deviation ellipse method to represent the trend development area of projects or solar energy resources. Two measurement indexes are introduced here, namely ellipticity and standard

centroid difference, and the calculation method is shown in equation (7).

$$
\begin{cases}
M = \sqrt{\left(\lambda_g - \lambda_D\right)^2 + \left(t_g - t_D\right)^2} \\
N = \dfrac{L}{T}
\end{cases}
$$

(7)

Where, M is the standard centroid difference; N is the ellipticity; λ_g and t_g are the horizontal and vertical coordinates of the center of mass of the standard deviation ellipse of each batch of project points, $g = 1, 2, 3..., 7, 8, 9$; L is the length of the long axis of the standard deviation ellipse; T is the length of the short axis of the standard deviation ellipse; λ_D and t_D are the horizontal and vertical coordinates of the center of mass of the GHI standard deviation ellipse.

The ellipse formed by GHI values shows the distribution of solar energy resources, and the ellipse formed by each batch of distributed photovoltaic project sites in Beijing shows the development trend of the batch of distributed photovoltaic power generation projects. The parameters of the standard deviation elliptic model are shown in **Table 1**.

Table 1. Parameter results of standard deviation ellipse model

Batch	Coordination of the center of mass		Long axis L	Short axis T	Ellipticity N	Standard centroid difference M	Rotation angle $\theta/(°)$
	λ_g	t_g					
1	116.62	40.13	0.41	0.05	8.20	0.23	83.20
2	116.33	40.03	0.40	0.31	1.29	0.08	59.97
3	116.44	40.11	0.24	0.10	2.40	0.06	110.94
4	116.54	39.97	0.24	0.02	12.00	0.17	179.80
5	116.34	39.85	0.36	0.19	1.89	0.22	63.39
6	116.43	40.00	0.53	0.23	2.30	0.07	58.09
7	116.49	39.93	0.52	0.28	1.86	0.16	70.62
8	116.39	40.06	0.36	0.34	1.06	0.01	44.19
9	116.46	40.00	0.49	0.40	1.23	0.08	10.97
GHI	116.40	40.06	0.60	0.39	1.54	0.00	61.16

Note: Rotation angle can reflect the deviation degree of development.

As can be seen from **Table 1**, due to the small number of distributed photovoltaic power generation projects in batches 1 to 4, the indexes of these four batches have great changes. The center of mass of the first batch of projects falls in Shunyi District, and the difference between the ellipticity and standard center of mass is 8.20 and 0.23, respectively, which deviates greatly from the development trend of resources. The second and third batches of project agglomeration centroids are

shifted to the west, and compared with the first batch of projects, the standard centroid difference has decreased, and the adaptability to the resource development trend has improved. The fourth batch of project centroid gradually shifted to the southeast. The fifth to ninth batches of projects gradually mature, the centroid basically stable in Fengtai District and Chaoyang District. The ellipticity maintains at about 1.67, showing a development trend of gradual expansion of

development areas, gradual increasing of marginal projects, and gradual decreasing trend of standard centroid difference. The fluctuation range is much smaller than the first four batches. The increasing adaptability to resource development trend and the better development trend indicates that the development of distributed photovoltaic power generation projects in Beijing are taking the central region as the starting point and gradually expanding to surrounding areas. In future development, attention should be paid to the development of southwest and northeast regions to enhance the adaptability of resources and project development trend.

5. Evaluation of spatio-temporal coupling suitability between solar energy resources and distributed photovoltaic power generation projects in Beijing

At present, the construction of distributed photovoltaic power generation projects in Beijing is still in the exploratory stage. Optimization of regional industrial development pattern and rational distribution of distributed photovoltaic power generation projects are important measures to achieve green energy development in the capital. This study applies the method of spatial overlay analysis and the amount of information in each area of Beijing solar energy resources with a distributed photovoltaic power generation project, on the basis of the data of solar energy resources and the coupling of time and space of distributed photovoltaic power generation project suitability evaluation (evaluation results can be divided into five level), to exploit the development potential of the development of distributed photovoltaic project in Beijing.

5.1 Steps for evaluating the suitability of spatiotemporal coupling

The spatio-temporal coupling suitability of distributed photovoltaic power generation projects and solar energy resource utilization is taken as the evaluation object. The evaluation process is mainly divided into four steps: determining data sources,

quantitative classification of indicators, assignment of index weights, and calculation of spatio-temporal coupling suitability.

5.1.1 Identification of data sources

The data are mainly from the Global Solar Atlas, the National Center for Meteorological Science, and the 2019 Statistical yearbook of Solar resources and distributed photovoltaic power generation projects in Beijing. According to the principle of independence, relevance, feasibility and importance, 12 indexes are selected from the perspective of natural, social, industrial and project conditions, and the factors are quantified, standardized and rasterized, and rasterized with Beijing's geographic data, using the grid data with spatial data and factor attributes as the basic analysis unit.

5.1.2 Quantitative classification of indicators

Combined with the actual development of distributed photovoltaic power generation projects in Beijing and the advantages and disadvantages of the experimental results of multiple grades, each index is divided into five grades by using the re-classification tool in ArcGIS software and the natural discontinuous separation method, namely, very suitable, relatively suitable, medium suitable, less suitable and not suitable.

The circle characteristic index and agglomeration characteristic index are normalized as follows:

$$\begin{cases} A_h = \begin{pmatrix} a_1 & a_2 & \cdots & a_h \end{pmatrix} \\ \dot{A}_h = \begin{pmatrix} \dot{a}_1 & \dot{a}_2 & \cdots & \dot{a}_h \end{pmatrix} \\ \dot{B}_f = \begin{pmatrix} \dot{b}_1 & \dot{b}_2 & \cdots & \dot{b}_f \end{pmatrix} \end{cases}$$

(8)

In the equation, A_h is the actual quantity set of projects in the GHI equivalent area; $\dot{A}_h$ is the descending set of projects in the GHI equivalent regional; $\dot{B}_f$ is the descending set of projects in the GHI equivalent region; a_h is the number of items corresponding to h area in A_h set. $\dot{a}_h$ is the number of projects in h^{th} region of $\dot{A}_h$; $\dot{b}_f$ is the GHI value of fth region in $\dot{B}_f$.

$$\begin{cases} \eta_h = \dfrac{a_h}{\tilde{a}_h} \\ \tilde{a}_h = \dot{a}_h \\ \delta_h = \dfrac{1}{|1.54 - M_h| N_h} \end{cases}$$

(9)

In the formula, η_h and δ_h are the evaluation values of circle characteristics and agglomeration characteristics corresponding to h region, respectively. $\widetilde{a_h}$ is the optimal number of projects in region h; M_h and N_h are the standard centroid difference and ellipticity corresponding to h region, respectively.

$$\begin{cases} \phi_h = \dfrac{\eta_h - \eta_{\min}}{\eta_{\max} - \eta_{\min}} \\ \Omega_h = \dfrac{\delta_h - \delta_{\min}}{\delta_{\max} - \delta_{\min}} \end{cases}$$

(10)

In the formula, ϕ_h and Ω_h are the final evaluation values of the circle layer characteristics and agglomeration characteristics after the normalization of h region, respectively. η_{max} and η_{min} were the maximum and minimum values of circle characteristics, respectively. δ_{max} and δ_{min} are the maximum and minimum evaluation values of agglomeration characteristics, respectively.

5.1.3 Assigning index weights

The selection of different types of regions with sensitivity, that is, by using the information content method to calculate the weight of the index and the weight is obtained by measuring each single factor and its mean. The calculation formula of index weight is as follows:

$$\begin{cases} \sigma_p = \sqrt{\dfrac{\sum\limits_{j=1}^{u} \left(C_{pj} - \overline{C}_{pj} \right)^2}{u}} \\ k_q = \dfrac{\sum\limits_{p=1}^{e} \sigma_p}{e} \\ H_q = \dfrac{k_q}{\sum\limits_{q=1}^{e} k_q} \end{cases}$$

(9)

Where, σ_p is the global mean square error of p region at $u = 5$ levels. q is the qth evaluation factor;

k_q is the mean value of the overall mean square deviation of the qth evaluation factor in different grades. H_q is the normalized value, which is the weight value of the final evaluation factor. The weight value of each indicator is calculated by ArcGIS software. e is the number of factors affecting the development and utilization of distributed photovoltaic power generation projects, including 12 factors. C_{pj} is the single factor suitability of the jth level in the pth region. $\overline{C_{pl}}$ is the average value of C_{pj}.

5.1.4 Calculation of spatio-temporal coupling suitability

By superimposing and reclassifying different factors and geographic areas to obtain the distribution of each factor in geographic areas, and then using the raster calculation tool to construct the suitability calculation function and weight different factors, we can finally obtain the classification results of the spatial and temporal coupling suitability of solar energy resources and distributed photovoltaic power generation projects in Beijing.

The expression of spatio-temporal coupling suitability is:

$$F = \sum_{q=1}^{e} H_q \cdot GRID(q)$$

(12)

Where, F is the evaluation value of time-space coupling suitability; $GRID(q)$ represents the suitability of single factor, which is described by grids. The spatio-temporal coupling comprehensive evaluation indexes and their grades of solar resources and distributed photovoltaic power generation projects in Beijing are shown in **Table 2**.

5.2 Comprehensive evaluation results

The spatio-temporal coupling comprehensive evaluation results of solar resources and distributed photovoltaic power generation projects in Beijing are shown in **Figure 5**. The spatio-temporal coupling of solar resources and distributed photovoltaic power generation projects presents five suitability types, among which, the very suitable development region, the relatively suitable development region and the moderately suitable

49

development region can all be considered as the preferred site selection and encouraged development region of distributed photovoltaic power generation projects. These regions can reach a relatively balanced level with the development of distributed photovoltaic power generation projects in terms of resource endowment and energy demand, and can rely on the distributed photovoltaic power generation projects originally gathered in the regions to reduce technical costs, improve the economic output value and benefits of enterprises, and thus optimize the layout. However, other energy sources should be considered for less suitable development areas and unsuitable development areas, so as to make use of energy according to local conditions.

As can be seen from **Figure 5**:

(1) For area very suitable for development, the evaluation value of the space-time coupling suitability is 118.95 ~ 131.83. This kind of area is mainly distributed in Daxing District, with abundant solar energy resources and moderate

Table 2. Comprehensive evaluation indexes and classification of space-time coupling between solar energy resources and distributed PV power generation projects in Beijing

Primary index		Secondary index	Grade scale					Weight
			Very suitable	Generally suitable	Suitable	Less suitable	Not suitable	
Resource side	Natural conditions (A)	GHI(A_1)/kWh·m^{-2}	≥1,422.68	1,406.11 ~ 1,422.68	1,402.90 ~ 1,406.11	1,395.60 ~ 1,402.90	<1,395.60	0.07
		Average annual temperature (A_2)/°C	≥12.00	11.50 ~ 12.00	11.00 ~ 11.50	8.00 ~ 11.00	<8.00	0.05
		Average annual sunshine hours (A_3)/h	≥2,764.0	2,588.6 ~ 2,764.0	2,519.0 ~ 2,588.6	2,384.3 ~ 2,519.0	<2,384.3	0.04
	Social conditions (B)	Population density (B_1)/person·km^{-2}	≥19,618	6,881 ~ 19,618	598 ~ 6,881	229 ~ 598	<229	0.06
		Per capita GDP (B_2)/ten thousand yuan·person^{-1}	≥29.51	9.90 ~ 29.51	5.29 ~ 9.90	4.36 ~ 5.29	3.90 ~ 4.36	0.04
		Proportion of urban population (B_3)/%	≥100.00	89.12 ~ 100.00	70.05 ~ 89.12	58.33 ~ 70.05	<58.83	0.05
		Proportion of tertiary industry (B_4)/%	≥91.20	80.00 ~ 91.20	56.06 ~ 80.00	45.81 ~ 56.06	<45.81	0.05
	Industry conditions (C)	Total power generation in the power industry (C_1)/100 million kWh	≥102.81	70.45 ~ 102.81	17.37 ~ 70.45	11.86 ~ 17.37	<11.86	0.17
		Administrative area power load (C_2)/100 million kWh	≥83.15	70.93 ~ 83.15	21.58 ~ 70.93	12.54 ~ 21.58	<12.54	0.15
Project side	Item condition (D)	Circle characteristics (D_1)	≥0.23	0.19 ~ 0.23	0.11 ~ 0.19	0.03 ~ 0.11	<0.03	0.07
		Agglomeration characteristics (D_2)	H-H	H-L	L-H	L-L	uncorrelated	0.13
		Development characteristics (D_3)	≥1.00	0.98 ~ 1.00	0.96 ~ 0.98	0.14 ~ 0.96	<0.14	0.12
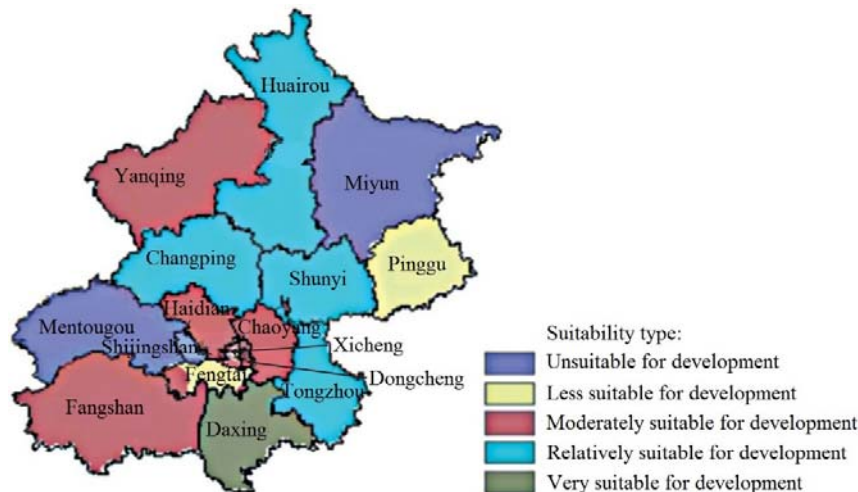
Figure 5. Comprehensive evaluation results of space-time coupling between solar energy resources and distributed PV power generation projects and in Beijing.

power demand. Since the 9th batch of projects, distributed photovoltaic power generation projects in Daxing District have gradually started to develop, and the distribution density has increased. Such areas are suitable for developing large-scale distributed photovoltaic power generation projects and improving the utilization level of solar energy resources by combining the advantages of local resources, power demand and existing power grids and projects.

(2) For areas relatively suitable for development, the evaluation value of the suitability of the space-time coupling is 114.20 ~ 118.95. Such areas are mainly distributed in Huairou District, Changping District, Shunyi District and Tongzhou District. Previously, the distribution density of distributed photovoltaic power generation projects in Huairou District was small, but since the 8th batch of projects, the development of the projects has gradually increased, showing a new development trend. Changping District, Shunyi District and Tongzhou District are rich in solar energy resources, with large user demand. Distributed photovoltaic power generation projects are not saturated, and the distribution of projects is relatively uniform. In the past, such areas had a certain foundation of project clusters, and in the future, it is necessary to promote the development of new projects on the basis of ensuring the development of existing projects.

(3) For areas moderately suitable development, the evaluation value of the suitability of spatial-temporal coupling is 108.26 ~ 114.20. This type of area is the most widely distributed, including Yanqing District, Haidian District, Dongcheng District, Xicheng District, Chaoyang District and Fangshan District. Among them, Yanqing District and Fangshan District are dominated by abundant solar energy resources, but the demand for electricity in these areas is relatively low, and the demand for distributed photovoltaic power generation is also relatively low. The solar energy resources in Haidian District, Dongcheng District, Xicheng District and Chaoyang District are relatively small, but there is a large demand for electricity. The distribution density of distributed photovoltaic power generation projects that have been built in moderately developed areas is relatively balanced, and local resources such as energy, roof and power grid are abundant, which can maintain the current growth trend and continue to develop in the future.

(4) For areas less suitable for development, the evaluation value of the spatial-temporal coupling suitability of this area is 104.20 ~ 108.26. This type of area is mainly distributed in Pinggu District, Fengtai District, and its common characteristics are that the foundation of the original distributed photovoltaic power generation project is weak, the distribution density of the project is small, and the population density and power load pressure are relatively small. Therefore, such areas are not suitable for large-scale concentrated development of distributed photovoltaic power generation projects, and future planning should consider developing small and medium-sized distributed photovoltaic power generation projects on the basis of accurate site selection.

(5) For areas unsuitable for development, the evaluation value of the suitability of space-time coupling is 98.86 ~ 104.20. This kind of area is mainly distributed in Mentougou District and Miyun District. Among them, Mentougou District has a good advantage in solar energy resources, but its users' energy demand and supporting facilities for the development of distributed photovoltaic power generation projects are few. Therefore, the next step in this area should be to integrate supporting facilities such as roofs and power grids, and carry out appropriate planning and development. The foundation of the original distributed photovoltaic power generation projects in Miyun District is weak, which is more suitable for developing smaller-scale distributed photovoltaic power generation projects.

6. Conclusion

This paper takes Beijing as an example, innovatively put forward the evaluation system of spatial-temporal coupling suitability of resources and projects by using spatial analysis methods such as nuclear density analysis and standard deviation ellipse method from the perspective of spatial-temporal coupling between regional solar

energy resources and distributed photovoltaic power generation projects to explore the spatial-temporal coupling relationship between regional solar energy resources and related distributed photovoltaic power generation projects, and scientifically evaluate the regional suitability of their development. The results show that:

(1) The spatial matching degree between solar energy resources and distributed photovoltaic power generation projects in Beijing is still low, and the spatial matching development between the northern region and the central region is weak, and the development trend is characterized by expanding from the central region to the surrounding regions.

(2) The development of solar energy resources and distributed photovoltaic power generation projects in Daxing District and other districts has reached a relatively balanced level; Miyun District, Mentougou District and other districts are no longer suitable for developing large-scale distributed photovoltaic power generation projects. In the future, other green energy development modes should be considered and optimized.

The research results can provide important reference for resource utilization, project layout and development planning of regional distributed photovoltaic power generation projects.

Acknowledgements

Conflict of interest

The authors declared no conflict of interest.

References

1. Zhang S, Fu H. Study on the incentive policy of distributed solar PV power in Beijing. Journal of North China Electric Power University (Social Science Edition) 2018; (6): 31–37.
2. Zhao Z, Fan W. Beijing shi kezaisheng nengyuan ziyuan Fengdu pingjia yu kongjian xiangguanxing fenxi (Chinese) [Abundance evaluation and spatial correlation analysis of renewable energy resources in Beijing]. Rural Electrification 2020; (6): 59–64.
3. Qi X, Wang M, An L, *et al*. Evaluation on development level of provincial renewable energy power generation projects in China. Renewable Energy Resources 2019; 37(6): 907–913.
4. Li G, Zhang Y, Xia L, *et al*. The feasibility study of distributed photovoltaic power generation system in Western Region of China. Advanced Materials Research 2015; 1070: 64–7.
5. Lu X, Lin D, Fan P, *et al*. Revenue budget of distributed PV power project. Solar Energy 2020; (3): 24–28.
6. Tran NH, Do CT, Hong CS, *et al*. Coordinated colocation datacenters for economic demand responce. ACM SIGMETRICS Performance Evaluation Review 2015; 43(3): 34–37.
7. Liu R, Liu Y, Jing Z. Impact of industrial virtual power plant on renewable energy integration. Global Energy Interconnection 2020; 3(6): 545–552.
8. Jo HC, Kim JY, Byeon G, *et al*. Optimal scheduling method of community microgrid with customer-owned distributed energy storage system. 2019 International Conference on Smart Energy Systems and Technologies (SEST); 2019 Sept 9–11; Porto, Portugal. IEEE; 2019. p. 1–6.
9. Zhao Z, Yuan S. Risk clustering analysis of regional wind power absorption based on spatial statistical model. Renewable Energy Resources 2020; 38(2): 225–232.
10. Jie C, Ren B, Wu K. The study of rainfall isosurface generation method. Electronic Design Engineering 2015; (16): 102–104.

REVIEW ARTICLE

Current situation of global manganese resources and suggestions for sustainable development in China

Hongwei Sun[1,2*], Jie Wang[1,2], Junping Ren[1,2], Weibo Zhang[3], Wenlong Tang[1,2], Xingyuan Wu[1,2], Alei Gu[1,2]

[1] Tianjin Center of China Geological Survey, Tianjin 300170, China. E-mail: shwcub@163.com

[2] North China Center for Geoscience Innovation, China Geological Survey, Tianjin 300170, China.

[3] Development and Reseach Center, China Geological Survey, Beijing 100037, China.

ABSTRACT

As an important metal mineral, manganese is widely used in metallurgy, chemical industry, national defense industry and other fields. Global manganese resources are characterized by extremely uneven distribution, highly concentrated production capacity, and serious separation between supply and demand. China's manganese resources are characterized by extensive distribution but insufficient reserves, low grade and poor quality, high external dependence, and imperfect resource guarantee system. In recent years, China's manganese industry has developed rapidly, and China has become the world's largest consumer of manganese resources. With the growth of new energy market, the contradiction between supply and demand of manganese resources in China will further increase in the future. Based on the actual situation that manganese ore is still in short supply and in great demand in China, in order to ensure the strategic safety of national manganese ore resources and promote the healthy development of China's manganese industry, this paper puts forward sustainable development suggestions such as formulating long-term supply planning, strengthening overseas layout, promoting capacity cooperation and establishing a diversified security system.

Keywords: Manganese Ore; Resource Distribution; Supply and Demand Situation; Resource Potential; Development Suggestions

1. Introduction

The average content of manganese in the earth's crust is about 0.1%, which is one of the important basic bulk raw material minerals for industrial production. More than 90% is used in the metallurgical industry. It is the element with the largest consumption in steel except iron, and is known as "no steel without manganese"[1,2]. In addition, it is also used in various fields of the national economy, such as light industry (used for batteries, printing paint, etc.), chemical industry (manufacturing all kinds of manganese salts), agriculture and animal husbandry (chemical fertilizers, fungicides, etc.), building materials industry (fading agents and colorants for ceramics and glass), and national defense industry. Therefore, manganese resources are important strategic materials for China's national economic construction. The most important non metallurgical use of manganese is as a depolarizer in dry batteries in the form of manganese dioxide. In the future, with the rapid growth of China's new energy market, the demand for manganese ore resources, especially battery grade manganese ore, will continue to increase.

In recent years, the output of manganese and manganese

containing alloys in China has ranked first in the world[3], and it is expected that the demand for manganese resources will further increase in the future. At the same time, the price of manganese in the international market has been fluctuating greatly. Since the outbreak of novel coronavirus, the price of manganese ore has risen rapidly due to the obstruction of mining in some areas[4]. How to ensure the safety of manganese resources in China has become an urgent problem to be solved. This paper will analyze the distribution characteristics, occurrence, supply and demand pattern and resource potential of global manganese resources, and on this basis, put forward measures and suggestions to ensure the strategic security of China's manganese resources.

2. Global resource distribution characteristics

2.1 Overview of global manganese resource distribution

The world's manganese resources are characterized by relatively rich total amount, but uneven distribution[5]. According to the statistical data[6], the global terrestrial manganese ore reserves in 2019 were 810 million tons, of which South Africa, Ukraine, Brazil and Australia accounted for more than 75% of the total global manganese ore reserves out 300 million tons of manganese resources (**Figure 1**). However, Ukraine's manganese ore grade is poor, and it has withdrawn from the ranks of major manganese ore producers in recent years. The world's high-grade manganese ore resources (with manganese content of more than 35%) are mainly concentrated in South Africa, Australia, Brazil and Gabon. In addition, the bottom of the ocean also contains ab in the form of modern manganese nodules, but due to technical reasons, a large number of manganese resources have not been exploited yet[7].

2.2 Distribution characteristics of manganese resources in China

China's manganese ore reserves are small, accounting for only 6.67% of the world's total reserves. Manganese ore deposits are characterized by small scale, low grade, complex co-associated components and high mining costs, resulting in low availability of manganese resources in China, and manganese ore has also become one of the scarce minerals in China[2,8,9].
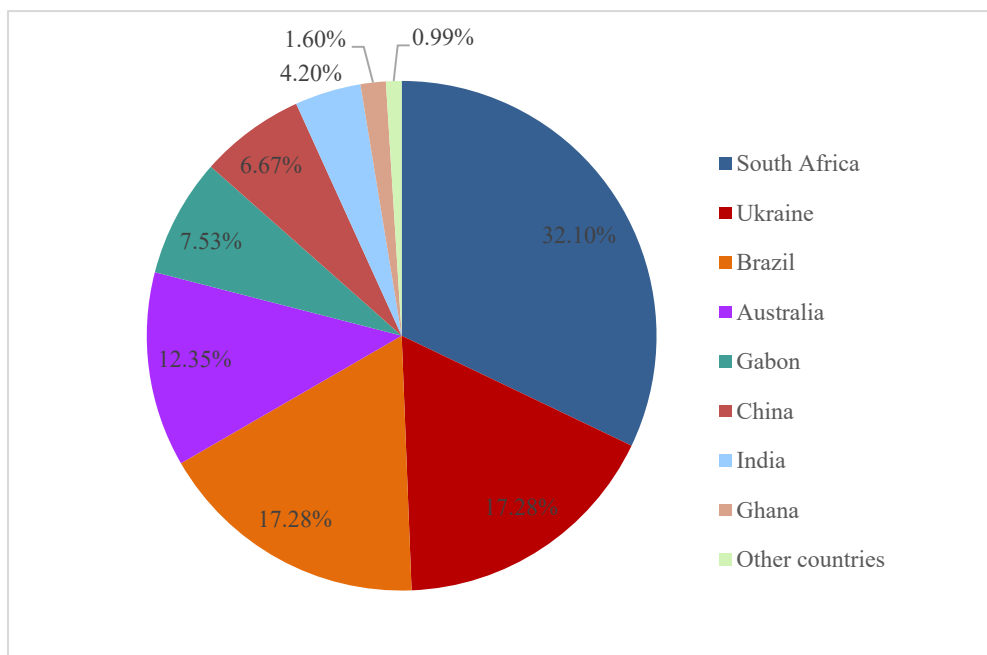
Figure 1. Proportion of global manganese reserves distribution.
Source: USGS[6].

Manganese resources in China are widely distributed in 24 provinces, cities and autonomous regions across the country. However, the distribution of resource reserves is extremely

uneven. According to the statistical data[5,10], China's manganese ore is mainly distributed in Guizhou, Guangxi, Hunan, Hebei and Yunnan provinces, of which the identified manganese ore resource reserves in Guizhou and Guangxi account for more than 60% of the total reserves in the country (**Figure 2**).

3. Production of global manganese resources

Figure 2. Distribution proportion of reserves of manganese resources in China. Source: Data are from Lei *et al*[5], Yin and Xiao[10].
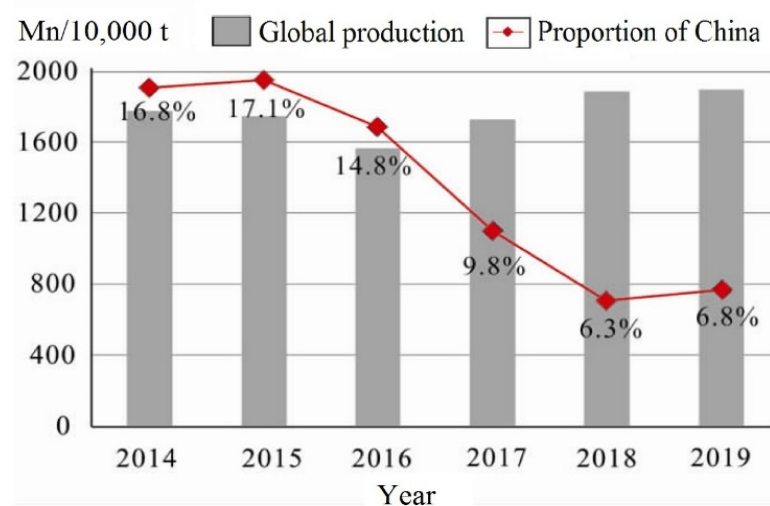
Figure 3. Global production of manganese metal from 2014 to 2019. Source: RTE[17].

3.1 Major manganese producing countries

In recent years, the total annual output of manganese metal in the world has basically remained between 16 and 19 million tons (**Figure 3**), of which South Africa, Australia and Gabon are the world's major manganese resource producers and exporters, accounting for more than 60% of the world's total output. China, Brazil, Ghana and India are also the world's major manganese resource producers. However, with the increase of domestic mining costs and strict environmental protection requirements in China, since 2015, China's manganese ore production has been declining, and its share in the world has also continued to decline (**Figure 3**).

3.1.1 South Africa

South Africa has the largest reserves of manganese ore in the world, and is dominated by high-grade manganese ore. In 2019, South Africa's manganese metal reserves were 260 million tons,

accounting for 32.1% of the total global reserves, ranking first in the world (**Table 1**). Manganese deposits in South Africa are widely distributed, mainly concentrated in Kalahari postmasburg manganese ore concentration area, especially the metamorphic sedimentary manganese deposits hosted in the Paleoproterozoic Transvaal supergroup[12,13].

3.1.2 Australia

Australia is the world's major producer and exporter of high-grade manganese ore. In 2019, Australia's manganese metal reserves were 100 million tons, accounting for 12.35% of the total global reserves (**Table 1**). Its manganese ore resources are mainly distributed in northern and western Australia, mostly open-pit mining, with high grade and easy sorting. Groote manganese ore

is the largest primary manganese oxide deposit in Australia. Manganese ore occurs in marine sedimentary deposits in sandy clay, and the manganese content of the ore is about 40%–50%[14,15].

3.1.3 Brazil

Manganese resources in Brazil are widely distributed, and manganese is found in most states of the country. By the end of 2019, Brazil's manganese metal reserves were 140 million tons, accounting for 17.28% of the world's total reserves (**Table 1**). Azul manganese ore area in Carajas area is the main manganese mine in Brazil at present, which mainly produces high-grade manganese ore with manganese content of 40% and high-grade battery manganese ore[15,16].

Table 1. Annual production data of the world's major manganese producers from 2014 to 2019

Serial number	Countries	Yield						Reserves
		2014	2015	2016	2017	2018	2019	
1	South Africa	520	590	530	540	580	550	26,000
2	Ukraine	42	41	42	73	51	54	14,000
3	Brazil	104	109	108	116	131	120	14,000
4	Australia	305	245	224	282	348	320	10,000
5	Gabon	186	202	162	219	233	240	6,100
6	China	300	300	233	170	120	130	5,400
7	India	94	90	74	73	96	100	3,400
8	Ghana	42	42	55	81	136	140	1,300
9	Other countries	187	131	142	176	195	246	800
10	Total	1,780	1,750	1,570	1,730	1,890	1,900	81,000

Note: The data in the table are manganese (unit: Mn/10,000 t).
Source: USGS[6].

3.1.4 Gabon

Gabon is the second largest manganese ore resource country in Africa, and is famous for its rich manganese ore (manganese content 50%–60%) and battery grade manganese ore. In 2019, Gabon's proven manganese (metal) reserves totaled 61 million tons, accounting for 7.53% of the world's

total (**Table 1**). Gabon's manganese resources are relatively concentrated, mainly in the Moanda area in the southeast of Gabon. Manganese ores are mostly hosted in the Paleoproterozoic (2.3–2.3 Ga) Francevillian supergroup, and the deposit type is mainly metamorphic sedimentary[13,15].

Table 2. The production of the world's leading manganese mining companies

Corporate name	Country	Main mines and locations	Ore output in 2018/t
South32 Ltd.	Australia	Groote in Australia, Hotazel in South Africa	4,983,300
Consolidated Minerals Ltd.	Australia	Nsuta, Ghana	4,100,000
Anglo American Plc	UK/South Africa	Hotazel in South Africa, Groote in Australia	3,322,200
CITIC Dameng Holdings Limited	China	China Daxin Manganese Mine, Gabon Bembele	2,989,040
ERAMET S.A.	France	Moanda in Gabon	2,763,740
Vale S.A.	Brazil	Azul, Urucum in Brazil	1,831,000
African Rainbow Minerals Ltd.	South Africa	Nchwaning, Gloria in South Africa	1,794,500
Jupiter Mines Ltd.	Australia	Tshipi Borwa in South Africa	1,757,609
Kudumane Manganese Resources	South Africa	Kudumane, South Africa	1,700,000

Source: RTE[17].

3.2 Major manganese mining enterprises

In 2018, there were 9 enterprises and 12 manganese mines in South Africa, Australia, Brazil, Gabon, Ghana and China, the world's major manganese ore producing countries, with an annual output of 25.2 million tons. See **Table 2** for details. Major ore miners account for about 56% of the world's output, and are the main controllers of the world's high-quality manganese rich resources, and play a leading role in the allocation of manganese resources.

4. Supply, demand and import of manganese ore in China

In recent years, with the rapid development of domestic metallurgical industry, China's demand for manganese ore, especially rich manganese ore, has increased sharply, while the domestic manganese ore resource endowment is poor, which makes the contradiction between supply and demand more prominent. China has become the world's largest importer of manganese ore for many consecutive years.

4.1 Highly concentrated importing countries

At present, the source countries of China's overseas manganese ore are mainly South Africa,

Australia, Gabon, Ghana and Brazil, which account for about 90% of China's total imports (**Table 3**), while the import volume from South Africa and Australia accounts for more than 60% (**Figure 4**). In order to ensure the strategic security of China's manganese resources, China has been trying to expand the import sources of manganese resources in recent years, but the import proportion of Australia and South Africa remains above 50%. There is a high supply risk.
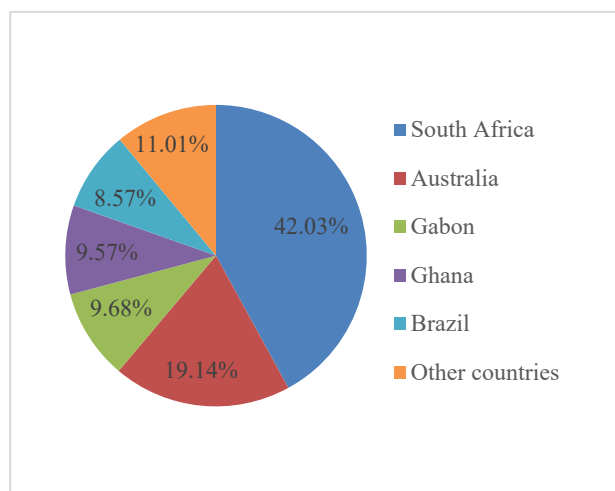
Figure 4. Proportion of China's manganese ore import sources in 2017. Source: RTE[17].

Table 3. China's manganese ore import volume and source in 2014–2018

Ranking	2014	2015	2016	2017	2018
First place (import volume)	South Africa 5,794,476	South Africa 6,329,742	South Africa 7,591,901	South Africa 8,935,753	South Africa 11,141,791
Second place (import volume)	Australia 5,162,516	Australia 4,297,605	Australia 4,073,938	Australia 4,069,536	Australia 5,221,954
Third place (import volume)	Gabon 1,478,570	Gabon 1,876,216	Ghana 1,548,971	Gabon 2,057,086	Ghana 3,508,550
Fourth place (import volume)	Ghana 1,059,407	Brazil 1,183,085	Gabon 1,256,172	Ghana 2,034,067	Gabon 2,524,817
Fifth place (import volume)	Brazil 880,039	Ghana 537177	Brazil 1,169,042	Brazil 1,822,121	Brazil 1,827,402
Total	14,375,008	14,223,825	15,640,024	18,918,563	24,224,514
Proportion in total	88.55%	90.12%	91.71%	88.99%	70.88%

Note: The data in the table is manganese concentrate data (unit: Manganese concentrate/t), which is derived from RTE[17].

4.2 The price fluctuates greatly

From the perspective of the average price of imported manganese ore in China (**Figure 5**), the lowest price was only 104.0 USD/t in 2006 and the highest was 458.2 USD/t in 2008. This is mainly due to the shortage of manganese ore products and the sharp rise in prices due to the financial crisis.

Since then, due to the implementation of China's domestic steel capacity reduction policy in 2014, China's demand for manganese ore has slowed down, falling back to 122.4 USD/t in 2015. However, after 2017, due to the continuous increase of domestic mine environmental protection requirements and mining costs, domestic production

has plummeted, external demand has increased, and the price of manganese ore in the international market has risen again. In 2018, the import price of manganese ore in China reached 212.2 USD/t, and since the outbreak of the epidemic in 2020, the global manganese ore price has increased rapidly. Even if the epidemic is stable, under the monopoly control of the world's manganese rich countries and giant manganese ore companies, the manganese ore price will not have much room for decline.
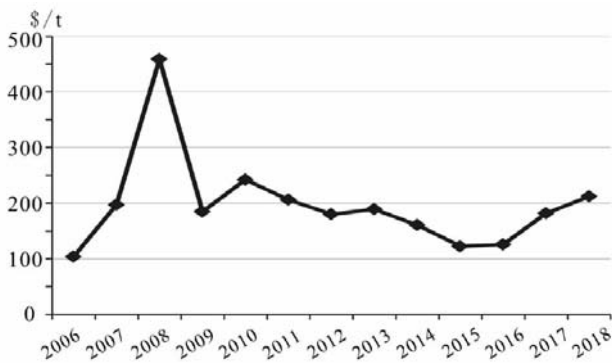
Figure 5. Import prices of Chinese manganese ores, 2006–2018. Source: RTE[17].

Statistics show that[4] the global manganese resource reserve production ratio has exceeded 40 years, but the effective exploration activities for manganese ore have increased rapidly in recent years (**Figure 6**), which may be related to the continuous growth of the global new energy market. Battery grade manganese ore is one of the main materials for producing power batteries (lithium manganate). With the further expansion of the new energy vehicle market, the demand for manganese ore will be very strong, which may push up the price of manganese ore.
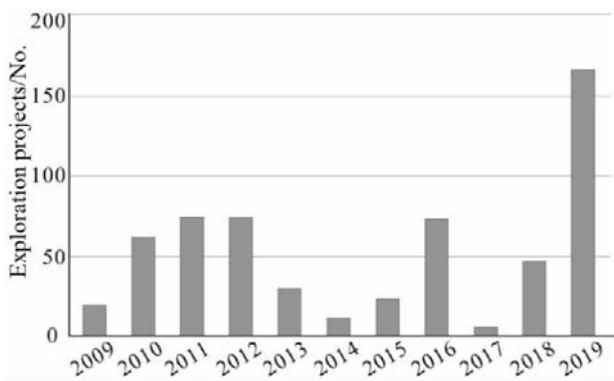
Figure 6. Statistics of global manganese ore exploration projects from 2009 to 2019. Source: Data are from SNL[4].

At present, the reasons for the fluctuation of

China's manganese ore import price mainly include the following aspects: first, the distribution and production capacity of rich manganese ore resources are very unbalanced, and countries and multinational companies rich in manganese ore resources almost monopolize the pricing power of manganese ore; secondly, there is less investment in the development of overseas manganese-rich mine resources in foreign countries, and there is a lack of international giant manganese ore groups; in addition, the change of ocean transportation cost will also affect the import price of manganese ore in China.

4.3 External dependence

After entering the 21st century, due to the rapid development of the iron and steel industry, China has become the world's largest importer of manganese ore. The import volume of manganese ore and manganese concentrate has increased year by year, and has maintained an external dependence of more than 50% since 2010[9]. The imported manganese ore is mainly rich manganese ore with a grade of more than 40%. In recent years, the degree of external dependence has exceeded 60% (**Figure 7**), and the contradiction between supply and demand is very prominent.
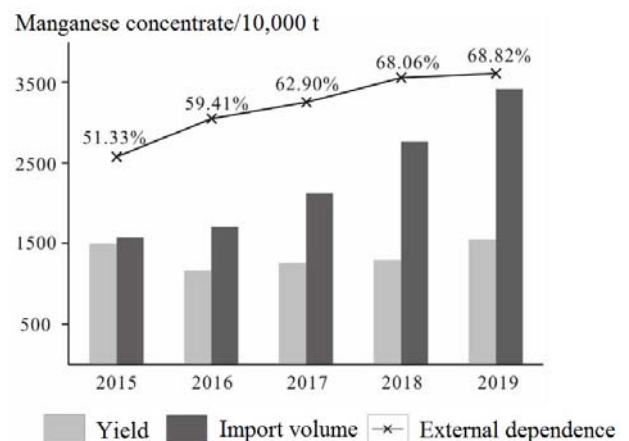
Figure 7. Yield and import of Chinese manganese ores, 2015–2019. Source: USGS and RTE[6,17].

5. Resource potential analysis

Limited by the metallogenic conditions[2,10,18], the current situation of the shortage of domestic manganese rich ores is difficult to change in the short term. Making full use of overseas manganese rich resources will help to realize resource

complementarity in China. With the application of some sophisticated exploration technologies[19,20], deep and peripheral exploration of the deposit will be conducive to achieving new breakthroughs in prospecting and providing technical support for China's manganese enterprises. However, with the rise of trade protectionism and unilateralism, the overseas market is also full of challenges. Identifying manganese potential areas will help domestic manganese enterprises go global.

At present, Africa and Oceania are the main sources of manganese resources overseas in China, and also the main concentration of manganese rich ores in the world. Especially, Africa has superior metallogenic geological conditions, and has become the largest source of imported manganese in China for many consecutive years. South Africa, Ghana and Gabon have large-scale and high-grade manganese mines, which are easy to realize industrial mining, and these countries account for a high proportion of mining investment, which is suitable for national manganese enterprises to settle in. The manganese mines in the Democratic Republic of Congo, Zambia and Namibia are small in scale, but there are many ore spots with high grade, and the investment is small and effective, which is conducive to the involvement of small and medium-sized private enterprises. In Australia and Brazil, because their manganese resources are firmly controlled by international mining giants, it is very difficult for large state-owned enterprises to enter, while small and medium-sized enterprises are trapped in environmental protection, human costs and other factors, which are difficult to make profits, which is not conducive to China's control of its manganese resources. Therefore, Africa will be the most important potential area of China's overseas manganese resources.

Through the comprehensive analysis of manganese ore-forming conditions and exploration and development degree in southern Africa[6,12,13,21-27], the exploration and development of manganese ore in southern Africa should focus on Kalahari–Postmasburg manganese ore concentration area in North Cape Town, South Africa, the central part of Limpopo Province, Haut–Ogoue and Moyen–Ogoue provinces in Gabon,

North Central Namibia, the adjacent area between southern Botswana and South Africa, Tete Province in Northwest Mozambique, Mansa–Mkushi–Kabwe area in central Zambia and Kisenge–Kamata area in Katanga Province in Southern Democratic Republic of Congo.

6. Conclusions and suggestions

6.1 Conclusion

The distribution of global manganese resources has the following characteristics: (1) the distribution of resources is extremely uneven, and South Africa, Australia and Gabon retain more than 60% of the global resource reserves; (2) the production capacity is highly concentrated, and the main ore producers account for more than 50% of the world's output, controlling the world's main high-quality manganese rich ore resources; (3) there is a serious separation between supply and demand. As the world's largest demander of manganese resources, China's reserves account for only about 5% of the world. Characteristics and demand trend of manganese resources in China: (1) widely distributed but insufficient reserves; (2) low grade, poor quality and limited manganese ore resources; (3) the external dependence is too high, the overseas channels are limited, and the manganese resource guarantee system is not perfect; (4) in the future, the contradiction between supply and demand of manganese resources in China will still exist, and southern Africa can be used as a key area for the exploration and development of overseas manganese resources in China.

6.2 Thoughts and suggestions

With the growth of domestic new energy market, the contradiction between supply and demand of manganese ore in China will become more prominent. In order to ensure the strategic safety of China's manganese resources and the healthy development of the manganese industry, domestic enterprises should seize the historical opportunities brought by the "going global" and the "the Belt and Road" initiatives, and promote a multi-level and multi-channel manganese resource utilization and guarantee system facing the world as

soon as possible. Specific suggestions are as follows:

Identify domestic assets and formulate domestic and foreign supply plans according to the demand gap. While finding out the current situation of domestic manganese resources, combined with the future development planning of major manganese application industries such as steel, new energy batteries and chemical industry, predict the demand gap of manganese resources, and make targeted import and export planning to ensure the sustainable development of domestic manganese industry.

Strengthen overseas layout and improve controllable manganese resource reserves. While increasing the investment in domestic manganese geological exploration, we should enter the manganese-rich resource countries with low degree of mining exploration and lack of technical personnel, such as southern Africa, where the metallogenic conditions is superior and the resource potential is huge. Relying on high-precision and cutting-edge technology, we should strengthen the exploration of manganese rich resources at home and abroad, and constantly seek new manganese resources. Promote production capacity cooperation, extend the industrial chain of resource development and processing in manganese resource countries, and increase the synergy of manganese development conditions. In the process of guiding domestic manganese mining enterprises to go global, there should be both a "national team" composed of large enterprises and a "self-employed" composed of small and medium-sized enterprises. The "national team" can actively participate in the development projects of manganese mines in the source countries, establish long-term strategic investment and cooperation relations with the target countries, and take acquiring world-class mines as the core strategy through various cooperation methods such as resource exploration, equity purchase and engineering for resources. We will do our utmost to ensure the safety of manganese resources supply in China. As a "self-employed" small and medium-sized enterprises, they cannot limit the size of the deposit, with the purpose of quickly and directly obtaining manganese rich

ores, blossom at multiple points, and constantly improve China's controllable manganese ore reserves. In addition, the beneficiation and smelting technology and the mining technology of marine manganese resources should be further improved to realize the comprehensive development and utilization of manganese resources.

Establish a diversified resource supply system and gradually gain the right to speak by using the scale of the domestic market. China is highly dependent on international manganese ores, but the manganese product suppliers and pricing power in the international market are mainly in the hands of several major foreign manganese miners, which has potential risks. In order to cope with the supply risks that may be caused by the great changes in the international situation, China should establish a multi-level and multi-channel manganese resource supply guarantee system facing the world as soon as possible, share trade risks, reduce the adverse impact of market fluctuations on the entire manganese industry, and further compete for the right to speak by using the scale of the domestic market.

Acknowledgements

Conflict of interest

The authors declared no conflict of interest.

References

1. Yan W, Gao H. The resource of Mn ore & its development of Mn-mining. China Manganese Industry 2009; (3): 14–19.
2. Cong Y, Dong Q, Xiao K, *et al*. Charateristics and predicted potential of Mn resources in China. Earth Science Frontiers 2018; 25(3): 118–137.

3. He H. A present situation of Mn-ore resources and its investigation. China Manganese Industry 2017; 35(1): 23–24.

4. SNL. Commodity profile-price chart [Internet]. Available from: https://platform.MarketIntelligence.spglobal.com/web/clientauth=inherit#industry/topProducingCompanies.

5. Lei X, Hu Y, Du Y, *et al*. Thinking of status and evelopment of the manganese ore sourcece utilization. China Mining Magazine 2015; 24(S1): 27–29.

6. USGS. Mineral Commodity Summaries 2020 [Internet]. USGS Publications Warehouse; 2020. Available from: https://pubs.usgs.gov/periodicals/mcs2020/mcs2020.pdf.

7. Wang Y, Li Z, Li H. A survey of processing techniques researches on sedbed Manganese nodules in China. China Manganese Industry 2006; 24(1): 17–20.

8. Liu Z, Zhang X, Xu H, *et al*. Overseas manganese resources distribution and proposals for Chinese mining companies. China Mining Magazine 2015a; 24(8): 8–15.

9. Liu Z, Xu H, Wang Q, *et al*. China's manganese supply-demand actuality and its sustainable development. Resources and Industry 2015; 161(6): 42–47.

10. Yin J, Xiao K. Resources potential analysis and metallogenic prospect of Mn resources in China. Geology in China 2014; 41(5): 1424–1437

11. Ye L, Fan D, Yang P. Zhongguo mengkuang chuang (Chinese) [Manganese deposits in China]. Beijing: Geological Publishing House; 1994. p. 80–552.

12. Gutzmer J, Beukes NJ. Mineral paragenesis of the Kalahari manganese field, South Africa. Ore Geology Reviews 1996; 11(6): 405–428.

13. Frost KS, Master S, Viljoen RP, *et al*. The great mineral fields of Africa introduction. Episodes Journal of International Geoscience 2016; 39(2): 285–318.

14. Huang C. Manganese mineral resources of Australia and its production and marketing. Guangxi Geology 1994; 7(3): 88–92.

15. Kuleshov V. Isotope geochemistry: The origin and formation of manganese rocks and ores. Amsterdam, Netherlands: Elsevier Inc.; 2016.

16. Song G. Baxi kuangye touzi huanjing fenxi (Chinese) [Analysis of mining investment environment in Brazil]. Natural Resources Information 2012; 8: 2–8.

17. RTE. Resource trade earth-manganese [Internet]. Available from: https://resource-trade.Earth/data?Year=2008&exporter=710&importer=156&category=182&units=weight.

18. Fu Y, Xu Z, Pei H, *et al*. Study on metallographic regularity of manganese ore deposits in China. Acta Geologica Sinica 2014; 88(12): 2192–2207.

19. Gu A, Wang J, Ren J, *et al*. Geological characteristics and mineralization potential analysis for the Pan-African Hook Batholith in Central Zambia. Geological Survey and Research 2020; 43(1): 63–71.

20. Zhong Z, Zhang S, Zhang W, *et al*. Application of interrated exploration to Yunyi concealed bauxite deposits in Shanxi province. Geological Survey and Research 2017; 40(2): 134–140.

21. De Putter T, Liegeois JP, Dewaele S, *et al*. Paleoproterozoic manganese and base metals deposits at Kisenge-Kamata (Katanga, DR Congo). Ore Geology Reviews 2018; 96: 181–200.

22. Gutzmer J, Du-Plooy AP, Beukes NJ. Timing of supergene enrichment of low-grade sedimentary manganese ores in the Kalahari Manganese Field, South Africa. Ore Geology Reviews 2012; 47(1): 136–153.

23. Ren J, Wang J, Gu A, *et al*. Zircon U-Pb geochronology and Lu-Hf isotopic composition of syenogranite, northeastern Zambia. Geological Survey and Research 2019; 42(3): 161–165.

24. Zhao P. Analysis of geological features and prospecting potential of manganese in Mansa District of Republic of Zambia. Mining Engineering 2015; 4: 15–16.

25. Sun H, Wang J, Ren J, *et al*. Metallogenic evolution and prospecting potential of the Katanga–Zambia polymetallic metallogenic belt in Central Africa. Geological Science and Technology Information 2019; 38(1): 121–131.

26. Sun H, Wang J, Ren J, *et al*. Analysis of uranium mineralization characteristics and resource potential in Lufilian area, Central Africa. Journal of Jilin University (Earth Science Edition) 2020; 50(6): 1660–1674.

27. Sun H, Ren J, Wang J, *et al*. Geological characteristics and prospecting direction of Pb–Zn–(Cu) deposits in Lufirian area, Central Africa. Geology and Exploration 2019; 55(4): 1101–1116.

ORIGINAL RESEARCH ARTICLE

Analysis and evaluation of solar energy resource change characteristics in the Wanshan Island area

Jun Wang[1], Fang Xi[2]

[1] *China Energy Engineering Group Guangdong Electric Power Design Institute Co., Ltd., Guangzhou 510663, China. Email: wangjun@gedi.com.cn*

[2] *CCCC-FHDI Engineering Co., Ltd., Guangzhou 510663, China.*

ABSTRACT

The total solar radiation and insolation hours in Wanshan Island were analyzed by linear regression analysis, distance level analysis method, 5-year sliding average method, and Mann-Kendall test method. The results showed that the total solar radiation in Wanshan Island showed a slight upward trend, and the total monthly solar radiation showed a unimodal distribution, with the highest in July and the lowest in February. The number of annual sunshine hours showed a weak downward trend, and the number of monthly sunshine hours showed a double-peak distribution, with the highest in July and the lowest in March. The analysis and evaluation of solar energy resources in the Wanshan Island area show that the annual average of total solar radiation in the Wanshan Island area is 4,996.25 MJ/m^2, belonging to a resource-rich area. The indicator of the stability of solar energy resources is 3.7, which belongs to the resources of more stable areas.

Keywords: Total Solar Radiation; Hours of Sunshine; Solar Energy Resources; Wanshan Island

1. Introduction

Since entering the 21st century, China's energy system is changing into a modern energy structure that is economical, efficient, clean, diversified, and safe and has gradually entered a stage of sustainable development, green and low-carbon energy development[1]. With unlimited reserves and ubiquitous properties, and its use has the advantages of cleanliness and economy, solar energy is internationally recognized as one of the most competitive future energy sources[2], and is also an important part of distributed energy resources.

At present, solar photovoltaic power generation technology has matured and has been widely used worldwide[3], and the primary task of photovoltaic power plants is to analyze and grasp the characteristics of local solar resource changes.

In this paper, the total solar radiation and sunshine hours of the Wanshan Island area are analyzed and studied, which provides a reference for the development and utilization of solar energy resources on the island and related scientific research[4,5].

2. Data selection and analysis methods

The Wanshan Island area has a subtropical oceanic climate with no severe cold in winter and abundant rainfall. Solar radiation observations are carried out at the Tai Tam Shan Meteorological Station in Macau,

which is located at a longitude of 113°33' east, the latitude of 22°09' north, and altitude of 110 m.

The main data in this paper are the total solar radiation of the Tai Tam Shan Meteorological Station from 1986 to 2011 and the monthly sunshine hours from 1981 to 2011 (the meteorological data in this article are from the Macao Geophysical and Meteorological Bureau).

Firstly, the linear regression analysis and distance analysis method were used to analyze the trend of total solar radiation and insolation hours in the region, and then the multi-year change characteristics of total solar radiation and sunshine hours in the region were verified and analyzed by the 5-year moving average method and the Mann-Kendall (M-K) rank correlation test. Finally, according to the solar resource assessment method, the solar energy resources in the Wanshan Island area are evaluated[6].

3. Characteristics of the change in total solar radiation

3.1 Analysis of inter-annual changes

Statistical analysis of the total solar radiation data in the Wanshan Island area from 1986 to 2011 shows that the total solar radiation average in the Wanshan Island area in the past 26 years is 4,996.25 MJ/m^2, of which the highest value appeared in 1986 at 5,512.70 MJ/m^2 and the lowest value appeared in 1994 as 4,526.44 MJ/m^2. The interannual variation of total solar radiation in the Wanshan Island area is shown in **Figure 1**.
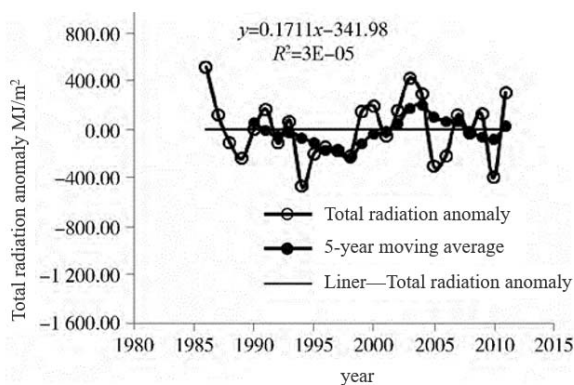
Figure 1. Annual variations of global solar radiation in Wanshan Islands area.

From **Figure 1**, it can be seen that: (1) The total solar radiation in the Wanshan Island area is in a weak upward trend, with an increase of only 1.711 MJ/m^2/10a; (2) From the 5-year sliding average to the parity, there was a clear downward trend before the end of the 1990s, and then recovered in the late 1990s, which is basically consistent with the trend of total solar radiation in South China[7], also in line with the climatic background of "global dimming" to "global lighting" in this period[8]; Since the beginning of this century, the total annual solar radiation has shown a state of fluctuation up and down, but the magnitude of the rise is slightly greater than the magnitude of the decline; (3) From the perspective of total solar radiation in different eras, the period in the late 1980s belonged to the high-value zone, which was higher than the multi-year average; In contrast, the total solar radiation in the 1990s was lower than the multi-year average; Since the beginning of this century, total solar radiation has rebounded, slightly above the multi-year average.

The sequence of total solar radiation in the Wanshan Island area was tested using the M-K method, and the results are shown in **Figure 2**.
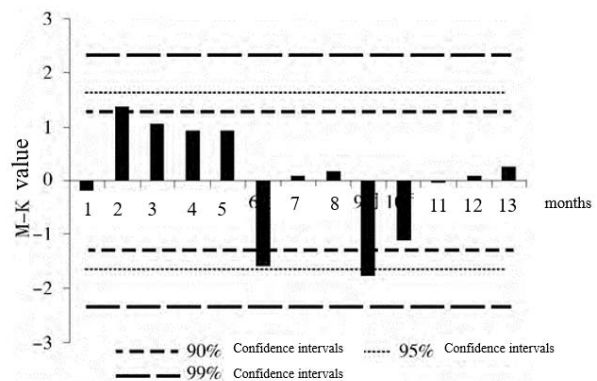
Figure 2. M-K statistics test value of global solar irradiance at different periods in Wanshan Islands area.

From **Figure 2**, it can be seen that the M-K test value of total solar radiation in the Wanshan Island area in recent decades is greater than zero, indicating that the total radiation in the region is on the rise, but it has not passed the significance confidence test. The M-K test value for January-6-September-October is less than zero, indicating that the total radiation in these four months is on a downward trend. The total radiation series in June passed the 90% significance confidence test, and the September total radiation series passed the 95%

significance confidence test; The M-K test for the remaining months of total radiation is greater than zero, showing an upward trend, with the February total radiation series passing the 90% significance confidence test and the remaining months total radiation series failing the significance test.

3.2 Analysis of intra-year changes

Figure 3 shows the characteristics of the annual change in the multi-year average total solar radiation in the Wanshan Island area from 1986 to 2011.
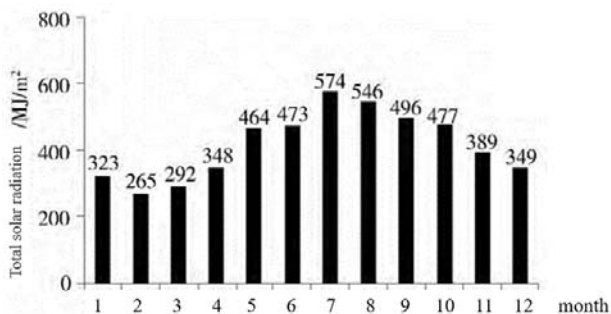
Figure 3. Monthly variations of global solar irradiance in Wanshan Islands area.

From **Figure 3**, it can be seen that the intra-year change of total solar radiation is mono-modal, with the highest in July and the second highest in August; February low, March second low; The highest value reaches 574.47 MJ/m^2 with a minimum value of just 265.16 MJ/m^2. This is related to the inter-month differences in astronomical radiation and precipitation characteristics in the Wanshan Island Area[7]: the maximum total astronomical radiation in this area occurs in June and the minimum value occurs at February 1st; However, due to the large number of rainy days in June, the total radiation reaching the ground is weakened, and July is controlled by subtropical high pressure, the number of rainy days is less than that of June, but the total astronomical radiation in July is second only to June in the whole year, so the total solar radiation in July is the highest throughout the year; Similarly, although the total astronomical radiation in February is less than that in February, because February is in the winter-spring transition season, the cold air in the north that frequently moves south and the warm and humid air flow of the ocean actively up the north confronts the region, resulting in

a high number of days of low temperature and rainy weather and less sunshine time, so that the total solar radiation from February to the ground is the lowest in the whole year.

4. Characteristics of changes in sunshine hours

4.1 Analysis of inter-annual changes

Statistical analysis of the sunshine hours in the Wanshan Island area from 1981 to 2011 shows that the average annual sunshine hours in the Wanshan Island area in the past 31 years have been as long as 1,766.5 h; The maximum number of sunshine hours for the year appeared in 1986 and was 2,081.4 h, the minimum value appeared in 2006, it is 1,542.8 h. The interannual variation in sunshine hours in the Wanshan Island area is shown in **Figure 4**.
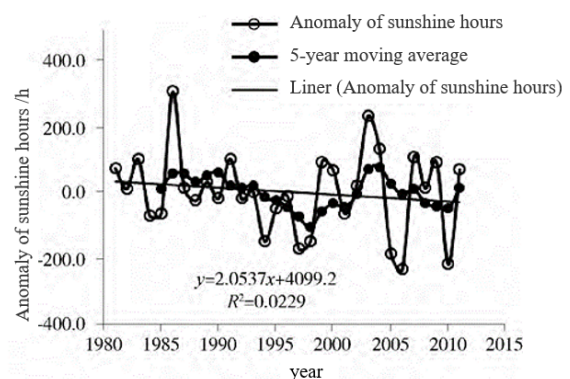
Figure 4. Annual variations of sunshine duration in Wanshan Islands area.

It can be seen from the figure: (1) The trend of sunshine hours in the Wanshan Island area is opposite to the total radiation change trend, showing a downward trend, with a decrease of 20 h/10 a; (2) From the perspective of the 5-year sliding average of the sunshine hours in previous years, before the end of the 1990s, the annual sunshine hours in the Wanshan Island area generally showed a large downward trend; Since the end of the 1990s, the number of sunshine hours has shown a short-lived, large upward trend; Since the beginning of this century, the annual sunshine hours have shown an upward and downward fluctuation state, but the amplitude is large; (3) Judging from the number of sunshine hours in different years, the end of the 1980s was a high value area of sunshine hours, which was higher than the multi-year average; The

1990s were low in sunshine hours, below the multi-year average; Since the beginning of this century, the average annual sunshine hours have been slightly lower than the average sunshine hours for many years. This is basically consistent with the results of the literature[9-13] of domestic scholars.

The M-K method test for the number of annual sunshine hours and the number of sunshine hours for each month in the Wanshan Island area is shown in **Figure** 5. It can be seen from the figure that the M-K test value of the number of sunshine hours in recent decades in the Wanshan Island area is less than zero, indicating that the trend of sunshine hours is decreasing, but it has not passed the significance confidence test. However, the change trend of each month is different, and the M-K test value from February to May and August is greater than zero, indicating that the trend of the number of sunshine hours in these 5 months is rising; The M-K test values for the remaining months are less than zero, indicating that the trend in the number of hours of sunshine for the remaining 7 months is decreasing. In terms of significance confidence tests, only 95% of the significance confidence tests passed in February and June, and none of the remaining 10 months passed the significance tests.

4.2 Analysis of intra-year changes

Figure 5 shows the characteristics of the multi-year average sunshine hours and years of change in the Wanshan Island area from 1981 to 2011.
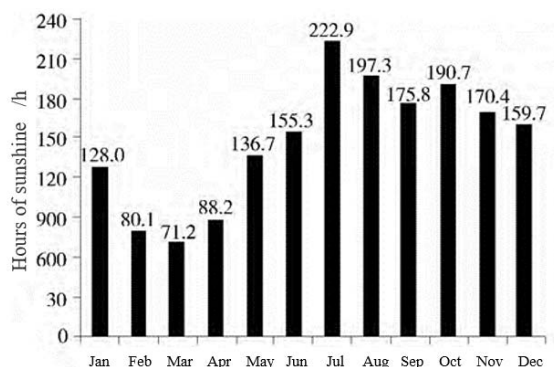
Figure 5. Monthly variations of sunshine duration in Wanshan Islands area.

It can be seen from the figure that the variation of the number of insolation hours in the Wanshan Island area during the year is large, showing a bimodal distribution, with two peaks appearing in July and October, and two valley values appearing in March and September, respectively. The longest number of hours of sunshine is in July, with hours of sunshine at 222.9 h, followed by August with sunshine hours of 197.3 h; The shortest number of sunshine hours is in March, with 71 hours of sunshine. 2 h, followed by February, with sunshine hours of 80.1 h. The difference between the longest and shortest months of sunshine hours is 157.1 h.

5. Solar resource assessment

The richness and stability of solar energy resources are used to evaluate solar energy resources at different levels.

5.1 Solar resource richness assessment

The abundance of solar energy resources is measured by the total annual solar radiation[14], which is divided into four levels according to the resource situation, as shown in **Table 1**.

Table 1. Richness grade of solar energy resources

Total annual solar radiation MJ/m^2/a	Richness
T1 ≥ 6,300	Most resourceful
5,040 ≤ T1 ≤ 6,300	Very resourceful
3,780 ≤ T1 ≤ 5,040	Resourceful
T1 < 3,780	Resources in general

Note: T1—Annual solar radiation per year.

According to the statistics of the total solar radiation data of the Wanshan Island area for many years, the annual average annual average of total solar radiation in the area is 4,996.25 MJ/m^2, which belongs to the resource-rich area.

5.2 Solar resource stability assessment

The stability of solar resources is expressed in K, the ratio of the maximum to a minimum number of days greater than 6 h per month[14], and its rank is shown in **Table 2**.

Table 2. Steady grade of solar energy resources.

Stability indicator	Degree of stability
<2	Stable resources
2—4	Resources are relatively stable
>4	Resource instability

From the statistics of the monthly sunshine hours greater than 6 h days in the Wanshan Island area over the years: the average number of days with more than 6 h in the region for many years is 160 d, accounting for 43.8%; Among them, July has

the most servings, reaching 19.7 d; March minimum, only 5.5 d; The difference between the two reaches 12.2 d. The multi-year average K value in the Wanshan Island area is 3.6, according to the stability level classification in **Table 2**, this area belongs to the area with more stable resources.

6. Conclusion

1) The total solar radiation in the Wanshan Island area showed a weak interannual upward trend, but failed the significance confidence test, and the increase was only 1.711 MJ/m^2/10 a; Total solar radiation varies undrilled during the year, peaking in July and lowest in February.

2) The number of sunshine hours in the Wanshan Island area showed a slight interannual downward trend, but failed the significance confidence test, and the decrease was 20 h/10 a; Sunshine hours vary bimodal over several years, with the largest in July and the smallest in March.

3) The solar energy resources in the Wanshan Island area are abundant and stable, and the total solar radiation has risen in recent years, which is beneficial to the development and utilization of solar energy in the region.

4) Similar to the previous research results, the trend of sunshine hours in the Wanshan Island area is decreasing; The trend of total solar radiation change in the Wanshan Island area is rising. It is generally believed that the factors that affect the total solar radiation and sunshine hours are mainly meteorological factors (such as cloud cover, precipitation, etc.) and environmental factors (such as aerosols, etc.). Especially since the beginning of the 21st century, the phenomenon of haze across the country has become increasingly serious, and the transparency of the atmosphere has continued to decline, resulting in a decrease in the number of sunshine hours, which should also affect the total solar radiation that is closely related to it. The author's analysis believes that this result is closely related to aerosol particulate matter, aerosol particulate matter may reduce direct solar radiation, but at the same time may increase scattered radiation, resulting in the total solar radiation composed of the sum of the above two parts is not significantly reduced. However, the degree and mechanism of the influence of various factors on the total solar radiation are not very clear at present, and relevant analysis and calculations need to be carried out in future studies.

Conflict of interest

The authors declared that they have no conflict of interest.

References

1. Huang X, Wang Z, Li Y, *et al*. Solar thermal electric generating technology. Beijing: China Electric Power Press; 2013.
2. Ma Q, Xie Y, Yang H. Characteristics and assessment of solar energy resources Variation in Yunnan Xijiekou Area. Electric Power Survey & Design 2013; (69): 306–308.
3. Jiang H, He G, Lan Y. Photovoltaic power station design technology. Beijing: China Electric Power Press; 2014.
4. Qi B, Shao B, Du R. Characteristics and assessment of solar energy resources variation in Hangzhou. Bulletin of Science and Technology 2012; 28(5): 59–61.
5. Yang F, Sun Z, Han E. Variation characteristics and assessment of solar energy resources in Lhasa area. Renewable Energy Resources 2014; 328(12): 1791–1796.
6. Fu Z, Wang Q. The definition and detection of the abrupt climatic change. Scientia Atmopherica Sinica 1992; 16(4): 482–493.
7. Li Y, He R, Du Y. Spatial and temporal variations of global solar irradiance in South China area. Renewable Energy Resources 2012; 30(1): 13–16.
8. Wild M, Gilgen H, Roesch A, *et al*. From dimming to brightening: Decadal changes in solar radiation at earth's surface. Science 2005; (308): 847–850.
9. Guo J, Ren G. Variation characteristics of sunshine duration in Tianjin in recent 40 years and influential factors. Meteorological Science and Technology 2006; 34(4): 415–420.
10. Yang X, Cai M, Zhao Y. Variation analysis of sunshine duration in Kashgar, in recent 39 years. Arid Zone Research 2011; 28(1): 158–162.
11. Lu X, Chen Y. Statistics and analysis of sunshine duration in Dongyang in 50 Years. Anhui Agriculture Bulletin 2008; 14(15): 99–101.
12. Chen B, Zhang P, Hao K, *et al*. Variation characteristics of sunshine duration in Chengdu in recent 50 years. Meteorological Science and Technology 2008; 26(6): 760–763.
13. Chen Z. Study on global solar irradiance in China during 1957—2000. Beijing: Graduate School of Chinese Academy of Sciences; 2005.
14. QX/T 89—2008. Assessment method of global solar irradiance. Beijing: Meteorological Press; 2008.

ORIGINAL RESEARCH ARTICLE

Research on solar energy resource assessment and development pathway in Singapore

Su Bai[1,2], Yi Gao[1,2]

[1] *Global Energy Interconnection Group Co., Ltd., Beijing 100031, China. E-mail: 744176958@qq.com*
[2] *Global Energy Interconnection Development and Cooperation Organization, Beijing 100031, China.*

ABSTRACT

Solar energy is the only renewable energy source likely to be developed on a large scale in Singapore. Singapore has limited land resources. According to the land use, the solar energy exploitable areas can be divided into five categories: rooftop photovoltaic, building surface photovoltaic, land-based photovoltaic, floating photovoltaic and infrastructure photovoltaic. The total development area of each type of photovoltaic is about $3,680 \times 10^4$ m^2. According to the assessment, Singapore has about 968×10^4 kW in 2050, of which distributed solar energy accounted for about 74%. Roof, building and infrastructure photovoltaic mainly adopt distributed development with high cost of per kWh; land-based and floating photovoltaic mainly adopt centralized development with low cost. According to the cost reduction speed and development degree of various kinds of solar energy, two solar energy development paths from 2030 to 2050 are proposed, namely, the full development path and the economic development path. The full development path aims at the full development of solar energy potential, and the economic development path considers the kilowatt-hour cost of solar energy development. The difference between the two paths focuses on the development degree of rooftop photovoltaic and building surface photovoltaic. Under the full development path, the electrification level reaches 61%, 16 percentage points higher compared with the economic development path; the installed renewable energy capacity reaches 51%, 19 percentage points higher compared with the economic development path. On the basis of two solar energy development paths, two 2050 energy scenarios adapted to different solar energy development paths are proposed. Singapore is unable to be carbon neutral in either development path or needs to increase transnational transmission.

Keywords: Solar Energy Resources; Photovoltaic; Full Development; Economic Development; kWh Cost; Singapore

1. Introduction

Singapore is a world-famous "pocket-size" developed country, short of fossil energy resources, but it takes advantage of its geographical advantages to embark on the road of export-oriented energy rich country with crude oil processing as the core. Aiming at urban greening, sustainable living and a green economy, Singapore has completed the transition from oil to natural gas in the past 50 years, and achieved clean electricity. With the climate change challenges of global warming, how to reduce carbon emissions and achieve carbon neutrality has become the focus of the Singapore government and research institutions. Developing renewable energy is an important measure to achieve carbon neutrality, but Singapore lacks renewable energy, without any hydro and geothermal resources. In terms of wind energy, except for coastal areas and offshore islands, the average wind speed is generally less than 2 m/s, and most coastal areas are used as

ports, moorings and waterways, so there is little potential for wind resource development. Solar energy is the most promising renewable energy source in Singapore, with an average annual irradiation intensity of 1,600 ~ 1,700 kW·h/m^2. Development of solar energy is the most viable renewable energy option in Singapore[1-7]. With solar energy as the core, this paper evaluates various types of solar energy exploitable resources in Singapore, calculates the cost changes of various types of solar energy, and gives two solar energy development paths of full development and economic development, as well as the Singapore 2050 energy scenario outlook to adapt to different solar energy development paths.

2. Assessment of solar energy resources

2.1 Assessment of developable area

Singapore has limited land resources, less land to build large-scale photovoltaic bases, and requires full use of various photovoltaic areas that can be developed. Based on land use, Singapore solar developable areas can be divided into the following five categories: rooftop, building surface, land-based, floating and infrastructure PV.

2.1.1 Rooftop PV

The assessment of the potential is based on a detailed 3D urban model of the Singapore Bureau of Land Management (SLA), which includes all 158,000 buildings in Singapore. After removing buildings with very small available surfaces (less than 10 m^2, not available for PV deployment), about 132,000 buildings participated in the assessment of rooftop PV development potential, with a total roof area of about 9,870 × 10^4 m^2. After the minimum irradiation amount, maximum inclination, minimum continuous area and building type screening, the total area of rooftop photovoltaic that can be developed is about 1,322.1 × 10^4 m^2, among which residential housing area is about 222.5 × 10^4 m^2, industrial building area is about 805.6 × 10^4 m^2, commercial building area is about 165.6 × 10^4 m^2, and buildings with other purposes area is about 128.4 × 10^4 m^2.

2.1.2 Building surface photovoltaic

The assessment of photovoltaic development potential on building surfaces is similar to the roof, based on the detailed 3D urban model of the Singapore Bureau of Land Management (SLA). The assessment includes all facade areas suitable for PV installation, regardless of the degree of integration of the building, that is, the building added PV (BAPV) and the building integrated PV (BIPV). The total area involved in the evaluation of the building surface is 2.14 × 10^8 m^2. After minimum irradiation, minimum continuous area, building window to wall ratio and surface orientation screening, the surface photovoltaic exploitable area of the existing building is about 787.7 × 10^4 m^2. Based on the average number of new buildings in Singapore over the past 10 years, 100 new buildings per year will be about 195 × 10^4 m^2 by 2050.

2.1.3 Land-based PV

Assessment of the land-based PV exploitable potential is based on the vacant land information system of Singapore Bureau of Land Management (SLA), and the assessment area includes vacant land on Singapore's main island and two larger islands that may be connected to the main island grid—Jurong Island and Pulau semakau Island. When assess whether it can be used for solar deployment, considering public acceptance, conflicts of interest, and economy, excluding fields, forests, nature reserves, unsuitable debris areas, and land reclamation areas. The total exploitable area of land-based PV is about 500 × 10^4 m^2, of which 35 × 10^4 m^2 is the main island, Jurong Island 380 × 10^4 m^2 and Pulau semakau Island 85 × 10^4 m^2. Most of the exploitable areas are concentrated in on Jurong Island[8].

2.1.4 Floating PV

Floating PV refers to the installation of solar photovoltaic systems on water bodies, and the assessment of the exploitable potential includes floating PV in inland water bodies and offshore waters. Singapore's total inland water area is about 6% of its total territory, but due to various restrictions, only a small fraction of them can be used for floating photovoltaic deployment. After

evaluation, the total area of solar photovoltaic power generation can be about 400×10^4 m^2. After deducting the waters designated to maintain buoys and safe buoys, the net photovoltaic area is about 250×10^4 m^2. Because Singapore's offshore space is very crowded, only areas known as the "Dead Sea space" are included in the assessment, excluding environmental requirements such as biodiversity, with about 211.6×10^4 m$^{2[9]}$.

2.1.5 Infrastructure and photovoltaic power

Infrastructure photovoltaic refers to the combining of existing infrastructure with a solar photovoltaic system without interfering with the original use of the land. The infrastructure included in the assessment includes land (open parking lots, agricultural areas, etc.), sound insulation barriers, flood control channels, roads, etc. Through new technical transformation such as 3D space expansion of existing infrastructure, about 415×10^4 m^2 can be used to install photovoltaic, including 250×10^4 m^2 land, 100×10^4 m^2 sound barrier, 25×10^4 m^2 flood control channel, and road about 40×10^4 m$^{2[10]}$. The exploitable area of various types of PV in Singapore is shown in **Table 1**.

Table 1. Developable area of all types of PV in Singapore

Solar type	Subclass	Developable area/10^4 m^2
Rooftop photovoltaics	Houses for residents	222.5
	Industrial buildings	805.6
	Commercial buildings	165.6
	Others	128.4
Building surface photovoltaics	Building renovation	787.7
	New buildings	195.0
Land-based photovoltaics	The island	35.0
	Jurong Island	380.0
	Pulau semakau Island	85.0
Floating photovoltaics	Inland	250.0
	Offshore	211.6
Infrastructure photovoltaics		415.0
Total		~ 3,680

2.2 Assessment of the exploitable potential

Based on the exploitable area of various types of solar energy to predict the area coefficient of the future PV system, then the exploitable potential of Singapore can be evaluated. In 2020, the most advanced photovoltaic panel area coefficient can reach 0.19 kW/m^2. According to the forecast of international Solar Energy Organization, the photovoltaic system area coefficient can reach 0.25 ~ 0.3 kW/m$^{2[11]}$ in 2050. The land-based photovoltaic area coefficient is taken as 0.3 kW/m^2, other types are measured as 0.25 kW/m^2. the developable PV potential in 2050 is about 968×104 kW, among them, rooftop photovoltaic has the greatest development potential, approximately 330×10^4 kW, accounting for 34%; the exploitable potential of building surface PV is about 246×10^4 kW, accounting for 25%; the land-based PV $150 \times$ 10^4 kW, accounting for 16%; the floating photovoltaic PV 138×10^4 kW, accounting for 14%; the infrastructure photovoltaic 104×10^4 kW, accounting for 11%. The exploitable potential of various PV products in Singapore is shown in **Table 2**.

3. Solar kWh cost

3.1 Prediction method of kWh cost

3.1.1 Calculation model

The levelized cost of energy (*LCOE*) is calculated in equation (1). The numerator is the project cost in the whole life cycle, including equity investment capital cost (*EPCI*), operating cost (*OM*), insurance (*IC*), inverter warranty extension cost (*IEI*). The year of the extended warranty depends on the inverter supplier, and the model assumes a warranty period of 20 years. The Loan (*LP*)

includes annual interest and amortization. The *OM*, *IC*, and *IEI* adjust for inflation rates after the first year. The denominator is the full life-cycle power generation of the system. The power generation in the first year of the system is calculated by

available irradiance (*IRD*) and performance ratio (*PR*). After the first year, the power generation is adjusted annually according to the system decline rate (*SDR*).

$$LCOE = \frac{EPCI + \sum_{n=1}^{N}\frac{OM^* + IC^*}{(1+DR)^n} + \frac{IEI^*_{n=5,10,15,20}}{(1+DR)^{n=5,10,15,20}} + \sum_{n=1}^{N}\frac{LP}{(1+DR)^n}}{\sum_{n=1}^{N}\frac{(IRD \times RP) \times (1-SDR)^n}{(1+DR)^n}}$$

(1)

The numerator and denominator are discounted by the nominal discount rate (*DR*) calculated from the net present value of the Weighted Average Cost of Capital (*WACC*).

$$WACC = (1-D) \times (RFR_{20} + b \times MRP) + D \times (RFR_{10} + DP)(1 - TR)$$

(2)

Table 2. Developable potential of various photovoltaics in Singapore

Solar type	Subclass	Developable potential/10^4 m^2
Rooftop photovoltaics	Houses for residents	56
	Industrial buildings	201
	Commercial buildings	41
	Others	32
Building surface photovoltaics	Building renovation	197
	New buildings	49
Land-based photovoltaics		150
Floating photovoltaics	Inland	75
	Offshore	63
Infrastructure photovoltaics		104
Total		968

The local risk-free interest rates (*RFR*) are based on Singapore government bond yield data, the cost of debt is 10 years (*RFR*$_{10}$), and the equity cost is 20 years (*RFR*$_{20}$). The cost of equity assumes that investment in solar systems shares the same risk with investment in the Singapore economy, the beta coefficient (*b*) is 1.0. The market risk premium (*MRP*) is calculated using the latest data from the Singapore National Electricity Market (*EMA*); the Debt ratio (*D*) is the percentage of an investment financed by an external lender; debt surcharge (*DP*) takes 3.07%; tax rate (*TR*) using the income tax rate of Singapore enterprises, 17%.

3.1.2 Basic assumptions

To simplify the calculation, following assumptions are made:

(1) **The investment cost**. Due to space constraints, the inefficient modules (polysilicon modules or below or equal to 300 W) is no longer taking into consideration; and the minimum cost of

photovoltaic module, central inverter and string inverter are set as 0.10 USD/W, 0.025 USD/W and \$0.035/W respectively[12]. Excluding solar grid connection and transmission costs; and to simplify analysis, excluding surplus value and decommissioning costs, assuming they are in balance.

(2) **The operating costs**. Excluding any rent fees; operating and maintenance costs range from 1% to 1.45% of capital expenditures, depending on system type (large size roof is 1%, small size is 1.45%). As capital expenditure decreases over time, the insurance cost is estimated to be between 0.4% and 0.6% of the capital expenditure. Based on the empirical data from the National Environment Agency of Singapore (NEA)[13], And the monthly data from 1991–2000 and 2010–2018, assuming that the constant annual irradiance of P50 is 1,644 kW·h/m^2. The performance ratio starts at 78%, and move up at 0.5% a year, until the upper limit of

82% of monocrystalline silicon is reached. Assuming that the performance ratio of floating PV system increases by 6% compared with rooftop PV and land-based PV systems[14]; the system decline rate remains constant throughout the forecast period, roof and land-based photovoltaic systems were 0.8%, inland reservoir floating photovoltaic power is 1%, offshore floating photovoltaic power is 1.5%.

3.1.3 Selection of basic financial parameters of the model

The loan term is 10 years; using a 25-year linear depreciation; the system life span is 25 years; operating costs (OPEX) inflation rate is 1.7%; no tax is included; no interest was available during the construction period, assuming that the lender provides a grace period; fixed exchange rates throughout the forecast period, 1 USD for 1.36 SGD; nominal debt ratio of 5% (risk-free interest rate of 1.92%, debt premium of 3.08%); equity cost of 8.75% ~ 9% (risk-free rate of 2.22%, market risk premium of 6.53%, Beta factor of 1.0); 100% equity financing $WACC = 9\%$.

3.2 Change forecast of kWh cost

According to the evaluation, the $LCOE$ changes of various PV types from 2025 to 2050 are shown in **Figure 1**. In 2025, the land-based photovoltaic $LCOE$ was 0.08 SGD/(kW·h), which is equivalent to the cost of gas and electricity, while the cost of other photovoltaic types is still high, between 0.12 and 0.19 SGD/(kW·h).

In 2030, land-based PV $LCOE$ continued to fall to 0.054/(kW·h); inland floating PV $LCOE$ fell to 0.07/(kW·h); rooftop PV, building surface PV, offshore floating PV and infrastructure PV $LCOE$ remains high at 0.09 ~ 0.11/(kW·h).

In 2050, land-based PV and inland floating PV $LCOE$ fell to 0.05/(kW·h); offshore floating PV and infrastructure PV $LCOE$ both fell to 0.076/(kW·h); roof and building surface PV to 0.09/(kW·h) and 0.105/(kW·h) respectively.
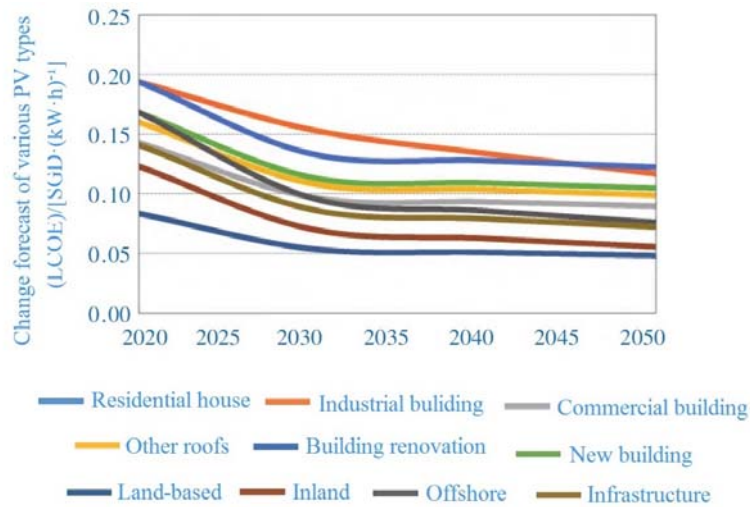
Figure 1. LCOE change prediction of various PV types from 2025 to 2050.

3.3 Path prediction of solar energy development

The path of solar energy depends not only on the rate of cost decline, but also on the government's attitude towards it. At present, Singapore Energy Market Authority plans to reach the solar installed capacity of 200×10^4 kW by 2030, but the medium and long-term development plan for solar energy is not clear, and it is difficult to give a clear solar energy development path according to existing policies and relevant data.

Therefore, in view of the policy uncertainty, this paper gives two solar energy development paths from 2030 to 2050, namely, the full development path and the economic development path.

3.3.1 Fully development path

On the basis of the installed solar capacity of 200×10^4 kW by 2030, the solar potential will be basically developed by 2050, and the installed solar capacity will reach 900×10^4 kW. The development order begins with the economic

solar types based on *LCOE*, the development focuses on land-based photovoltaic by 2030, inland floating photovoltaic, infrastructure photovoltaic and a small number of rooftop photovoltaic by 2040, all types of solar energy development completed by 2050. The changes of solar energy installed capacity from 2030 to 2050 under the full development path are shown in **Figure 2**.

3.3.2 Economic development Path

On the basis of the plan of the solar installed capacity to reach 200×10^4 kW in 2030, the development of certain economic solar energy begins. When the *LCOE* of solar energy falls to 0.08 SGD/(kW·h), the development of this kind of solar energy begins. It is predicted that the solar installed capacity will reach 600×10^4 kW by 2050. The development plan concentrates on land-based PV by 2030, land-based photovoltaic, infrastructure photovoltaic and inland floating photovoltaic by 2040, and full development of land-based photovoltaic, infrastructure photovoltaic and
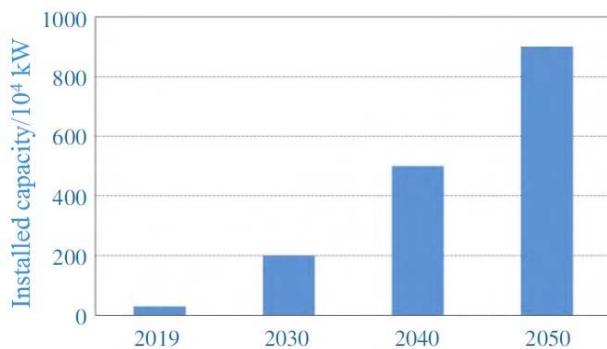
Figure 2. Changes of solar energy installed capacity—full development path.
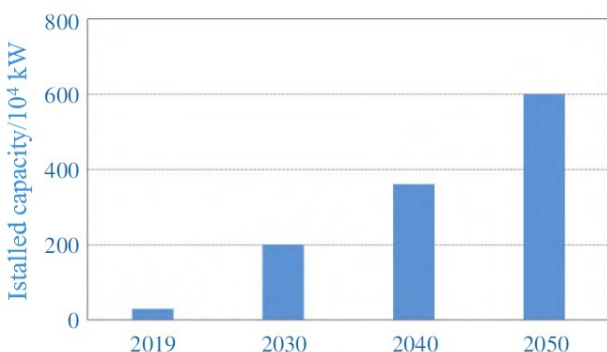
Figure 3. Changes in solar energy installed capacity—economic development path.

floating photovoltaic by 2050. A small amount of rooftop photovoltaics will be developed, and wall photovoltaics will be developed on a pilot basis. It

is estimated that the total cost of solar energy development is only half of the full development path. The changes of solar energy installed capacity from 2030 to 2050 under the economic development path are shown in **Figure 3**.

The comparison of two solar development paths is shown in **Figure 4**. By 2050, the development of land-based photovoltaic, infrastructure photovoltaic and floating photovoltaic will be basically completed, and the difference between the two development paths focuses on the development degree of rooftop photovoltaic and building surface photovoltaic. Due to the high cost of rooftop photovoltaic and building surface photovoltaic kWh, it is difficult to conduct large-scale centralized development. In the economic development path, the development of rooftop photovoltaic will only be carried out in the pilot form from 2030 to 2040, and from 2040 to 2050, cheaper industrial rooftop photovoltaic will be developed and the pilot development of building photovoltaic will be carried out.

4. 2050 energy scenario outlook for different solar energy development paths

4.1 Scenario construction method

On the basis of the development of the two solar energy paths, according to the consumption of renewable energy, the decommissioning of gas and power units and the transnational Internet situation, the two energy and power development scenarios are obtained, including the full development scenario of renewable energy and the economic development scenario of renewable energy. These two scenarios are discussed, and the specific path of energy and electricity development in Singapore is given in two extreme scenarios, comparing the energy structure, power structure, cost difference and interconnection degree of the two extreme scenarios.

Constraints for the two scenarios include the Singapore 2030 Energy and Power Plan, renewable energy installations following their own solar energy development path, power balance and energy terminal consumption balance.

The development goal of the full development scenario of renewable energy is to achieve the highest proportion of renewable energy as possible. In order to achieve the goal, no restraints to the transnational channel capacity, energy structure changes, and gas-power units will only serve for 30 to 40 years. The development goal of the economic development scenario of renewable energy is to keep cost as low as possible. In order to achieve the priority of self-sufficiency of target power of, existing industries are not electrified (the new part is not limited), and gas power units are in service for 50 years. The constraints and development goals for the two energy scenarios in Singapore are shown in **Figure 5**.
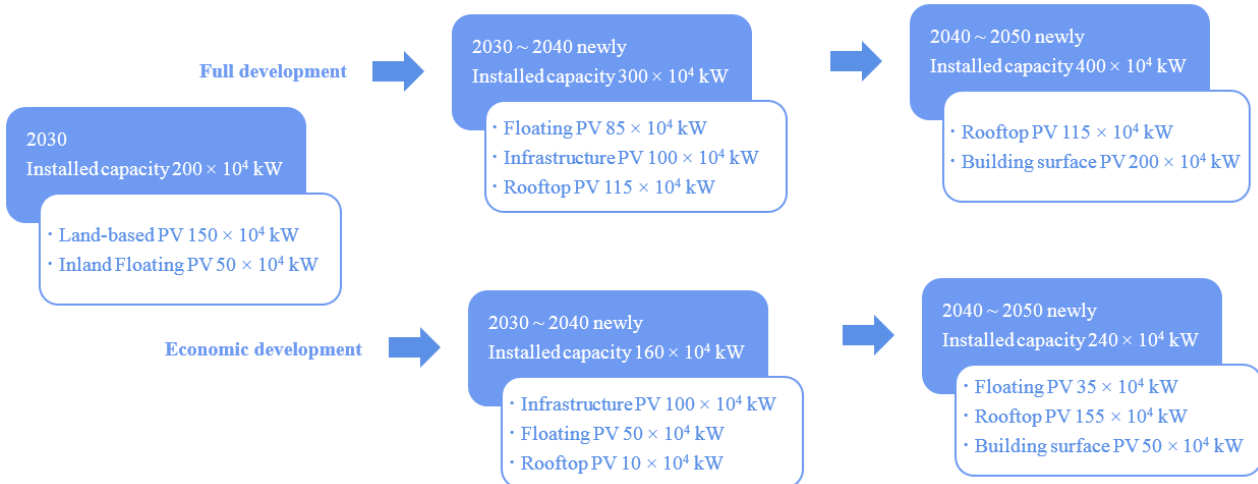
Figure 4. Comparison of solar energy development path.
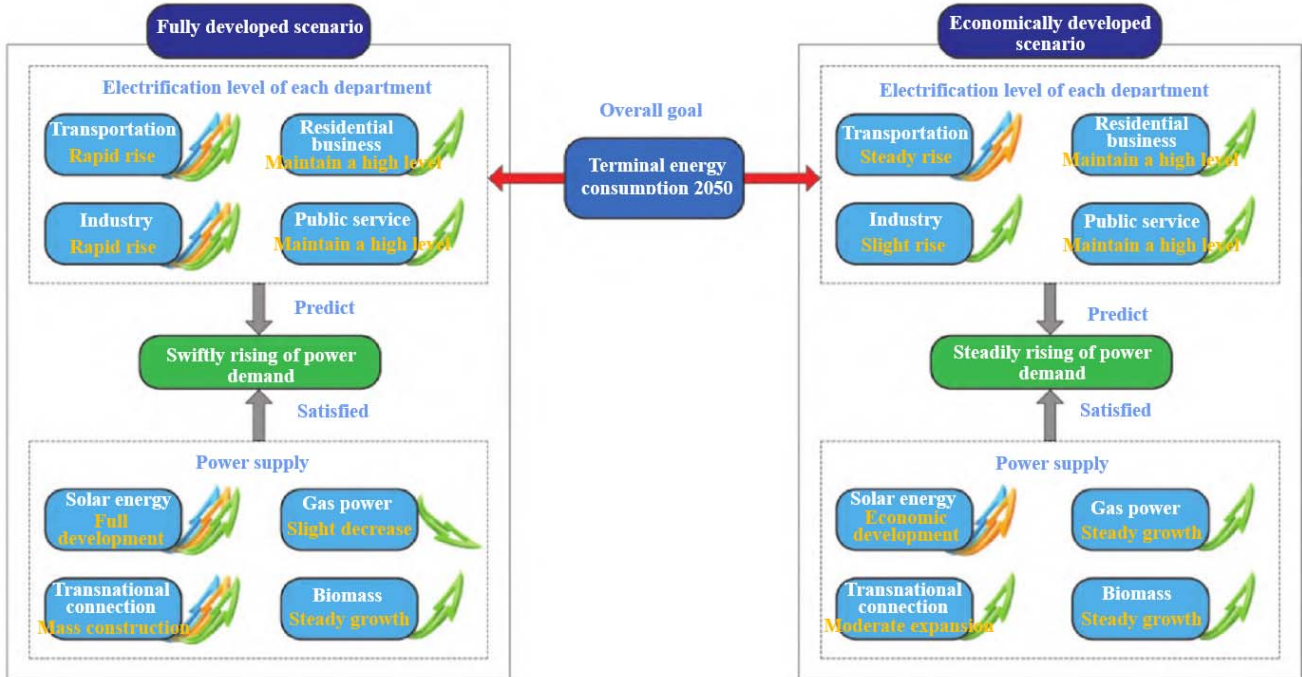
Figure 5. Constraints and development goals for the two energy scenarios.

4.2 Full development scenario solar energy

4.2.1 Energy transformation mode

The transportation department considers the electric energy replacement for fuel vehicle such as cargo vehicles, and aircraft and ships are not considered. The calculation equation of the terminal energy electrification rate in the transportation department is shown in the equation (3).

$$I = \frac{E_{EV}}{E_{EV} + E_{FV} + E_{others}}$$
$$E_{EV} = M(1 + r_V)^n \cdot R_{EV} \cdot L \cdot K_E$$
$$E_{FV} = M(1 + r_V)^n \cdot (1 - R_{EV}) \cdot L \cdot K_F$$

(3)

73

In the equation: I is the terminal energy electrification rate of the transportation department; E is the energy consumption of various transportation terminals , for example, E_{EV} is the terminal energy consumption of electric vehicle, while E takes the energy consumption of plane, ship and other transportation terminals in 2020, assuming it is constant; M is the total existing vehicles; r_V is the annual vehicle growth rate; n is the growth year, for example, if 2050 is the target year, then n is 30; R_{EV} is the target annual electric vehicle ratio; L is the average vehicle mileage; K is the terminal energy consumption per unit mileage.

According to the data of Singapore Land Transport Authority (LTA), the number of cars in Singapore was about 600,000 in 2018. Limited by land resources and road tolerance, the annual growth rate of Singapore cars will not exceed 0.2% in the future[15-17]. It's estimated that the share of electric car in Singapore will be 30% by 2030, with more than 200,000 vehicles. Under the full development path, the electric car in Singapore will account for 80% by 2050, with more than 500,000 vehicles, and electricity will account for 55.8% of energy consumption in the transportation sector, as shown in **Figure 6**.
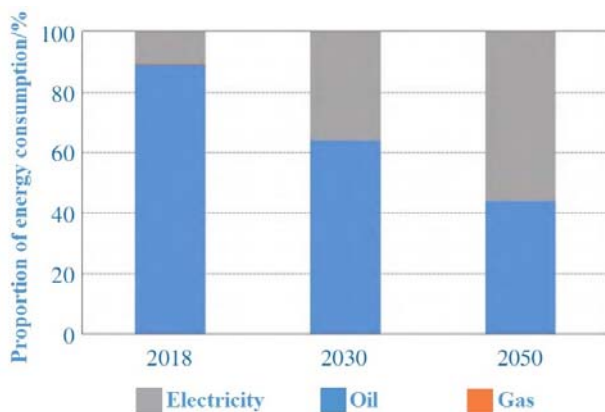
Figure 6. Energy consumption change in the transportation sector—full development path.

The energy mix of Singapore's industrial sector is not expected to shift significantly by 2030, with a small proportion of oil-fired equipment used for heating to be converted to gas and electricity, and the share of oil in end consumption falling to 57.3%, gas rising to 15.9%, electricity rising to 25%, and coal remaining at 1.8%. Under the full development path, considering the cost and technical factors, oil-fired equipment will be converted to hydrogen combustion or electrification respectively according to their respective characteristics, and coal equipment will be completely eliminated. By 2050, the share of oil in end consumption decreases to 39.5%, natural gas is 15.8%, and electricity rises to 44.7%, as shown in **Figure 7**.
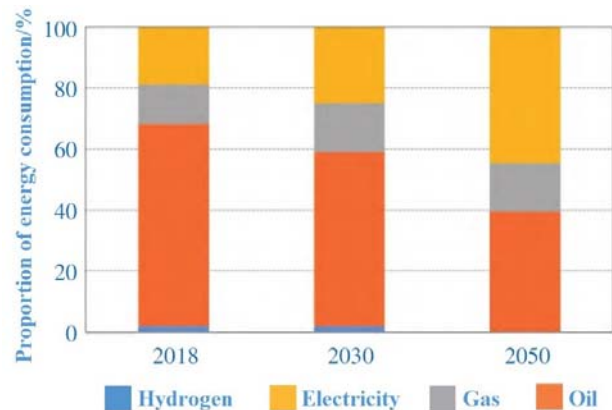
Figure 7. Changes in industrial sector energy consumption—full development path.

The structure of Singapore's energy consumption in 2050 under the full development path is shown in **Figure 8**, with electricity consumption of 9,219.9 kt standard oil, natural gas consumption of 1,427.7 kt standard oil, and oil consumption of 4,536 kt standard oil. The power sector reduces carbon emissions by developing renewable energy sources and importing clean electricity, and the carbon emissions from the fully developed pathway are estimated to be about $3,140 \times 10^4$ t according to the carbon emission factors given by the IPCC for each type of energy source (see **Table 3**).
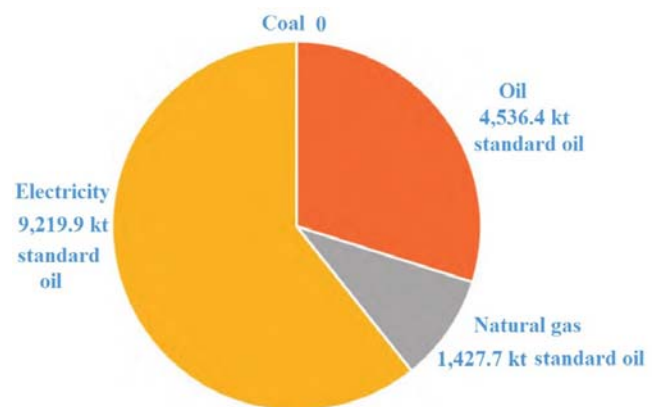
Figure 8. Energy consumption structure of Singapore in 2050—full Development path.

74

Table 3. Carbon emission factors of various types of energy consumption

Types of energy consumption	CO_2 emission factors
Coal	94,600 kg/TJ
Oil	71,900 kg/TJ
Natural gas	56,100 kg/TJ
Electricity	0.4 kg/(kW·h)

4.2.2 Power supply mode

According to the terminal energy demand, the power demand of Singapore in 2030 is 711×10^8 kW·h and maximum load is 981×10^4 kW; the power demand in 2050 is $1,100 \times 10^8$ kW·h and maximum load is $1,500 \times 10^4$ kW. In 2050, the total installed capacity was $1,850 \times 10^4$ kW, among which solar energy resources were basically developed, and the installed capacity reached 900×10^4 kW, installed capacity of gas power and biomass reached 900×10^4 kW, and 50×10^4 kW respectively, as shown in **Figure 9**.
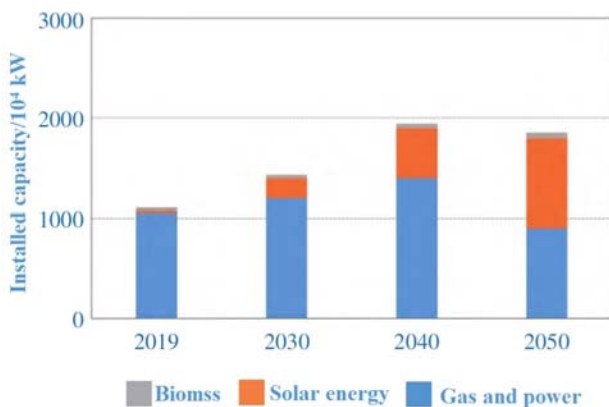
Figure 9. Installation structure changes—full development path.

According to the power balance analysis, due to the decrease of solar energy output at 7:00 pm, 900×10^4 kW of gas power installed capacity and 50×10^4 kW of biomass installed capacity cannot meet the power demand of about $1,500 \times 10^4$ kW. Considering the standby, about 850×10^4 kW of electricity should be added internationally. Transnational power transactions exceed 50% of the maximum load.

Combined with Singapore's geographical location, the power industry is diversified, importing 300×10^4 kW of electricity from Malaysia and Indonesia and 250×10^4 kW of electricity from Australia.

4.3 Economic development scenario of solar energy

4.3.1 Mode of energy transformation

Transportation department and the prediction method is consistent with the full development path. It is expected that electric vehicles in Singapore will account for 30% in 2030, with a total of more than 200,000 vehicles, and the new electricity demand of 68×10^8 kW·h. The electrification rate of the transportation sector has increased from 11% in 2018 to 36% in 2030. In 2050, the proportion of electric vehicles in Singapore will reach 48%, with more than 300,000 vehicles, the new electricity demand will increase by 100×10^8 kW·h compared with 2030, and the electrification rate of the transportation sector will increase to 48.5%, as shown in **Figure 10**.
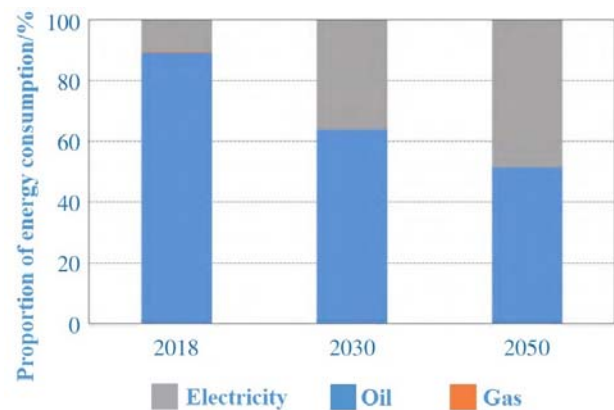
Figure 10. Changes in energy consumption of transportation sector—economic development path.

In the industrial sector, only considering using electricity to replace oil, the electrification rate in the industrial sector is expected to rise to 27% from 19% in 2018 by 2030. In 2050, with a pilot hydrogen replacement of new natural gas consumption, electrification in the industrial sector slowly grew to 30%.

Under the economic development path, the energy consumption structure of Singapore in 2050 is shown in **Figure 11**. Among them, electricity consumption 6,939.9 kt oil equivalent, natural gas consumption 1,727.7 kt oil equivalent, oil consumption 6,516 kt oil equivalent and coal consumption 130 kt oil equivalent. According to the IPCC carbon emission factor, the carbon emission of the economic development path is about $4,100 \times 10^4$ t.
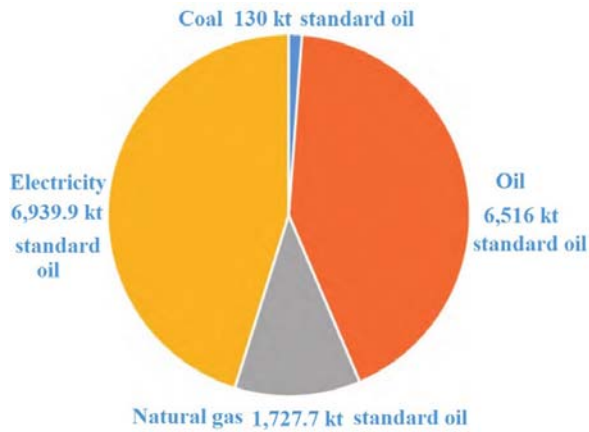
Figure 11. Energy consumption structure of Singapore by 2050—economic development path.

4.3.2 Power supply mode

According to the terminal energy demand, the power demand of Singapore in 2030 is 711×10^8 kW·h, the maximum load is 981×10^4 kW; the power demand in 2050 is 820×10^8 kW·h, and the maximum load is $1,300 \times 10^4$ kW. Under the economic development path, the installed solar energy capacity in 2030 will reach 200×10^4 kW, achieving the planning target. In 2040, with the economic development of infrastructure photovoltaics and inland floating photovoltaics, the installed solar capacity will increase by 360×10^4 kW; in 2050, all of Singapore's economical solar energy resources will be basically developed, with an installed capacity of about 600×10^4 kW, as shown in **Figure 12**.
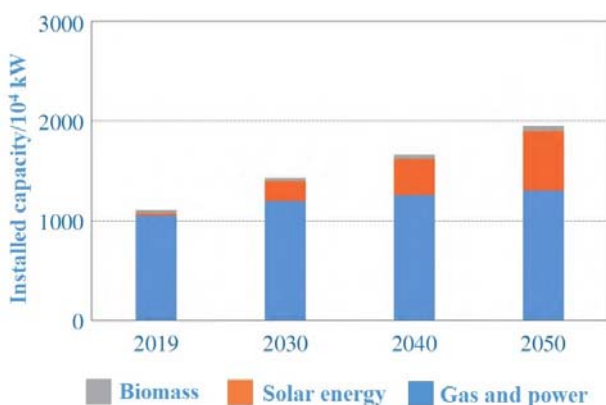
Figure 12. Changes in installed capacity structure—economic development path.

5. Conclusion

(1) According to the evaluation, in 2050, Singapore photovoltaic exploitable potential is about 968×10^4 kW, including rooftop photovoltaic

about 330×10^4 kW, building surface photovoltaic about 246×10^4 kW, land-based photovoltaic about 150×10^4 kW, floating photovoltaic about 138, 104 kW, infrastructure photovoltaic about 104×10^4 kW, distributed solar accounted for about 74%. By 2050, roof, building and infrastructure PV will mainly be distributed development with high kWh cost, roof PV 0.09 ~ 0.12 SGD/(kW·h), building surface PV 0.10 ~ 0.12 SGD/(kW·h) and infrastructure PV 0.072 SGD/(kW·h). Land-based and floating photovoltaic are mainly developed with low cost, namely 0.038 SGD/(kW·h) and 0.04 ~ 0.06 SGD/(kW·h) respectively.

(2) Solar energy is the only renewable resource in Singapore that can be developed on a large scale. Two development paths are proposed according to the development degree and cost change of solar energy resources. Under the full development path, the electrification level reaches 61%, 16% higher compared with the economic development path; the installed renewable energy capacity is 51%, 19 percentage points higher compared with the economic development path.

(3) Singapore is unlikely to become carbon neutral by only relying on its own renewable energy resources, and needs to increase the proportion of cross-border transmission. Singapore has scarce renewable resources, wind and water energy, and solar energy is abundant. However, the land area is small, and it is difficult to carry out the construction of large-scale solar energy bases. Neither of the two development paths of research and planning can achieve carbon neutrality. In 2050, Singapore's carbon emissions under the full development path were $3,140 \times 10^4$ t, and about $4,100 \times 10^4$ t under the economic development path. Singapore needs to develop solar energy, upgrade the transnational transmission scale, install carbon capture systems, reduce carbon emissions, and achieve carbon neutrality.

Load Access" (No.: SGGEIG00JYJS2100033).

Conflict of interest

The authors declared no conflict of interest.

References

1. Khew EE. Renewable energy and its relevance for Singapore in 2065. In: Quah E (editor). Singapore 2065: Leading insights on economy and environment from 50 Singapore icons and beyond. Singapore: World Scientific Publishing Co. Pte. Ltd.; 2015. p. 113–118.
2. Energy Market Authority. Singapore electricity market outlook (SEMO) 2018 [Internet]. Singapore: EMA; 2019. 3rd ed. Available from: https://www.ema.gov.sg/cmsmedia/Singapore%20Electricity%20Market%20Outlook%202018%20Final.PDF.
3. Karthikeya BR, Negi S, Srikanth N. Wind resource assessment for urban renewable energy application in Singapore. Renewable Energy 2016; 87: 403–414.
4. Amin ZM, Hawlader MNA. A review on solar assisted heat pump systems in Singapore. Renewable and Sustainable Energy Reviews 2013; 26: 286–293.
5. King S, Wettergren P. Feasibility study of renewable energy in Singapore. Stockholm: KTH Royal Institute of Technology; 2011.
6. Quek A, Ee A, Ng A, et al. Challenges in environmental sustainability of renewable energy options in Singapore. Energy Policy 2018; 122: 388–394.
7. He J. Renewable bioenergy development in Singapore and recent discoveries on biofuel generation. 2012 AIChE Annual Meeting; 2012 Oct 28–Nov 2; Pittsburgh, PA, USA. New York: American Institute of Chemical Engineers; 2012.
8. Solar Energy Research Institute of Singapore. Solar photovoltaic (PV) roadmap for Singapore [Internet]. Singapore: SERIS; 2020. Available from: https://www.nccs.gov.sg/docs/default-source/default-document-library/solar-photovoltaic-roadmap-for-singapore-a-summary.pdf.
9. Dong Z, Yang D, Reindl T, et al. Satellite image analysis and a hybrid ESSS/ANN model to forecast solar irradiance in the tropics. Energy Conversion and Management 2014; 79: 66–73.
10. Ng H. Tender called for 3rd phase of railway noise barrier works [Internet]. Available from: https://www.straitstimes.com/singapore/tender-called-for-3rd-phase-of-railway-noise-barrier-works.
11. Zumbo L, Lerat JF, Connelli C, et al. Influence of defects on silicon heterojunction solar cell efficiency: Physical model and comparison with data. AIP Advance 2021; 11(1): 015044.
12. Gandhi O, Rodríguez-Gallegos CD, Gorla NBY, et al. Reactive power cost from PV inverters considering inverter lifetime assessment. IEEE Transactions on Sustainable Energy 2018; 10(2): 738–747.
13. Singapore National Environment Agency. E^2 Singapore [Internet]. Singapore: NEA; 2010. Available from: http://www.e2singapore.gov.sg/DATA/0/docs/Booklet/E2S%20Publication.pdf
14. Kokate A, Wagh M. Experimental analysis of performance ratio of solar rooftop photovoltaic system (SRTPV) for various roof orientation and tilt. Journal of Physics: Conference Series 2019; 1172(1): 012067.
15. Oh S, Seshadri R, Azevedo CL, et al. Accessing the impacts of automated mobility-on-demand through agent-based simulation: A study of Singapore. Transportation Research Part A: Policy and Practice 2020; 138: 367–388.
16. Li MZF, Lau DCB, Seah DWM. Car ownership and urban transport demand in Singapore. International Journal of Transport Economics 2011; 38(1): 47–70.
17. Fwa TF. 50 Years of transportation in Singapore: Achievements and challenges. Singapore: World Scientific Publishing Co. Pte. Ltd.; 2016. p. 1–576.

Natural Resources Conservation and Research

Focus and Scope

Natural Resources Conservation and Research is a peer-reviewed, open-access journal that delivers high-quality original articles significant in all disciplines of resources conservation and sustainable management. Contributions may have relevance at regional, national or international scales and may focus at any level of research from individual resources or technologies to whole sectors or systems of interest. Contributors may emphasize any of the aforementioned aspects as well as scientific and methodological issues. NRCR aims to provide a communication and information exchange platform for conservationists, environmentalists, ecologists, researchers and professionals. Articles from related fields that are interested to a broad readership are particularly welcomed.

Topics include but are not limited to:

1. Research and proposal on natural ecosystem.

2. Research on ecology and biomass energy, including pesticide degradation, biodiversity, the impact of human activities on ecological energy.

3. Transformation of the natural resource system towards more sustainable production and consumption patterns, including instruments, methods, and process of change.

4. Technical, societal, economic, business and policy aspects of strategies to improve the sustainability.

5. Research on substitution of renewable or regenerative alternatives.

6. Climate strategy of natural resources protection.

7. Strategies or methods to serve the regenerative ecosystem.

8. Technological interventions for sustainable conservation of natural resources, including but not limited to biotechnology, physical technology, genetic technology, garden technology.